



DE83005696

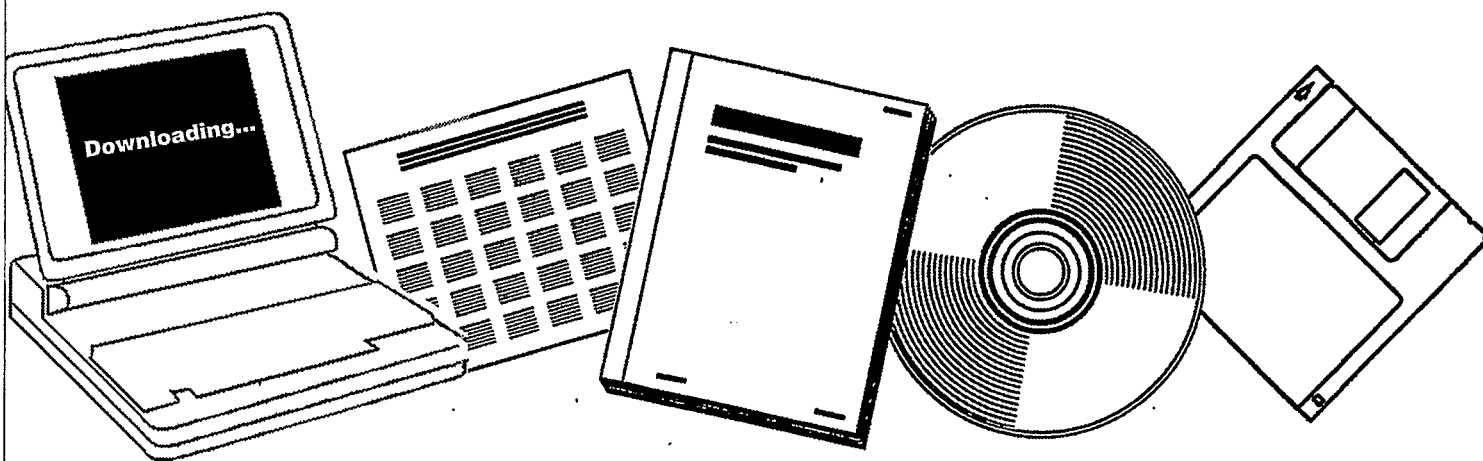
**NTIS**

One Source. One Search. One Solution.

**CHEMISTRY AND CATALYSIS OF COAL  
LIQUEFACTION: CATALYTIC AND THERMAL  
UPGRADING OF COAL LIQUID AND HYDROGENATION  
OF CO TO PRODUCE FUELS. QUARTERLY PROGRESS  
REPORT, OCTOBER-DECEMBER 1982**

UTAH UNIV., SALT LAKE CITY. DEPT. OF  
MINING AND FUELS ENGINEERING

JAN 1983



U.S. Department of Commerce  
**National Technical Information Service**

DOE/ET/14700-13  
(DE83005696)

Distribution Category UC-90d

Chemistry and Catalysis of Coal Liquefaction  
Catalytic and Thermal Upgrading of Coal Liquid  
and Hydrogenation of CO to Produce Fuels

Quarterly Progress Report  
for the Period Oct - Dec 1982

Dr. Wendell H. Wiser

University of Utah - Department of  
Mining and Fuels Engineering  
Salt Lake City, Utah 84112

Date Published - January 1983

Prepared for the United States Department  
of Energy  
Under Contract No. DE-AC22-79ET14700

## CONTENTS

II	Objective and Scope of Work	3
III	Highlights to Date	7
IV	Task 1 Chemical-Catalytic Studies	8
	Task 2 Carbon-13 NMR Investigation of CDL and Coal	12
	Task 3 Catalysis and Mechanism of Coal Liquefaction	43
	Task 4 Momentum, Heat and Mass Transfer in Co-Current Flow	Discontinued
	Task 5 The Fundamental Chemistry and Mechanism of Pyrolysis of Bituminous Coal	46
	Task 6 Catalytic Hydrogenation of CD Liquids and Related Polycyclic Aromatic Hydrocarbons	55
	Task 7 Denitrogenation and Deoxygenation of CD Liquids and Related N- and O- Compounds	57
	Task 8 Catalytic Cracking of Hydrogenated CD Liquids and Related Hydrogenated Compounds	61
	Task 9 Hydropyrolysis (Thermal Hydrocracking) of CD Liquids	62
	Task 10 Systematic Structural-Activity Study of Supported Sulfide Catalysts for Coal Liquids Upgrading	69
	Task 11 Basic Study of the Effects of Coke and Poisons on the Activity of Upgrading Catalysts	77
	Task 12 Diffusion of Polyaromatic Compounds in Amorphous Catalyst Supports	83
	Task 13 Catalyst Research and Development	90
	Task 14 Characterization of Catalysts and Mechanistic Studies	Inactive
V	Conclusion	115

## OBJECTIVE AND SCOPE OF WORK

### I. The chemistry and Catalysis of Coal Liquefaction

#### Task 1 Chemical-Catalytic Studies

Coal will be reacted at subsoftening temperatures with selective reagents to break bridging linkages between clusters with minimal effect on residual organic clusters. The coal will be pretreated to increase surface area and then reacted at 25 to 350°C. Reagents and catalysts will be used which are selective so that the coal clusters are solubilized with as little further reaction as possible.

#### Task 2 Carbon-13 NMR Investigation of CDL and Coal

Carbon-13 NMR spectroscopy will be used to examine coal, coal derived liquids (CDL) and residues which have undergone subsoftening reactions in Task 1 and extraction. Improvements in NMR techniques, such as crosspolarization and magic angle spinning, will be applied. Model compounds will be included which are representative of structural units thought to be present in coal. Comparisons of spectra from native coals, CDL and residues will provide evidence for bondings which are broken by mild conditions.

#### Task 3 Catalysis and Mechanism of Coal Liquefaction

This fundamental study will gain an understanding of metal salt chemistry and catalysis in coal liquefaction through study of reactions known in organic chemistry. Zinc chloride and other catalytic materials will be tested as Friedel-Crafts catalysts and as redox catalysts using coals and selected model compounds. Zinc chloride, a weak Friedel-Crafts catalyst, will be used at conditions common to coal liquefaction to participate in well defined hydrogen transfer reactions. These experiments will be augmented by mechanistic studies of coal hydrogenation using high pressure thermogravimetric analysis and structural analysis. The results of these studies will be used to develop concepts of catalysis involved in coal liquefaction.

#### Task 4 Momentum Heat and Mass Transfer in CoCurrent Flow of Particle-Gas Systems for Coal Hydrogenation

A continuation of ongoing studies of heat and transport phenomena in cocurrent, co-gravity flow is planned for a one-year period. As time and development of existing work permits, the extension of this study to include a coiled reactor model will be undertaken. Mathematical models of coal hydrogenation systems will utilize correlations from these straight and coiled reactor configurations.

#### Task 5 The Fundamental Chemistry and Mechanism of Pyrolysis of Bituminous Coal

Previous work at the University of Utah indicates that coal pyrolysis, dissolution (in H-donor) and catalytic hydrogenation all have similar rates and activation energies. A few model compounds will be pyrolyzed in the range of 375 to 475°C. Activation energies, entropies and pro-

duct distributions will be determined. The reactions will assist in formulating the thermal reaction routes which also can occur during hydro-liquefaction.

## II. Catalytic and Thermal Upgrading of Coal Liquids

### Task 6 Catalytic Hydrogenation of CD Liquids and Related Polycyclic Aromatic Hydrocarbons

A variety of coal derived (CD) liquids will be hydrogenated with sulfided catalysts prepared in Task 10 from large pore, commercially available supports. The hydrogenation of these liquids will be systematically investigated as a function of catalyst structure and operating conditions. The effect of extent of hydrogenation will be the subject of study in subsequent tasks in which crackability and hydrolysis of the hydrogenated product will be determined. To provide an understanding of the chemistry involved, model polycyclic arenes will be utilized in hydrogenation studies. These studies and related model studies in Task 7 will be utilized to elucidate relationships between organic reactants and the structural-topographic characteristics of hydrogenation catalysts used in this work.

### Task 7 Denitrogenation and Deoxygenation of CD Liquids and Related Nitrogen- and Oxygen-Containing Compounds

Removal of nitrogen and oxygen heteroatoms from CD liquids is an important upgrading step which must be accomplished to obtain fuels corresponding to those from petroleum sources. Using CD liquids as described in Task 6, exhaustive HDN and HDO will be sought through study of catalyst systems and operating conditions. As in Task 6, catalysts will be prepared in Task 10 and specificity for N- and O-removal will be optimized for the catalyst systems investigated. Model compounds will also be systematically hydrogenated using effective HDN/HDO catalysts. Kinetics and reaction pathways will be determined. A nonreductive denitrogenation system will be investigated using materials which undergo reversible nitridation. Conditions will be sought to cause minimal hydrogen consumption and little reaction of other reducible groups.

### Task 8 Catalytic Cracking of Hydrogenated CD Liquids and Related Polycyclic Naphthenes and Naphthenoaromatics

Catalytic cracking of hydrogenated CD liquid feedstocks will be studied to evaluate this scheme as a means of upgrading CD liquids. Cracking kinetics and product distribution as a function of preceding hydrogenation will be evaluated to define upgrading combinations which require the minimal level of CD liquid aromatic saturation to achieve substantial heteroatom removal and high yields of cracked liquid products. Cracking catalysts to be considered for use in this task shall include conventional zeolite-containing catalysts and large-pore molecular sieve, CLS (cross-linked smectites) types under study at the University of Utah. Model compounds will be subjected to tests to develop a mechanistic understanding of the reactions of hydro CD liquids under catalytic cracking conditions.

#### Task 9 Hydropyrolysis (Thermal Hydrocracking) of CD Liquids

Heavy petroleum fractions can be thermally hydrocracked over a specific range of conditions to produce light liquid products without excessive hydrogenation occurring. This noncatalytic method will be applied to a variety of CD liquids and model compounds, as mentioned in Task 6, to determine the conditions necessary and the reactivity of these CD feedstocks with and without prior hydrogenation and to derive mechanism and reaction pathway information needed to gain an understanding of the hydropyrolysis reactions. Kinetics, coking tendencies and product compositions will be studied as a function of operating conditions.

#### Task 10 Systematic Structural-Activity Study of Supported Sulfide Catalysts for Coal Liquids Upgrading

This task will undertake catalyst preparation, characterization and measurement of activity and selectivity. The work proposed is a fundamental study of the relationship between the surface-structural properties of supported sulfide catalysts and their catalytic activities for various reactions desired. Catalysts will be prepared from commercially available. Supports composed of alumina, silica-alumina, silica-magnesia and silica-titania, modification of these supports to change acidity and to promote interaction with active catalytic components is planned. The active constituents will be selected from those which are effective in a sulfided state, including but not restricted to Mo, W, Ni and Co. The catalysts will be pre-sulfided before testing. Catalyst characterization will consist of physico-chemical property measurements and surface property measurements. Activity and selectivity tests will also be conducted using model compounds singly and in combination.

#### Task 11 Basic Study of the Effects of Coke and Poisons on the Activity of Upgrading Catalysts

This task will begin in the second year of the contract after suitable catalysts have been identified from Tasks 6, 7 and/or 10. Two commercial catalysts or one commercial catalyst and one catalyst prepared in Task 10 will be selected for a two-part study, (1) simulated laboratory poisoning/coking and (2) testing of realistically aged catalysts. Kinetics of hydrogenation, hydrodesulfurization, hydrodenitrogenation and hydrocracking will be determined before and after one or more stages of simulated coking. Selected model compounds will be used to measure detailed kinetics of the above reactions and to determine quantitatively how kinetic parameters change with the extent and type of poisoning/coking simulated. Realistically aged catalysts will be obtained from coal liquids upgrading experiments from other tasks in this program or from other laboratories conducting long-term upgrading studies. Deactivation will be assessed based on specific kinetics determined and selective poisoning studies will be made to determine characteristics of active sites remaining.

#### Task 12 Diffusion of Polyaromatic Compounds in Amorphous Catalyst Supports

If diffusion of a reactant species to the active sites of the catalyst is slow in comparison to the intrinsic rate of the surface reaction, then only sites near the exterior of the catalyst particles will be utilized effectively. A systematic study of the effect of molecular size on the sorptive diffusion kinetics relative to pore geometry will

be made using specific, large diameter aromatic molecules. Diffusion studies with narrow boiling range fractions of representative coal liquid will also be included. Experimental parameters for diffusion kinetic runs shall include aromatic diffusion model compounds, solvent effects, catalyst sorption properties, temperature and pressure.

### III. Hydrogenation of CO to Produce Fuels

#### Task 13 Catalyst Research and Development

Studies with iron catalysts will concentrate on promoters, the use of supports and the effects of carbiding and nitriding. Promising promoters fall into two classes: (1) nonreducible metal oxides, such as CaO, K<sub>2</sub>O, Al<sub>2</sub>O<sub>3</sub> and MgO, and (2) partially reducible metal oxides which can be classified as co-catalysts, such as oxides of Mn, Mo, Ce, La, V, Re and rare earths. Possible catalyst supports include zeolites, alumina, silica, magnesia and high area carbons. Methods of producing active supported iron catalysts for CO hydrogenation will be investigated, such as development of shape selective catalysts which can provide control of product distribution. In view of the importance of temperature, alternative reactor systems (to fixed bed) will be investigated to attain better temperature control. Conditions will be used which give predominately lower molecular weight liquids and gaseous products.

#### Task 14 Characterization of Catalysts and Mechanistic Studies

Catalysts which show large differences in selectivity in Task 13 will be characterized as to surface and bulk properties. Differences in properties may provide the key to understanding why one catalyst is superior to another and identify critical properties, essential in selective catalysts. Factors relating to the surface mechanism of CO hydrogenation will also be investigated. Experiments are proposed to determine which catalysts form "surface" (reactive) carbon and the ability of these catalysts to exchange C and O of isotopically labelled CO. Reactions of CO and H<sub>2</sub> at temperatures below that required for CO dissociation are of particular interest.

#### Task 15 Completion of Previously Funded Studies and Exploratory Investigations

This task is included to provide for the orderly completion of coal liquefaction research underway in the expiring University of Utah contract, EX-76-C-01-2006.

### III Highlights to Date

Task 10 Tests for HDS and hydrogenation activities of a number of catalysts carried out at both atmospheric and elevated pressure in the same reactor showed good correlation between low and high pressure results. This means that the atmospheric pressure tests adopted for ranking of activity of various catalysts should be the same under high pressure test conditions.

Task 11 Enhancement of HDS activity of thiophene at levels of 2,6-dimethylpyridine adsorbed on a commercial CoMo/Al<sub>2</sub>O<sub>3</sub> catalyst was confirmed in repeat experiments. This very unusual result (other N-compounds tested gave expected lowered HDS activity) indicates that adsorption on a site adjacent to the HDS site can activate the HDS site, provided that the HDS site is not itself blocked, e.g., by steric hindrance of the adsorbed molecule.

#### Papers and Presentations

"The Effects of Pyridine and Coke Poisoning on Benzothiophene Hydrodesulfurization over CoMo/Al<sub>2</sub>O<sub>3</sub> Catalyst," R. Ramachandran and F.E. Massoth, Chem. Eng. Commun., 18, 239 (1982).

"Mechanism of High-Pressure Hydrogenolysis of Hokkaido Coals (Japan), 3, Chemical Structure Changes in Coal Asphaltene During Hydrogenolysis," R. Yoshida, Y. Yoshida, D.M. Bodily and G. Takeya, Fuel Proc. Tech., 6, 225 (1982).

## Task 1

### Comparison of Catalysts for Coal Conversion at Softening Conditions

Faculty Advisor: L.L. Anderson  
Graduate Student: T.C. Miin

#### Introduction

Since the last report another thirty catalysts have been studied. The results accompanied by results reported in the last report are presented together and a detailed discussion follows. The conclusion still shows that only borderline cationic salts with nonhard anionic counterparts are better catalysts.

#### Project Status

The relationship between the softness property of catalysts and coal conversion was further investigated. The classification of acids and bases is shown in Reference 1.

Group IIB metal salts (the Periodic Table of the Elements) fit the above conclusion perfectly and is shown in Table I. The activity of zinc chloride is much greater than that of cadmium and mercury because zinc is borderline, and both cadmium and mercury cations are soft.

Of the different zinc halide catalysts, the fluoride ion has the least activity, because it is hard. The chloride ion and the bromide ion belong to the borderline category and the iodide ion belongs to the soft. The difference in activity of these catalysts is due to the difference in softness of the anion which influences the softness of the cation.

The fluoride anion is so hard that it hardens the cation, and all of the fluoride catalysts tested had very low activity. The other three halide anions in the zinc salts have moderate hardness properties and thus do not influence the cation very much. Therefore there is very little influence on the zinc, whose borderline property is mainly responsible for the high catalytic activity. Nevertheless, the small differences in softness of these halides still produces small differences in activity.

The sulfite anion belongs to the borderline category also, but it is comparatively harder than the chloride.<sup>3</sup> This makes sulfites less effective than chlorides. Nonetheless, sulfates are not as effective as a catalyst as are sulfites because the sulfate anion is hard. The same reasoning can be applied to phosphate and phosphide.

Cadmium halides have lower activity than zinc halides because the  $\text{Cd}^{++}$  is softer than the  $\text{Zn}^{++}$ . One of the most fascinating points of the application of the HSAB principle is seen by the effectiveness of the cadmium fluoride catalyst. The fluoride anions harden both zinc and cadmium cations, but it hardens zinc too much and makes  $\text{ZnF}_2$  less effective than  $\text{ZnCl}_2$ . Fluoride anions also harden cadmium cations and make the  $\text{Cd}^{++}$  in

CdF<sub>2</sub> harder (but not to the extent of borderline). Thus CdF<sub>2</sub> is a better catalyst than ZnF<sub>2</sub>.

As shown in Table II, Ge<sup>+4</sup>, Sn<sup>+2</sup>, Sn<sup>+4</sup> are very effective catalysts, while Pb<sup>+2</sup> is not. This is due to lead (II) being softer than Sn<sup>+2</sup>, Sn<sup>+4</sup> and Ge<sup>+4</sup>, although all of them belong to the borderline category. Tin(IV) is generally better than Sn (II), because of the slightly softer property of the former.

Stannic tetraiodide (SnI<sub>4</sub>) gives 99% conversion, and the softness of SnI<sub>4</sub> and its Lewis acidity are the best parameters for catalytic activity for coal conversion under mild conditions. To find a way to quantify the softness and Lewis acidity will probably provide the best technique for coal conversion under mild conditions. Obviously, optimum conversion conditions need to be reinvestigated. Also it can be predicted that lead (IV) will have better activity than the lead (II) compounds already studied.

Since Zn and Sn are potent catalysts, Ga, In and Bi are also expected to be good catalysts based on their position in the Periodic Table. Indium and Ga will be investigated later. However, Bi does give the expected results (see Table III). The activity of bismuth trihalides reaches a maximum for conversion for bromide. Other Bi compounds may be synthesized by a slight modification of the softness of the compounds by replacing the anions with some suitable inorganic or organic anions, thus providing better results.

Table IV shows the effect of some transition metal halides. Once again the activity trend can be explained by the softness of catalysts. It is interesting that both strong Lewis acids, Ce<sup>+3</sup> and Fe<sup>+3</sup>, are hard and have very low activity.

### Future Work

Forty more catalysts will be investigated to complete the test of the applicability of the HSAB principle in the fuels field. However, from the present data, weak Lewis acidity and borderline cationic species accompanied by nonhard anions are the most important two properties of good catalysts for coal conversion. To build the quantitative table of softness of catalysts in the fuels field, it is necessary for future work to be directed to obtain more general quantitative information. Such quantitative information has not been available since the beginning of the introduction of the HSAB principle.<sup>1</sup>

The properties of stannic iodide will be investigated in detail. Liquids produced by different catalytic reactions will be analyzed and compared. The reason for the activity of borderline catalysts will be explained. The results may lead to a better understanding of the catalysis of the conversion of coal and other solid fuels as well as an indication of the chemical structures participating in the catalytic conversion reactions.

### References

1. H. Tse-Lok, "Hard and Soft Acids and Bases Principle in Organic Chemistry," Academic Press, New York, New York, 1977.
2. R.D. Ernst, University of Utah, Department of Chemistry, personal communication, 1982.
3. T.C. Miin, personal analysis, 1982.

Table 1. Conversion of HV bituminous coal (Hiawatha, Utah) with treatment by H<sub>2</sub> at 2000 psi and 290°C for 3 hours. Yields in weight percent of THF extracted coal.<sup>a</sup> Catalysts are Group IIB.

Catalyst	Liquid	Gas	Total
ZnO	7.8	1.2	0.9
ZnF <sub>2</sub>	9.0	1.0	10.0
ZnCl <sub>2</sub>	70.0	8.0	78.0
ZnBr <sub>2</sub>	82.0	12.0	94.0
ZnI <sub>2</sub>	77.0	7.0	84.0
ZnSO <sub>3</sub>	27.0	2.0	29.0
ZnSO <sub>4</sub> ·H <sub>2</sub> O	12.5	2.0	14.5
ZnOAc	19.0	1.0	20.0
Zn <sub>3</sub> (PO <sub>4</sub> ) <sub>2</sub>	13.0	0.7	14.0
Zn <sub>3</sub> P <sub>2</sub>	17.0	0.5	18.0
CdF <sub>2</sub>	21.0	2.4	23.4
CdCl <sub>2</sub> ·2.5H <sub>2</sub> O <sup>b</sup>	8.0	1.0	9.0
CdBr <sub>2</sub>	24.0	0.9	25.0
CdI <sub>2</sub>	12.4	2.7	15.1
HgCl <sub>2</sub>	18.0	1.0	19.0

<sup>a</sup>Raw coal was pre-extracted as completely as possible with THF in soxhlet extractor before catalytic treatment.

<sup>b</sup>Needs repeat.

Table II. Catalysts: Group IVA (Ge, Sn, Pb)

Catalyst	Liquid	Gas	Total
GeCl <sub>4</sub>	81.0	4.3	85.3
SnO	5.0	3.0	8.0
SnF <sub>2</sub>	10.0	3.0	13.0
SnF <sub>4</sub>	27.0	12.0	39.0
SnCl <sub>2</sub> ·2H <sub>2</sub> O	77.0	9.0	86.0
SnCl <sub>4</sub>	71.0	1.5	73.0
SnCl <sub>4</sub> ·5H <sub>2</sub> O	90.0	2.0	92.0
SnBr <sub>2</sub>	80.0	13.0	93.0
SnBr <sub>4</sub> <sup>a</sup>	75.0	4.4	79.4
SnI <sub>2</sub>	80.0	13.0	93.0
SnI <sub>4</sub>	95.2	3.7	99.0
PbF <sub>2</sub>	13.4	2.3	16.0
PbCl <sub>2</sub>	15.0	1.3	16.3
PbBr <sub>2</sub>	42.2	2.0	44.2
PbI <sub>2</sub>	34.1	2.5	37.0

<sup>a</sup>Needs repeat.

Table III. Group VA<sup>n+</sup>  
(As, Sb, Bi)

Catalyst	Liquid	Gas	Total
SbCl <sub>3</sub>	20.0	2.0	22.0
BiF <sub>3</sub>	12.5	3.2	16.0
BiCl <sub>3</sub>	51.4	4.3	56.0
BiBr <sub>3</sub>	60.8	8.0	69.0
BiI <sub>3</sub>	29.7	8.9	39.0

Table IV. Transition Metals

Catalyst	Liquid	Gas	Total
CrCl <sub>3</sub> ·6H <sub>2</sub> O	34.2	1.5	36.0
FeF <sub>2</sub>	11.0	1.5	13.0
FeCl <sub>2</sub> ·4H <sub>2</sub> O	21.0	2.5	24.0
FeCl <sub>3</sub>	3.5	1.5	5.0
FeBr <sub>2</sub>	41.5	1.5	43.0
FeI <sub>2</sub>	37.4	3.3	41.0
FeS	10.0	1.4	11.4
CoCl <sub>2</sub> ·6H <sub>2</sub> O	18.0	0.6	19.0
CoS	17.6	0.9	18.5
RhCl <sub>3</sub> ·H <sub>2</sub> O	14.0	13.0	27.0
NiCl <sub>2</sub> ·6H <sub>2</sub> O	18.4	2.5	21.0
NiS	9.0	1.0	10.0
CuCl <sub>2</sub> ·2H <sub>2</sub> O	10.0	3.0	13.0
Cu <sub>2</sub> Cl <sub>2</sub>	13.0	2.0	15.0
CeCl <sub>3</sub> ·7H <sub>2</sub> O	4.0	1.0	5.0

## Task 2

### Carbon-13 NMR Investigation of CDL and Coal

Faculty Advisor: R.J. Pugmire  
Postdoctor Associate: D.K. Dalling

#### Introduction

The solid NMR work on this project suffers from the loss of one postdoctoral (K.W. Zilm) who left the University last spring. A commitment has been made to a Ph.D. student in the Department of Chemistry who will join the project in about two months after he finishes his thesis. In the meantime, Dr. Warner Woolfenden will join the project for a portion of his time.

#### Project Status

Dr. Woolfenden will begin a detailed NMR analysis of a set of 24 samples obtained from Dr. Richard Neavle at Exxon. These samples were selected from the Exxon Coal Data Bank. We will carry out routine CP/MAS analyses and dipolar dephasing studies on these coals in an effort to correlate structure with conversion behavior as determined in the EDS process.

During the past quarter we submitted the manuscript, "Application of New Carbon-13 NMR Techniques to the Study of Products from Catalytic Hydrodeoxygenation of SRC-II Liquids," based on Dr. Haider's thesis. The manuscript has been accepted for publication in Fuel after minor changes. A copy of the preprint, as submitted, is attached.

During the period 15-29 October I visited the Institute for Carbochemistry at Tychy-Wyry, Poland as a consultant for the United Nations Industrial Development Organization (UNIDO). UNIDO is cooperating with the Polish government on a coal conversion process. I was invited as an "Expert on Mission" to advise the Institute on the use of NMR in their coal conversion studies. While in Poland I gave three lectures on NMR. The scientists and engineers were particularly interested in the work described in the attached paper.

**Application of New Carbon-13 NMR Techniques to the Study of Products  
From Catalytic Hydrodeoxygenation of SRC-II Liquids**

**Don K. Dalling**

**University of Utah Research Institute**

**420 Chipeta Way**

**Salt Lake City, Utah 84108**

**Ghulam Haider, Ronald J. Pugmire and Joseph Shabtai**

**Department of Fuels Engineering**

**University of Utah**

**Salt Lake City, Utah 84112**

**and**

**William E. Hull**

**Bruker Scientific Instruments**

**Karlsruhe, Germany**

## ABSTRACT

A middle-heavy SRC-II distillate (b.p. 230-455° C), containing 3.03 wt% of oxygen, has been studied by means of carbon-13 nuclear magnetic resonance at 75 and 125 MHz. The magnetization refocussing techniques INEPT and J-resolved two-dimensional Fourier transform have been utilized to demonstrate methods by which resonance line multiplicities may be determined in complex liquid mixtures. Products derived from the above coal liquid by hydrodeoxygenation at temperatures from 200-370° C, using sulfided Co-Mo and Ni-W catalysts, were also examined. The fraction aromatic carbon in the hydrotreated liquids was found to correlate directly with their C/H atomic ratio and inversely with the weight percent of contained hydrogen. Comparison of O/C atomic ratios with  $f_a$  values for these liquids indicates that hydrogen uptake below 260° C is associated primarily with hydrogenolytic oxygen removal without attendant ring hydrogenation, while at temperatures between 260-350° C hydrodeoxygenation is accompanied by ring hydrogenation and dealkylation reactions.

(Keywords: SRC-II middle-heavy distillate, J-resolved 2-D spectroscopy, hydrodeoxygenation, hydrotreating)

## INTRODUCTION

Carbon-13 nuclear magnetic resonance (NMR) has seen increasing use as a tool for analysis of coal-derived liquids. NMR studies have provided information relative to the gross nature of coal derived liquids (CDL's) such as fraction of aromatic carbon and average length of aliphatic chains.<sup>1-12</sup> In recent work <sup>13</sup>C NMR has been utilized in the examination of coal tar anthracene oil<sup>13</sup> and in the analysis of neutral, acidic, and basic heteroatom containing components produced by coal hydrogenation.<sup>14</sup> Methods for best determining the aromatic bridgehead carbon content of coal-derived products have been explored.<sup>15</sup> However, due to the complex nature of spectra obtained from CDL's, a more comprehensive analysis has proven difficult without carrying out fractionation and/or separation steps in order to provide simpler starting materials. In the present work we explore the possibility of applying some novel pulsing techniques, termed INEPT and J-resolved two-dimensional FT NMR, to a complex SRC-II distillate, in order to elucidate more fully the nature and quantity of the structural species present. Structural changes described in catalytically hydrotreated liquids obtained from the original feedstock are also discussed

## EXPERIMENTAL

All of the INEPT and J-resolved 2D Fourier transform NMR spectra (hereafter referred to as J-resolved 2D spectra) were acquired on a Bruker WM-500 superconducting spectrometer, operating at 125 MHz for carbon-13, resident in Karlsruhe, Germany. Other spectra were acquired on the University of Utah Varian SC-300 superconducting spectrometer with a <sup>13</sup>C resonance frequency at 75 MHz.

The original feedstock was a middle-heavy SRC-II distillate, boiling between 230-455° C, and containing 3.03 wt% of oxygen. The catalysts used in the study of hydrogenation-hydrodeoxygenation reactions of

the liquids were sulfided Co-Mo and Ni-W, supported on alumina. Reactions were performed in a semi-batch autoclave reactor at 1750 psig hydrogen pressure. The reaction time in each case was one hour, and the products were monitored as a function of reaction temperature (200-370°). Details are reported elsewhere.<sup>16</sup>

## RESULTS

The <sup>13</sup>C NMR spectrum at 125 MHz of the SRC-II derived distillate is presented in Figure 1. It may be noted that a wealth of detail is evident there, but we will mention only a few points of interest. In the aliphatic region the presence of straight chain alkanes or alkyl groups is signaled by the usual lines at 14, 23, 32, 29, and 29.5 ppm for the α-, β-, γ-, δ-, and ε-, etc. carbons, respectively. The resonance line due to the interior carbons (ε-, etc., 29.5 ppm) has been clipped in order to allow a larger vertical scale to be used. The full intensity of that line indicates an average n-alkyl chain length of 10-12 carbons. The chemical shifts of methyls in branched alkyls are clustered in the range from 10-15 ppm. In addition to straight chain and branched C-2 carbons the area from 18 to 25 ppm is characteristic of methyls attached to aromatic (20-22 ppm) or hydroaromatic rings. The chemical shifts from 15 to 16.5 ppm may be attributed to the methyl portion of ethyl aromatics; unfortunately the CH<sub>2</sub> of such ethyl groups is found among the δ and ε carbon lines near 29 ppm. From 32 to about 45 ppm are found the resonances of interior carbons which are at, or immediately adjacent to, a branching point. Branched centers near the end of a chain generally occur in the region around 28-30 ppm.

In the region of the spectrum characteristic of aromatic carbons, signals in the range of 150-160 ppm indicate the presence of aryl ethers

and phenols or anilines. Non-substituted benzenoid carbons ortho or para to oxygen or nitrogen substituents tend to produce resonance lines from 114 to 122 ppm. These are also evident in the spectrum. Resonances above 114 ppm in the aromatic region are usually due to carbons which are part of five-membered aromatic heterocycles such as the C-2 position in benzofuran. However, carbons in 1-alkenes are also found in this spectral region.

The tentative assignments given above are made on the basis of chemical shifts observed in model compounds. In the past it has been extremely difficult to verify directly the multiplicities of given signals because of the overwhelming complexity of the coupled spectra. However, the development of multiplicity-dependent, magnetization refocussing techniques makes it possible to determine the coupled nature of carbon resonance signals by indirect means.

The first of these novel techniques to be illustrated here has been given the acronym INEPT.<sup>17</sup> The requisite pulse sequence is given in Figure 2. Some results for the SRC-II distillate of Figure 1 are presented in Figures 3 and 4. In Figure 3 delay intervals have been set so that resonance signals from methyls and methynes are positive, while those from methylenes are negative. There are areas of cancellation where positive and negative signals overlap, but many of the tentative assignments made above can be verified. It is clear that the bulk of the 22-38 ppm range are due to CH<sub>2</sub> groups. In Figure 4, signals due to CH carbons are enhanced while others are (approximately) nulled. Many of the methynes, which are identified with some difficulty in Figure 3 because of the presence of much more intense CH<sub>2</sub> and CH<sub>3</sub> resonances, may be easily recognized here.

A second method for determining resonance line multiplicities is J-resolved two-dimensional NMR.<sup>18</sup> The pulse sequence is given in Figure 5.

The experiment is performed numerous times with varying delay sequences. The resulting array of data is then Fourier transformed along both time axes, producing results which may be plotted like those given in Figures 6-8 for the same SRC-II distillate of Figure 1. The lower portion of these figures is an expansion of the traditional spectrum as given in Figure 1. The upper portion of the figures can be viewed as a topographical map produced by a direct overhead view. In principle, the multiplicity of every line may be determined. The densely plotted lines result from rapidly changing contours, corresponding to the peaks of the multiplets associated with the signals directly below them on the lower trace. Hence, the resonances in Figure 6 near 21 ppm are associated with quartets (the outside lines are aliased), indicating methyl carbons, while those near 23 ppm, being triplets, result from CH<sub>2</sub>'s. There is a prominent doublet near 23.8 ppm, which must be associated with a CH carbon.

In Figure 7, one views a portion of the aromatic region of the spectrum. Most of the lines in the region displayed are associated with doublets corresponding to protonated aromatic carbons. However, the lines near 130.0 and 130.3 ppm appear to be accidentally degenerate, having both singlet and doublet components at the same resonance position. Evidence of fine multiplet structure also appear in a number of lines (e.g., 129.7) indicating the long range coupling due to CH<sub>3</sub> groups. Figure 8 was extracted from the area of unprotonated aromatic carbons which produce singlets. The point of interest here is the observation that these peaks also exhibit small multiplets resulting from long range coupling to protons attached to other carbons. For example, the lines at 139.0 and 139.1 ppm show small quartets indicating that these carbons are probably bonded to methyl groups. Such observations obviously provide valuable additional information relative to the environment of these carbons.

The SRC-II derived liquid described above was subjected to hydrodeoxygenative treatment using sulfided Co-Mo and Ni-W catalysts. In Figure 9 the aliphatic portion of the  $^{13}\text{C}$  spectrum of the feedstock liquid is compared to that which is obtained after hydrodeoxygenation with Co-Mo catalyst at  $350^\circ$ . After the hydrotreatment there is a noticeable increase in the intensity and/or number of resonance lines in the spectrum near 12, 23.5, 27, and 35 ppm regions of the spectrum. These results are consistent with formation of additional hydroaromatic rings by hydrogenation of aromatic rings as well as with increased alkyl branching (methyls at 12 ppm), probably as a result of ring dealkylation followed by skeletal isomerization of derived alkyl groups. In Figure 10 a similar comparison is made for the aromatic spectral regions. In the hydrotreated sample, many of the resonance lines in the areas of 150-160 ppm and 110-120 ppm are now absent, while additional resonances are noted in the region from 125 to 130 ppm. These observations are consistent with the anticipated removal of aryl heteroatoms as a result of the hydrotreatment. Similar results may be noted in the spectrum after hydrodeoxygenation with sulfided Ni-W catalyst.

The fraction aromatic carbon ( $f_a$ ) of the hydrotreated products was determined by use of  $^{13}\text{C}$  NMR for each reaction temperature. The resulting values are plotted in Figures 11 and 12 for Co-Mo and Ni-W catalysts, respectively. For both catalysts the aromaticity is seen to decrease above  $260^\circ\text{C}$  with increasing reaction temperature to a minimum in the range of  $320\text{-}350^\circ\text{C}$ . At that point the  $f_a$  again begins to increase. This upturn is believed to result from a shift in the hydrogenation-dehydrogenation equilibria toward dehydrogenation, as well as to hydrodealkylation of hydrogen-rich alkyl groups (as reflected in some  $\text{C}_1\text{-C}_4$  gas formation under these conditions).<sup>16,19</sup>

A careful comparison of Figures 11 and 12 also reveals an interesting fact regarding the rate of ring hydrogenation. While both catalysts cause no apparent ring hydrogenation at temperatures  $< 260^{\circ}$  C, the rate of change in aromaticity associated with use of the Ni-W catalyst is significantly greater than that of the Co-Mo system: i.e.,  $f_a = 0.49$  vs.  $0.57$  at  $290^{\circ}$  C for the Ni-W and Co-Mo, respectively. Furthermore, it is noted that the minimum value of  $f_a$  is lower for the Ni-W catalyst (ca.  $0.38$ ) than for the Co-Mo catalyst (ca.  $0.45$ ). Hence a difference in depth of hydrogenation with these two catalyst systems is apparent. Mechanistic details for these observations will be discussed elsewhere.<sup>19</sup> Also in Figures 11 and 12 the C/H atomic ratios of the hydrotreated products are plotted as a function of temperature. One may note that there is general agreement in the shape of the curve for the two catalysts. The C/H curves are also found to compare qualitatively with the  $f_a$  curves. In Figures 13 and 14 the carbon aromaticity of the hydrotreated products is contrasted with the weight percent hydrogen of the same. In this case an inverse correlation is observed between the two curves. In both cases, the hydrogen content increases through a maximum and then decreases. At low temperatures ( $260^{\circ}$  C and below) the  $f_a$  value practically does not change while the hydrogen content slightly increases. On the other hand, the heteroatom content decreases monotonically with temperature. The O/C ratio is compared to  $f_a$  values in Figures 15 and 16 for the two catalysts. It is seen that the oxygen content decreases with increase in hydrotreatment temperature. Further, the data indicate that the initial decrease in oxygen is accompanied by some increase in hydrogen content but that, initially, the  $f_a$  does not vary. Only at temperatures above  $260^{\circ}$  does one observe a change in aromaticity.

Hence, the data suggest that initial hydrogen uptake (below 260° C) is associated primarily with oxygen removal without attendant ring hydrogenation, e.g., sterically unhindered hydrogenolytic removal of phenolic and arylalkyl etheric groups.<sup>16,19</sup> At temperatures between 260° and 350° C, on the other hand, hydrodeoxygenation is accompanied by ring hydrogenation and dealkylation. Above 320° C oxygen removal still occurs but dehydrogenation reactions also become important. The details of possible reactions and reaction mechanisms are beyond the scope of the present communications and will be described elsewhere.<sup>19</sup>

### CONCLUSIONS

The <sup>13</sup>C NMR data obtained on an SRC-II liquid has demonstrated the wealth of chemical information that can be obtained. Using modern high field spectrometers, adequate resolution is obtained to qualitatively characterize major structural changes occurring in catalytic upgrading of coal liquids. Employing multiple pulse decoupling and J-resolved 2-D techniques, structural detail is observed that represents major improvement in the analytical characterization of the complex mixtures present in syn-fuel samples. Furthermore, the data obtained on products derived from the feedstock when subjected to different catalytic hydrotreatment conditions provides a means for following overall processes as well as competing processes associated with heteroatom removal, hydrogenation, and dehydrogenation reactions.

## ACKNOWLEDGMENT

Support for this work was provided by the Department of Energy, Office of Fossil Energy under Contract Number AC0176ET 10527.

## REFERENCES

1. (a) Retcofsky, H. L. and Friedel, R. A., in Spectrometry of Fuels, (Ed. R. A. Friedel), Plenum Press, New York, 1970, Ch. 8;  
(b) Ibid, Fuel 1968, 47, 487;  
(c) Ibid, Chem. Ind. 1966, 455;  
(d) Ibid, Fuel, 1976, 55, 303;  
(e) Ibid, in "Coal Science" (Ed. R. F. Gould), Advan. Chem. Ser. No. 55, 1966, p. 503, Amer. Chem. Soc., Washington, D. C.
2. (a) Wooton, D. L., Dorn, H. C., Taylor, L. T., and Coleman, W. M., Fuel 1976, 55, 224;  
(b) Ibid, Fuel 1978, 57, 17.
3. Pugmire, R. J., Grant, D. M., Zilm, K. W., Anderson, L. L., Oblad, A. G., and Wood, R. E., Fuel 1977, 56 295.
4. Zilm, K. W., Pugmire, R. J., Grant, D. M., Wood, R. E., and Wiser, W. H., Fuel, 1979, 58, 11.
5. (a) Bartle, K. E. and Jones, D. W., Analytical Methods for Coal and Coal Products (C. Karr, Jr., Ed.) Academic Press, New York, 1978, Vol. II, Chap. 23;  
(b) Retcofsky, H. L. and Link, T. A., Ibid, Chap. 24.
6. Retcofsky, H. L., Appl. Spectroscopy, 1977, 31, 116.
7. Maekawa, Y., Yoshida, T., Yoshida, Y. and Imanari, I., Nenryo Kyokai-shi 1977, 56, 351.
8. Cantor, D. M., Anal. Chem. 1978, 50, 1185.
9. Seshadri, K. S., Ruberto, R. G., Jewell, D. M., and Malone, H. P., Fuel 1978 57, 549.
10. Ladner, W. R. and Snape, C. E., Fuel 1978, 57, 658.
11. Yokoyama, S., Bodily, D. M., and Wiser, W. H., Fuel 1979, 58, 162.
12. Joseph, J. T. and Wong, J. L. Fuel 1980, 59, 777.
13. Stadelhofer, J. W. and Gerhards, R., Fuel 1981, 60, 367.
14. Yoyoyama, S., Uchino, H., Kato, T., Sananda, Y. and Yoshida, T., Fuel 1981, 60, 254.
15. Mashima, K., Nakayama, I., Kiya, K., and Wainai, T., Fuel 1982, 61, 193.
16. (a) Haider, G., Ph.D. thesis, University of Utah 1981;  
(b) Shabtai, J. and Haider, G., Proc. Internat. Confer. Coal Science, Dusseldorf, Germany 1981.

17. Doddrell, D. M. and Pegg, D. T., J. Am. Chem. Soc., 1980 102, 6388.
18. Freeman, R., Morris, G. A., and Turner, D. L., J. Mag. Res. 1977, 26, 373.
19. Shabtai, J., and Haider, G., manuscript in preparation.

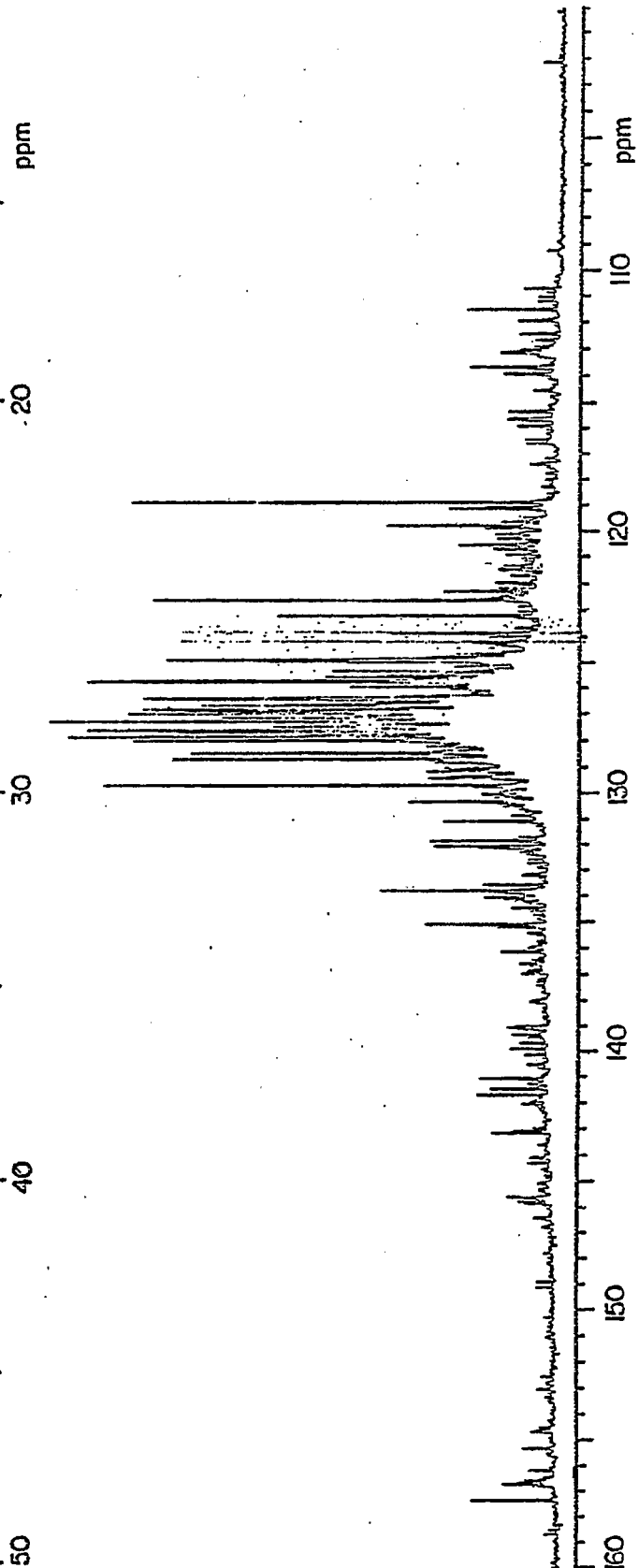
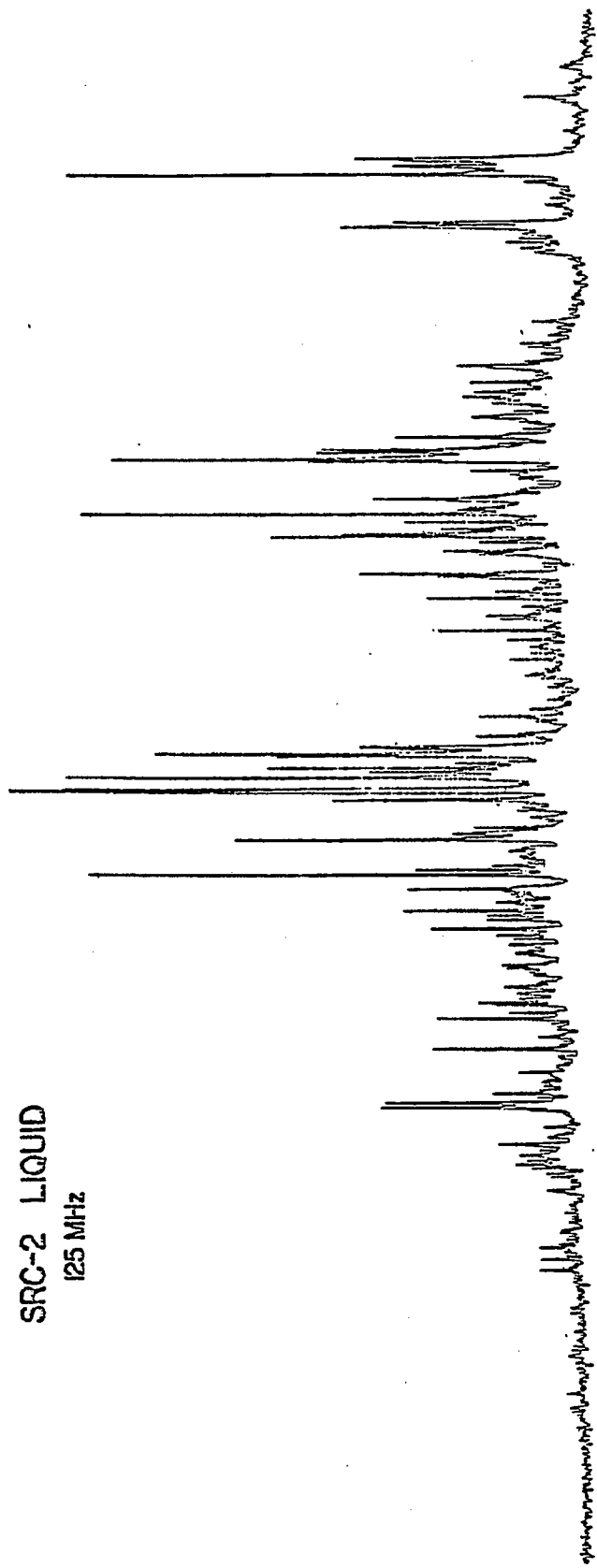
## FIGURE CAPTIONS

- Figure 1. The  $^{13}\text{C}$  NMR spectrum at 125 MHz of a distillate obtained from a coal derived liquid produced by the SRC-II process.
- Figure 2. The proton and carbon-13 pulsing sequence utilized to produce INEPT spectra.
- Figure 3. The aliphatic region of the spectrum shown in figure 1, acquired using an INEPT pulse sequence. Resonance lines due to  $\text{CH}_2$ 's are inverted compared to those due to  $\text{CH}_3$ 's and  $\text{CH}$ 's.
- Figure 4. The same spectrum as given in Figure 3 except in this case the resonance lines due to  $\text{CH}$ 's are preserved, while those due to  $\text{CH}_2$ 's and  $\text{CH}_3$ 's are (mostly) nulled.
- Figure 5. The proton and carbon-13 pulse sequence necessary to produce J-resolved two-dimensional FT NMR spectra.
- Figure 6. The lower trace is an expansion of a portion of the spectrum given in Figure 1. The upper plot is a presentation of the J-resolved 2-D spectrum of the same region as if viewed from directly overhead. Note the presence of quartets (aliased), triplets, and doublets.
- Figure 7. The same as figure 6 except in the aromatic region. Most of the resonances are associated with doublets due to aromatic  $\text{CH}$  carbons, but near 130.0 and 130.3 ppm singlets and doublets appear superimposed.
- Figure 8. The same as Figure 7 except further into the aromatic region. These lines are all due to unprotonated carbons, but the resonances exhibit fine structure as a result of coupling to hydrogens on adjacent carbons.
- Figure 9. A comparison of the aliphatic region of the SRC-II distillate of Figure 1 with that resulting after hydrodeoxygenation of the same using sulfided Co-Mo catalyst at 350°C.
- Figure 10. The aromatic region of the same spectra given in Figure 9.
- Figure 11. A comparison of the temperature dependence of the percent aromatic carbon (open circles) and C/H atomic ratio (filled circles) of products produced by hydrodeoxygenation of the SRC-II distillate of figure 1 using sulfided Co-Mo catalyst. The lines connecting the points are cubic splines and have no theoretical significance. Feedstock values were 82.0% for  $f_a$  and 0.87 for C/H.

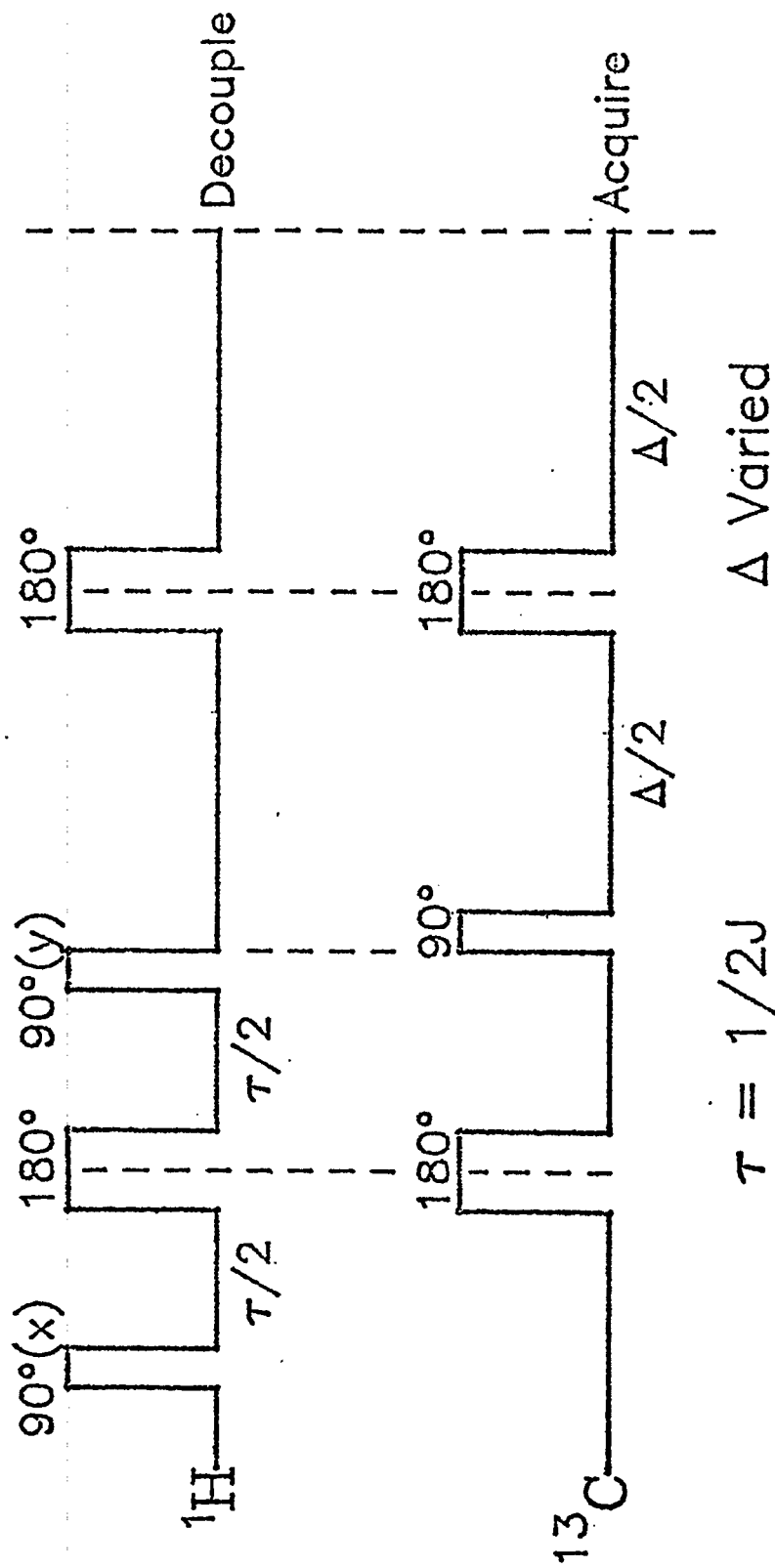
- Figure 12. The same as Figure 11 except using sulfided Ni-W catalyst.
- Figure 13. A comparison of percent aromatic carbon (open circles) with hydrogen content by weight (filled circles) for catalytically upgraded SRC-II liquid using Co-Mo. The hydrogen content of the feedstock was 8.23%.
- Figure 14. Similar to Figure 13, but using Ni-W catalyst.
- Figure 15. A comparison of the O/C ratio to carbon aromaticity for the products resulting from hydrotreatment of a SRC-II liquid in the presence of Co-Mo catalyst. The O/C ratio in the untreated liquid was 3.52%. The line through the points was derived by least-squares, linear regression ( $R=0.98$ ).
- Figure 16. The same as Figure 15, but with Ni-Was catalyst. For this case linear regression gave  $R=0.95$ .

SRC-2 LIQUID

125 MHz



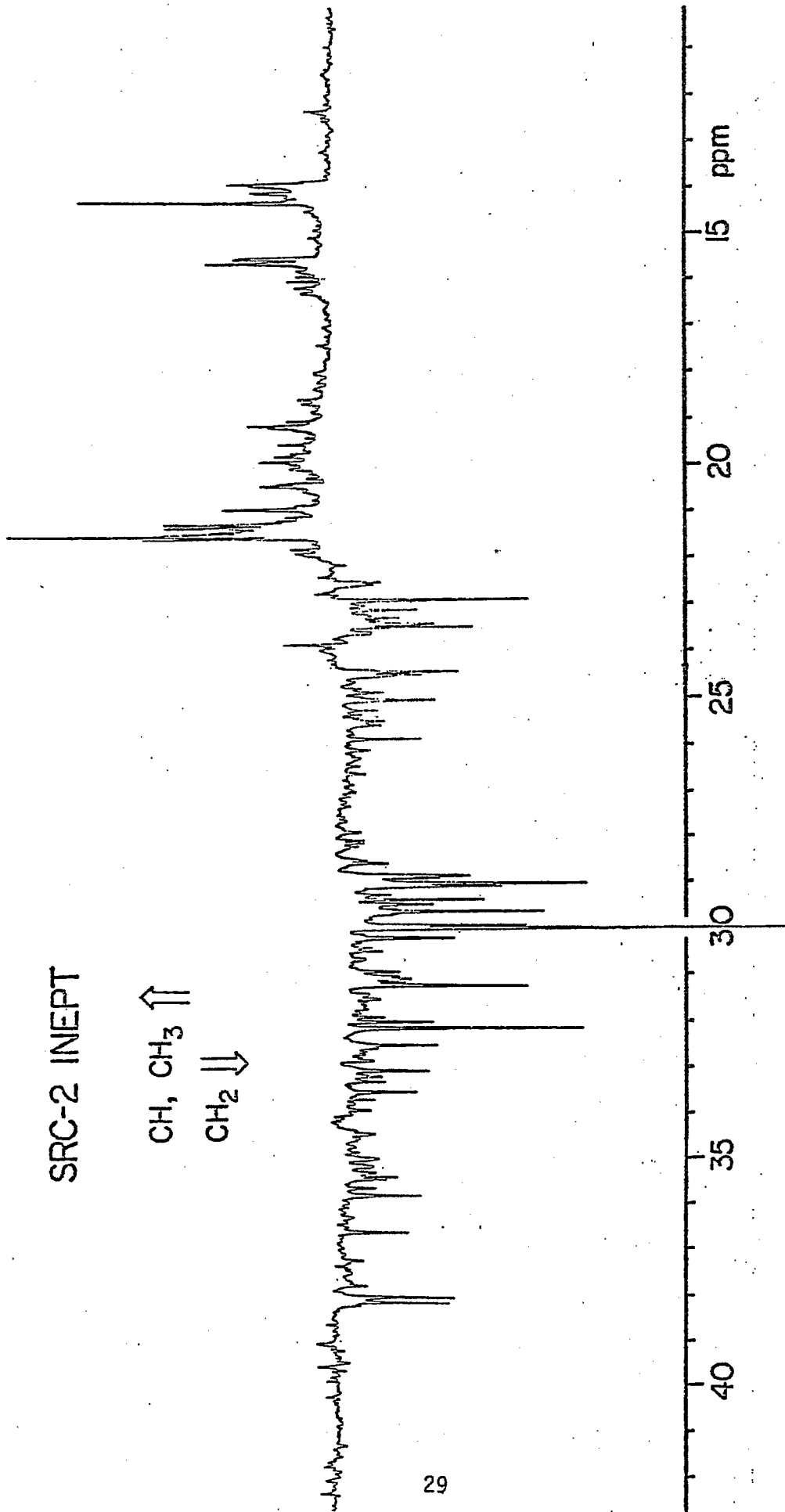
# INEPT



SRC-2 INEPT

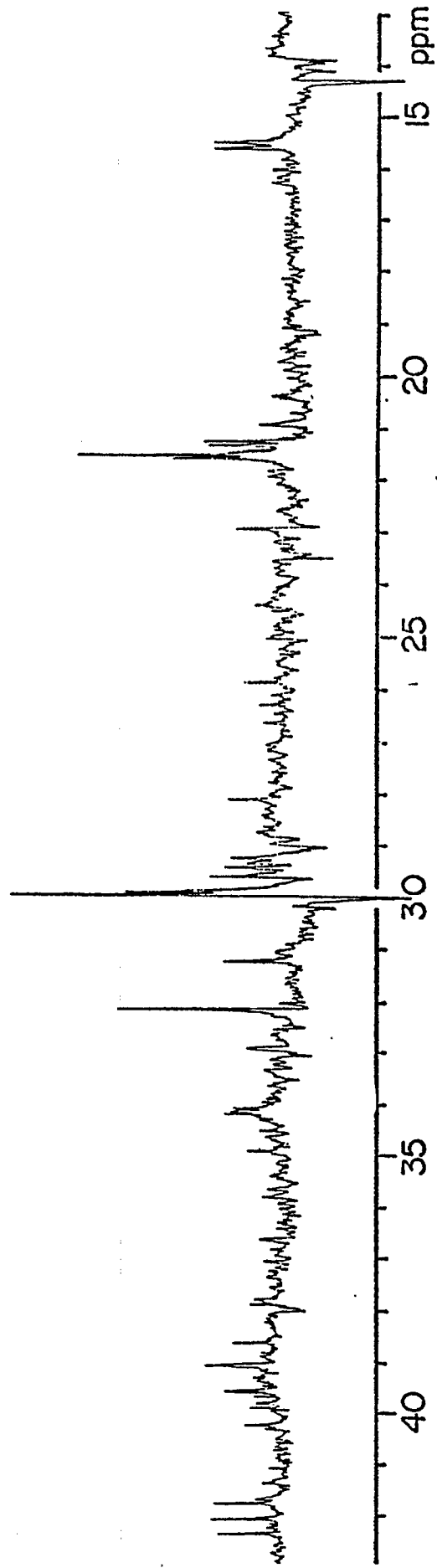
CH, CH<sub>3</sub> ↑

CH<sub>2</sub> ↓

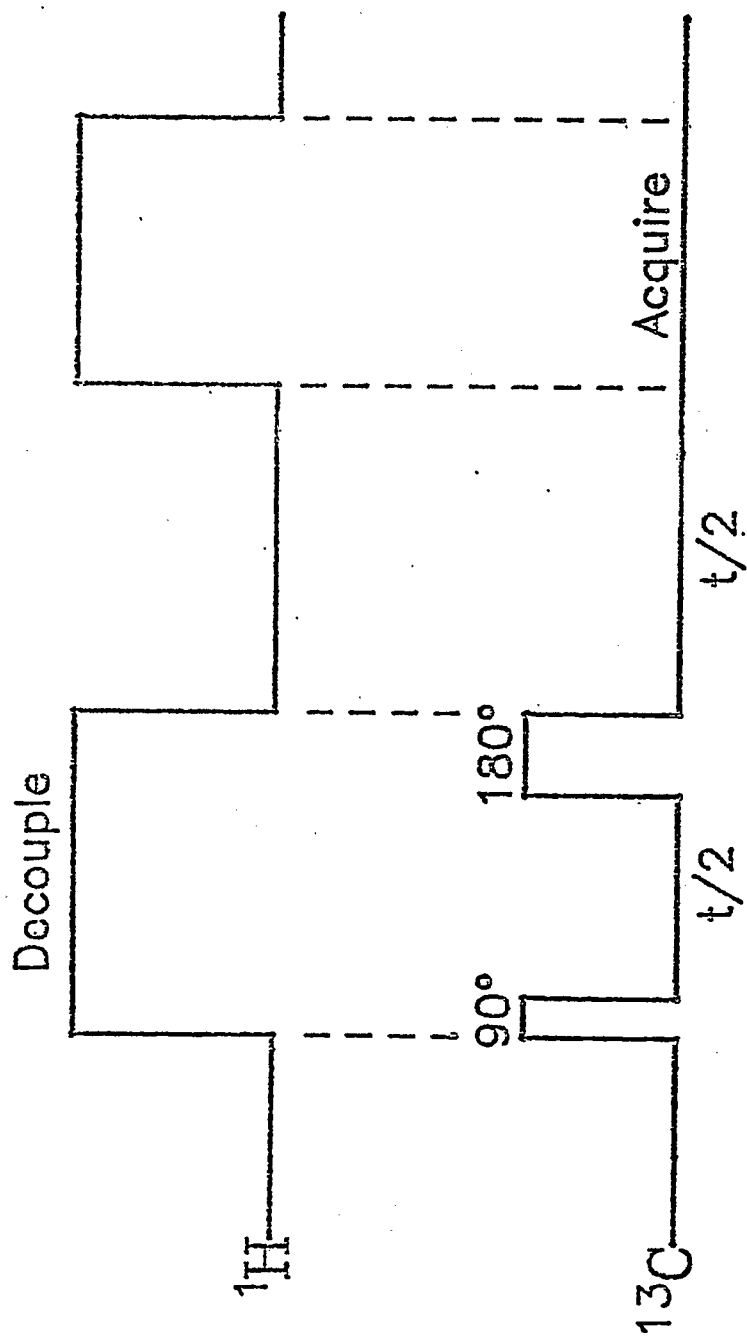


SRC-2 INEPT

CH only

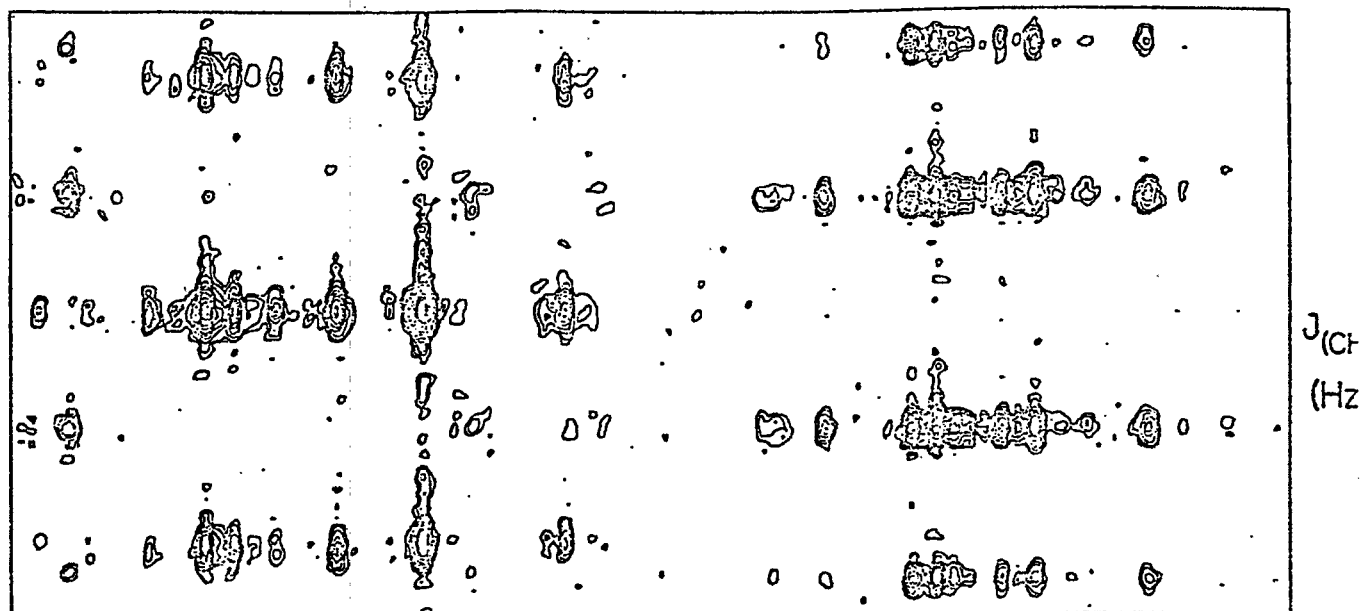


# J-Resolved 2-D

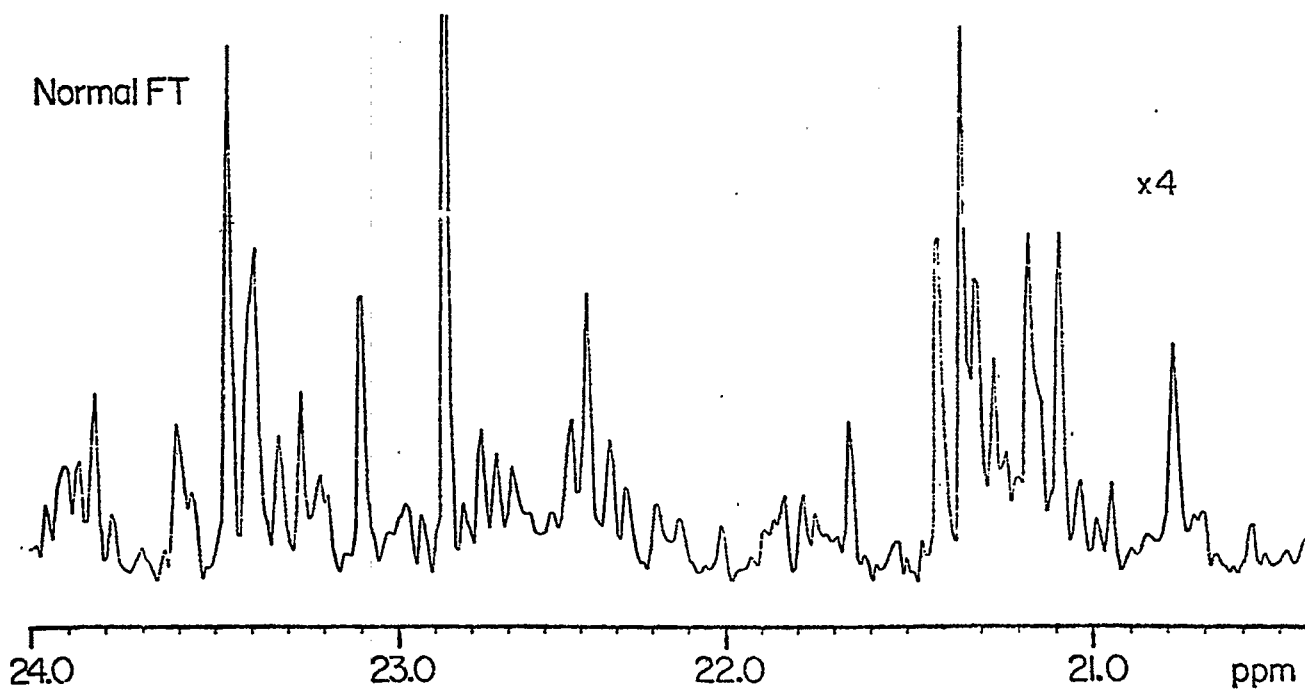


2D FT  
J Resolved

SRC-2 LIQUID

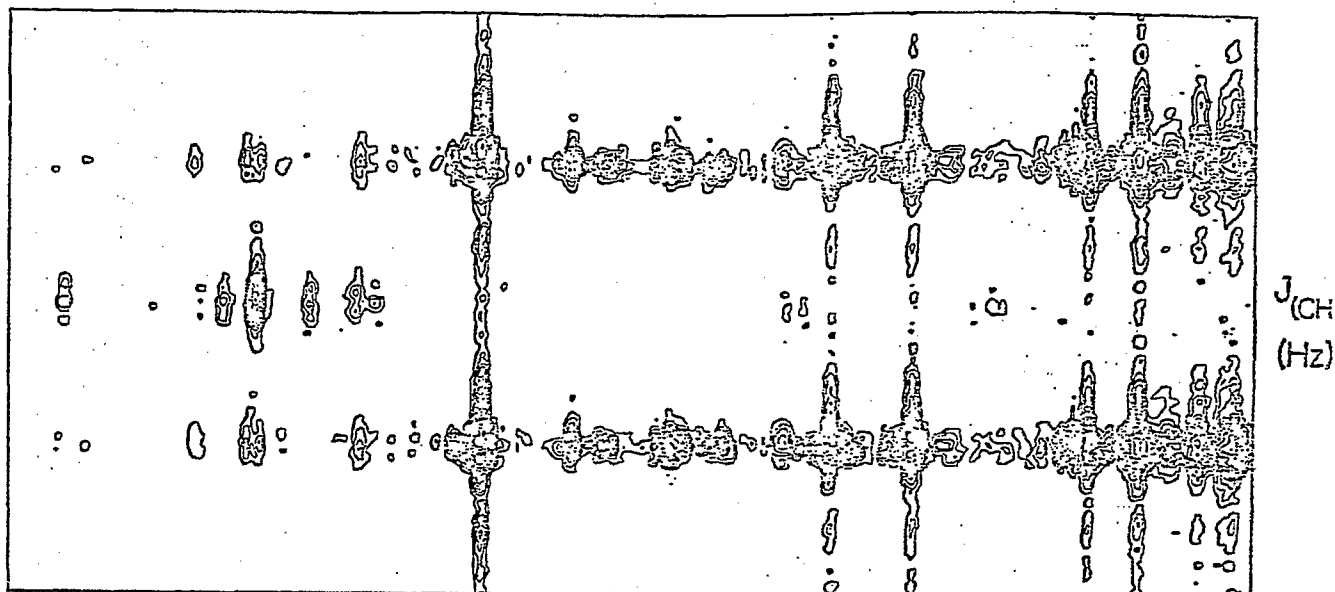


Normal FT



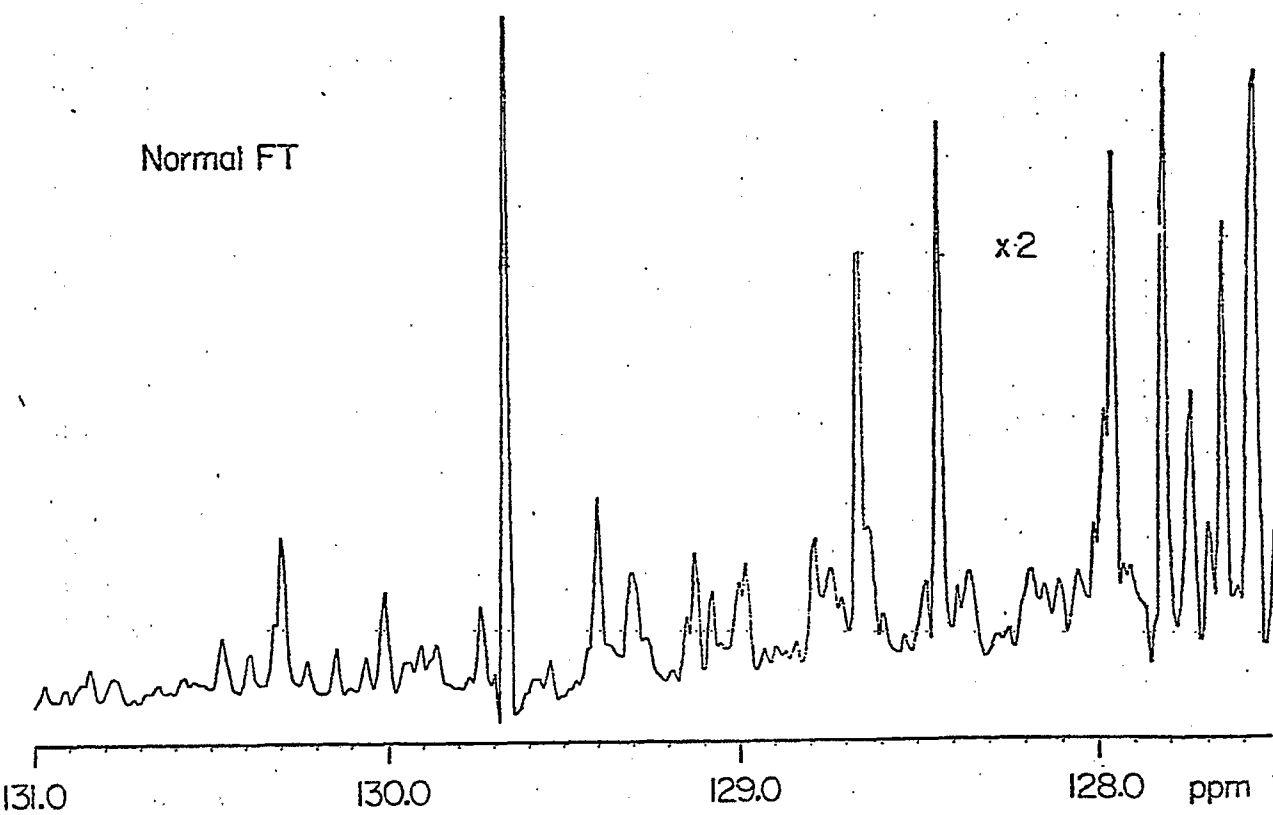
2D FT  
J Resolved

SRC-2 LIQUID



Normal FT

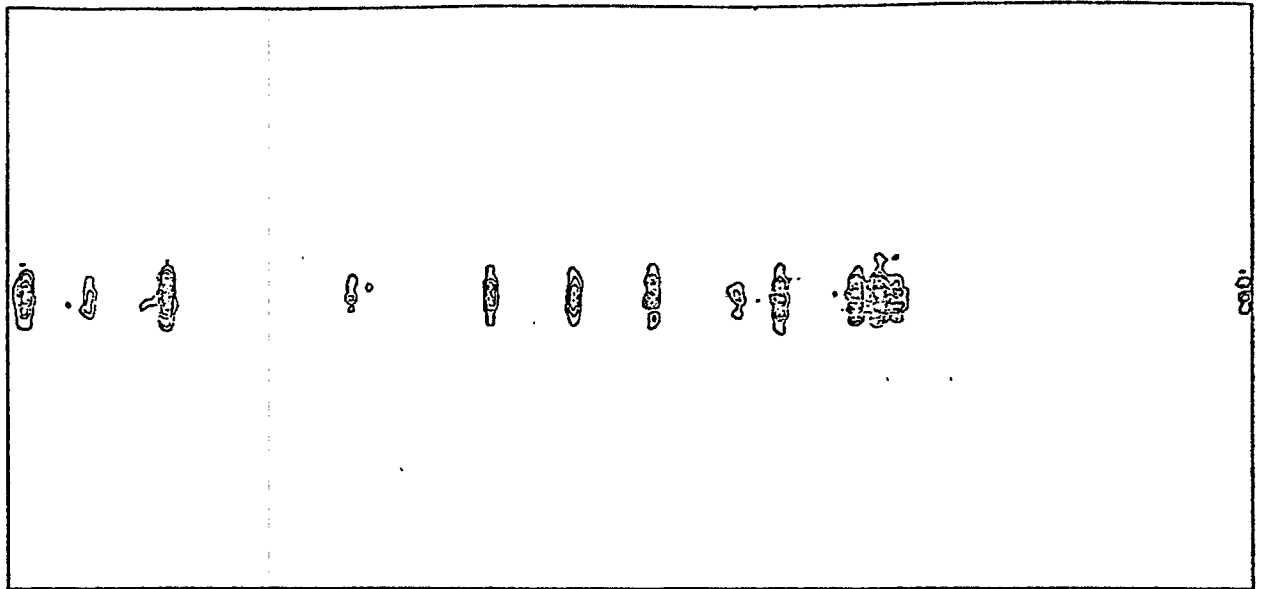
x2



Dubing et al  
Fig. 7

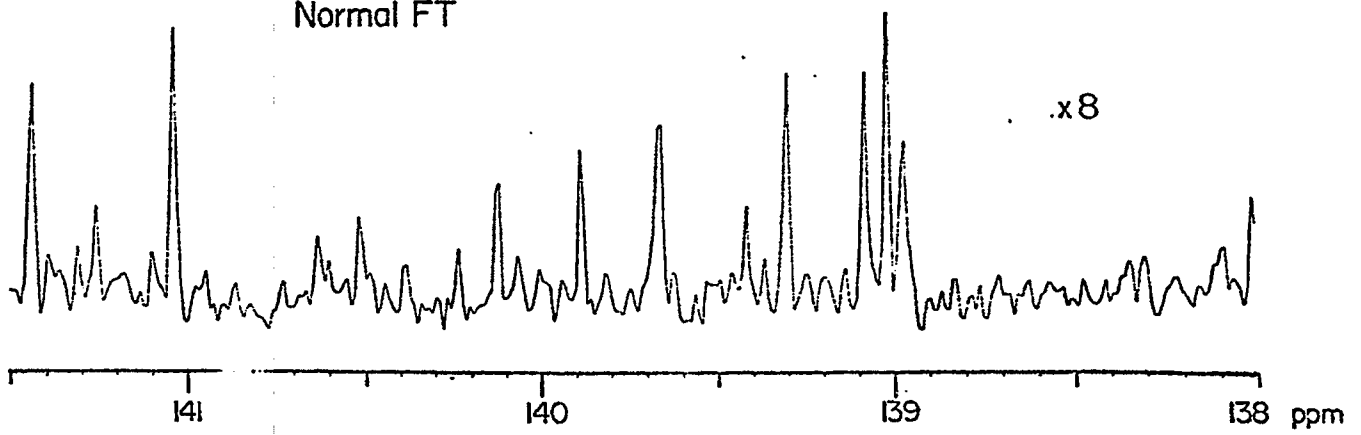
SRC-2 LIQUID

2D FT  
J Resolved

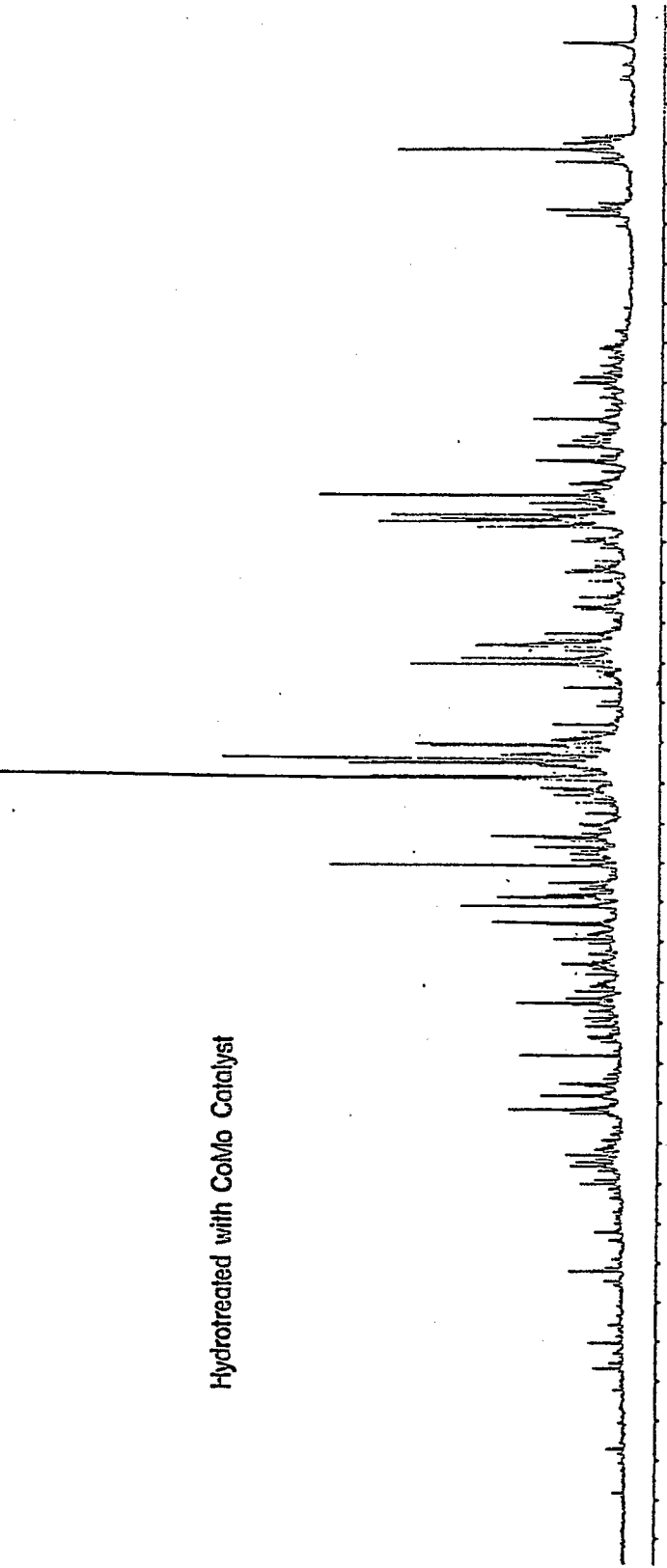


J (CH)  
(Hz)

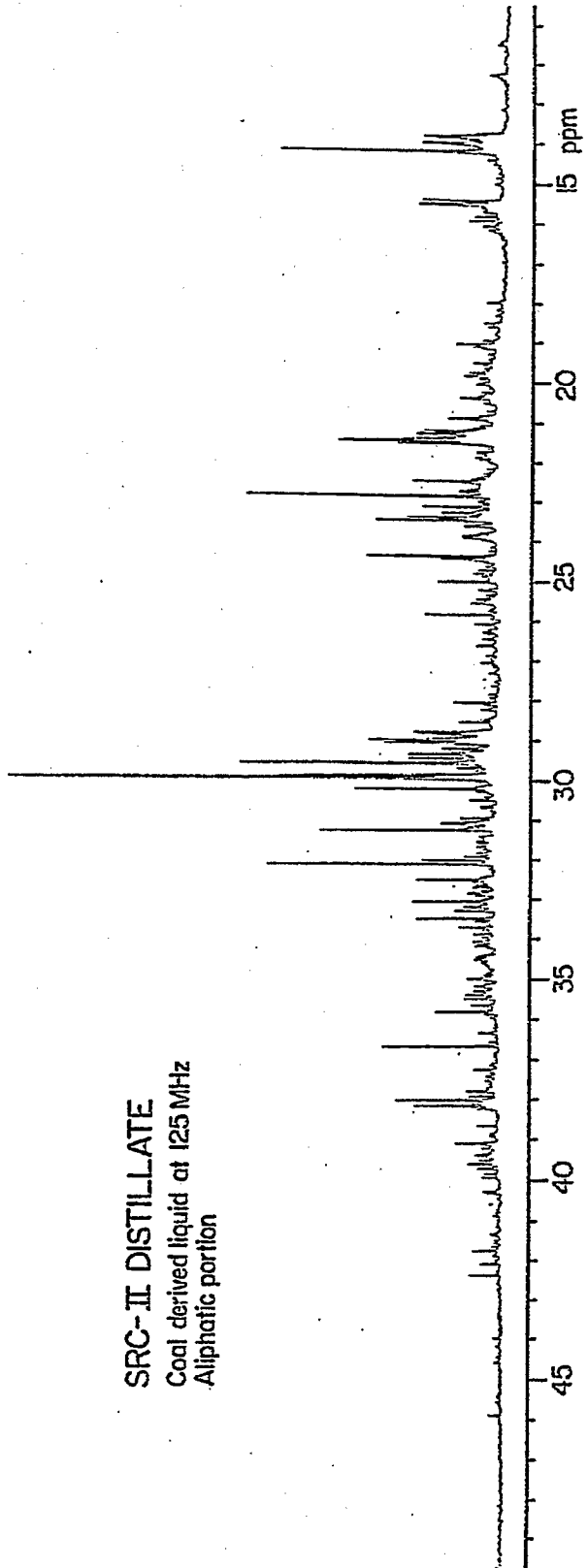
Normal FT



Hydrotreated with CoMo Catalyst

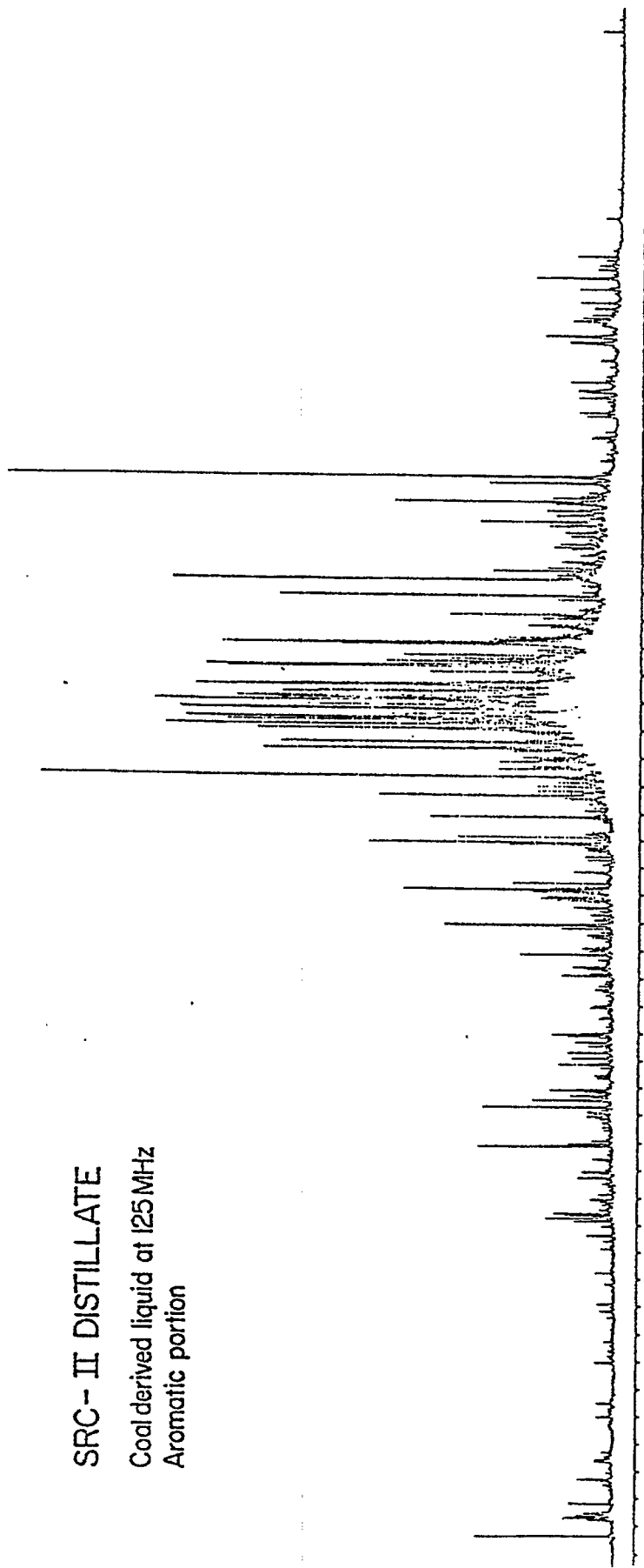


SRC-II DISTILLATE  
Coal derived liquid at 125 MHz  
Aliphatic portion



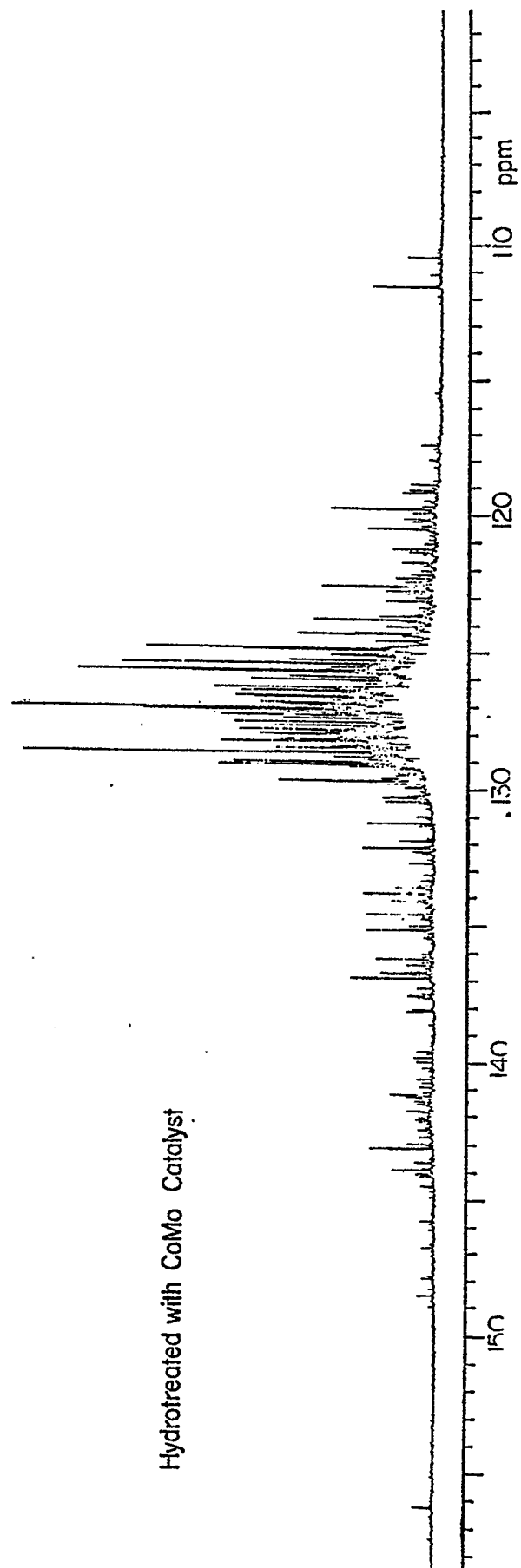
SRC- II DISTILLATE

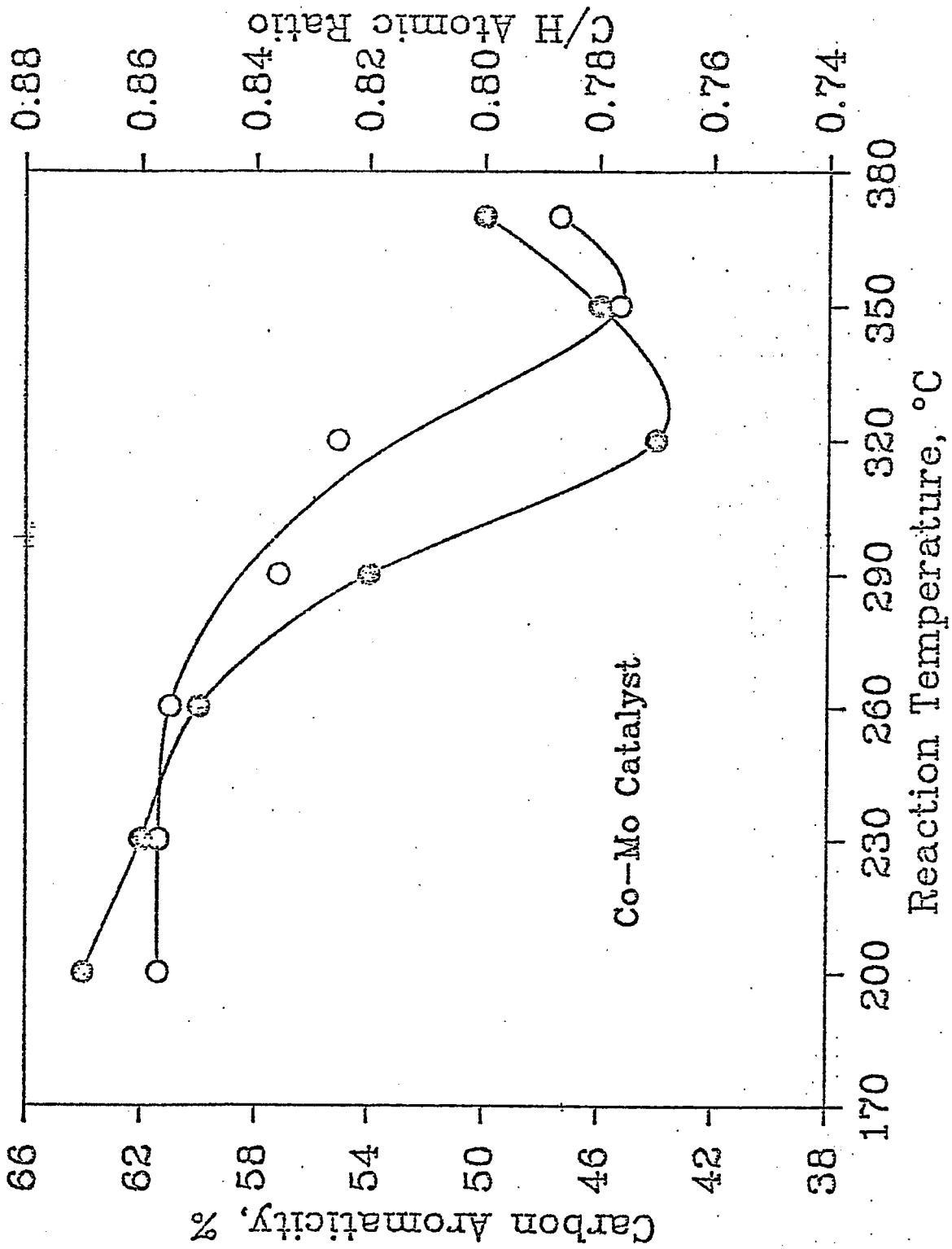
Coal derived liquid at 125 MHz  
Aromatic portion

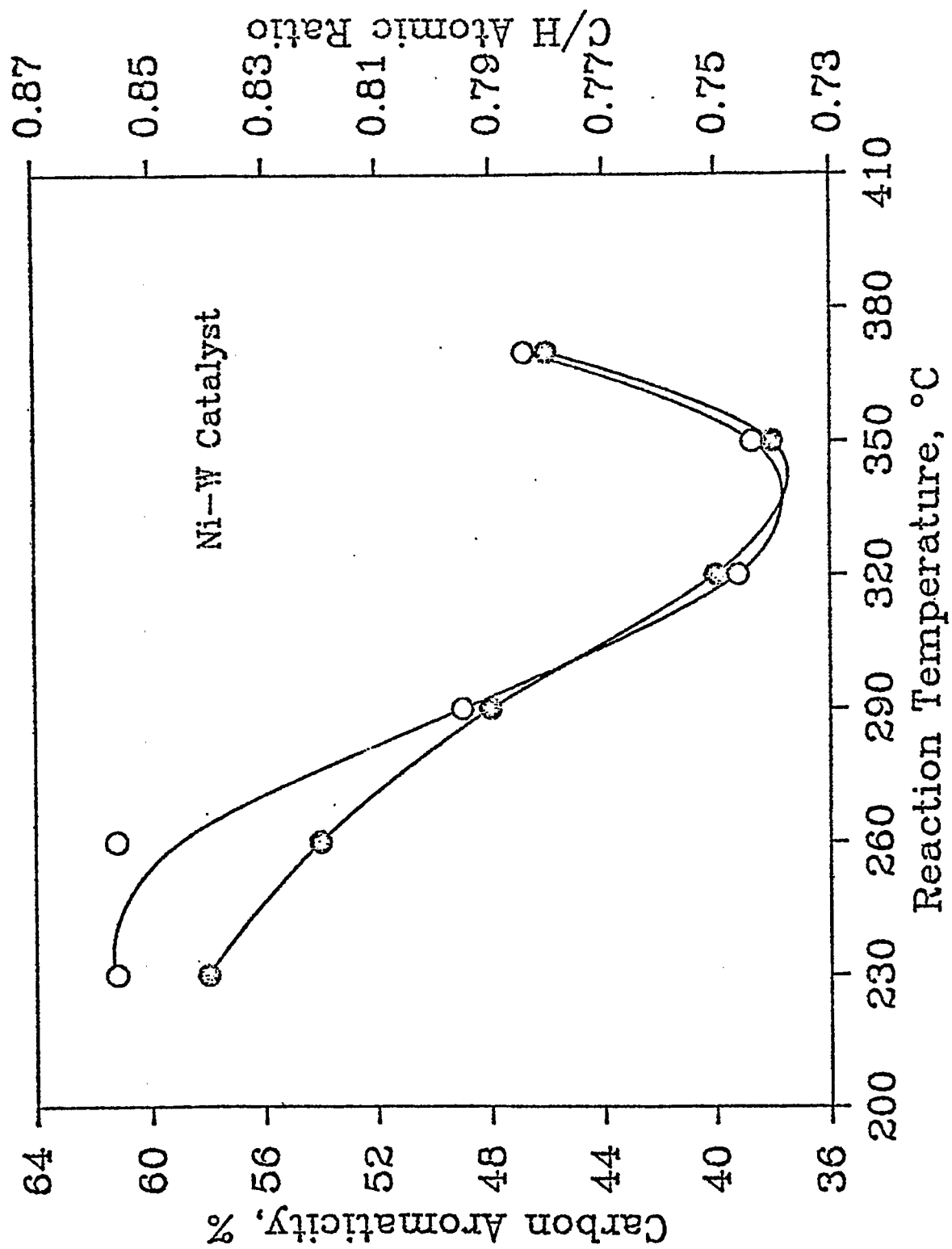


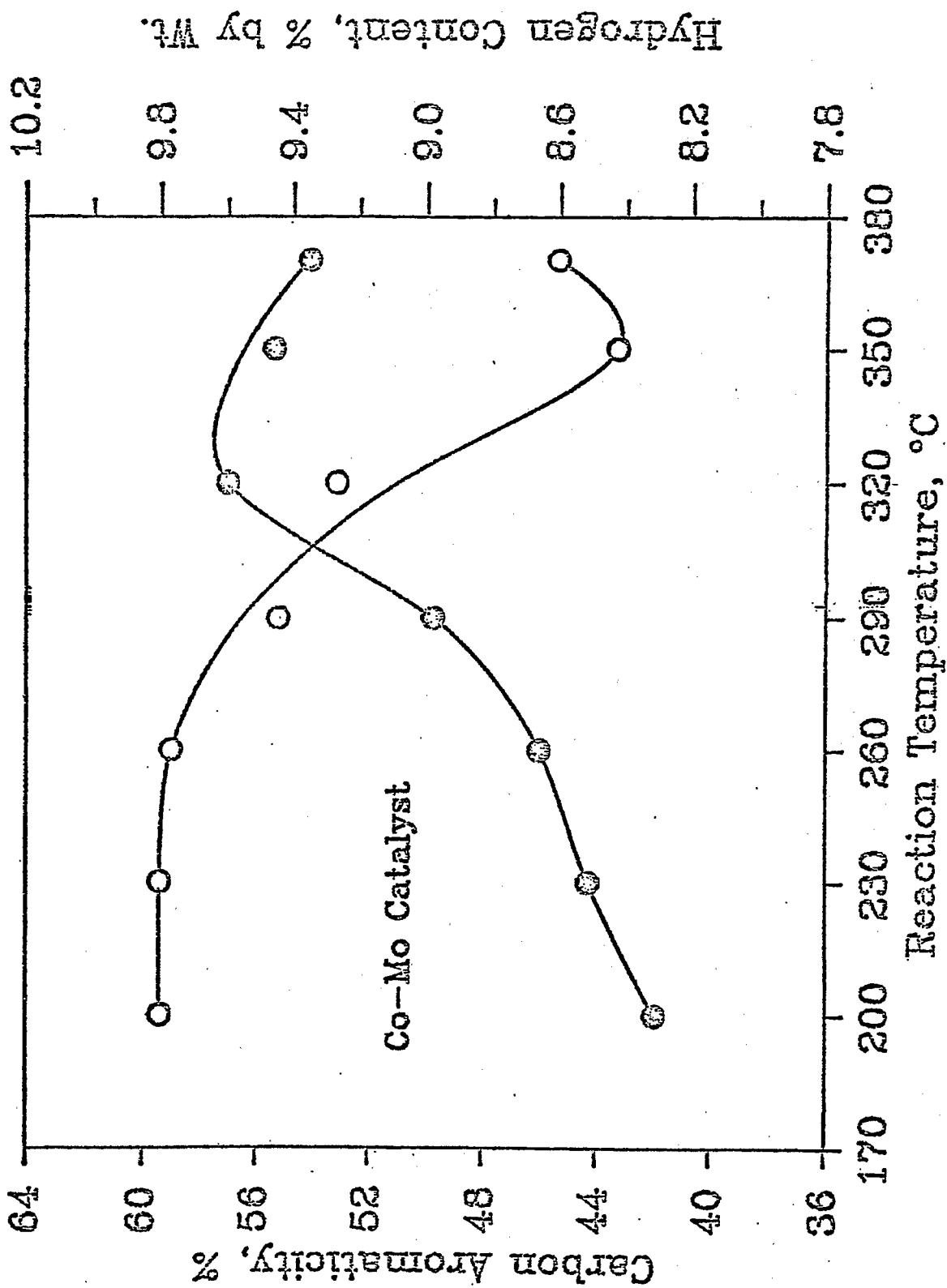
36

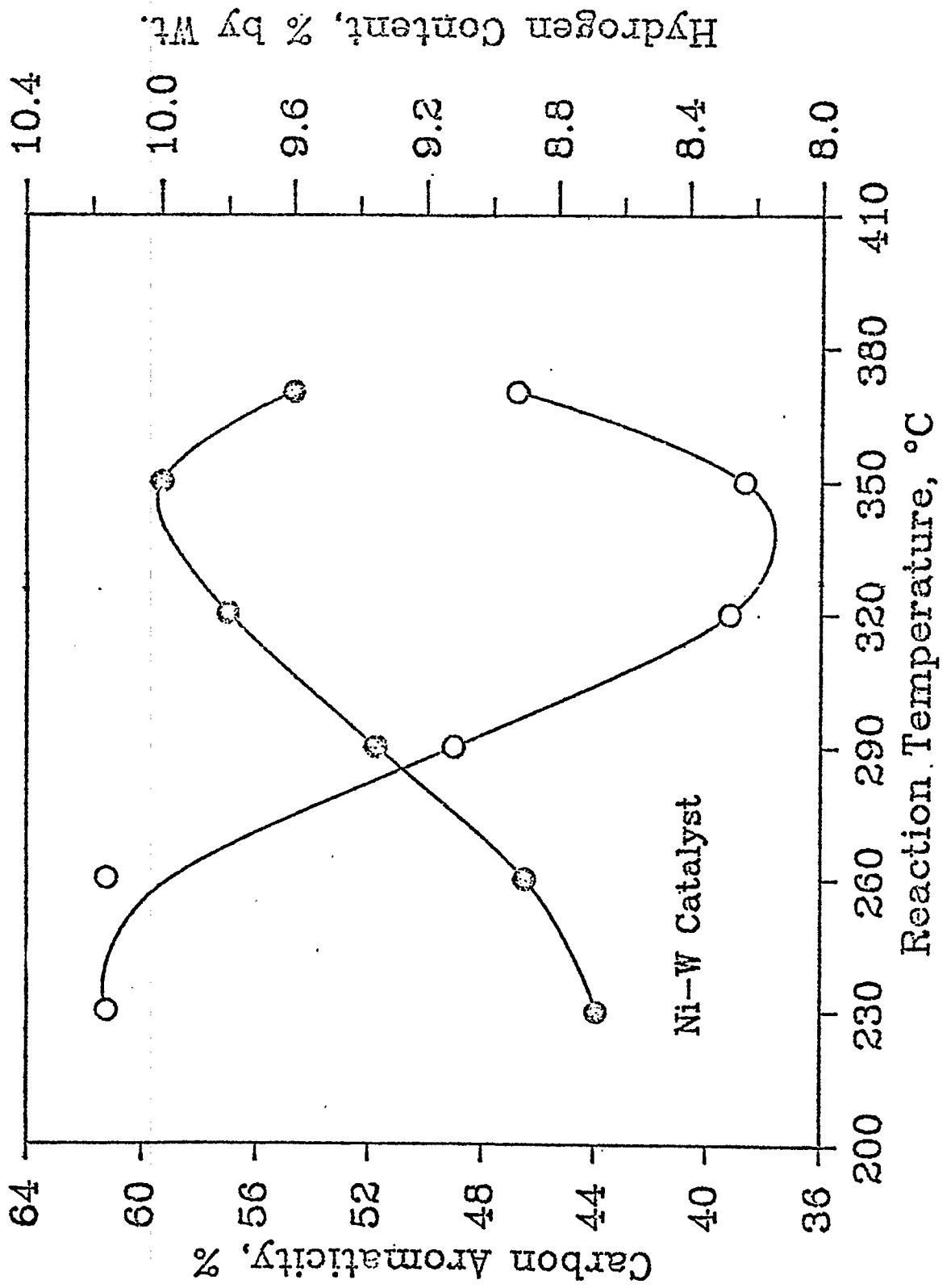
Hydrotreated with CoMo Catalyst

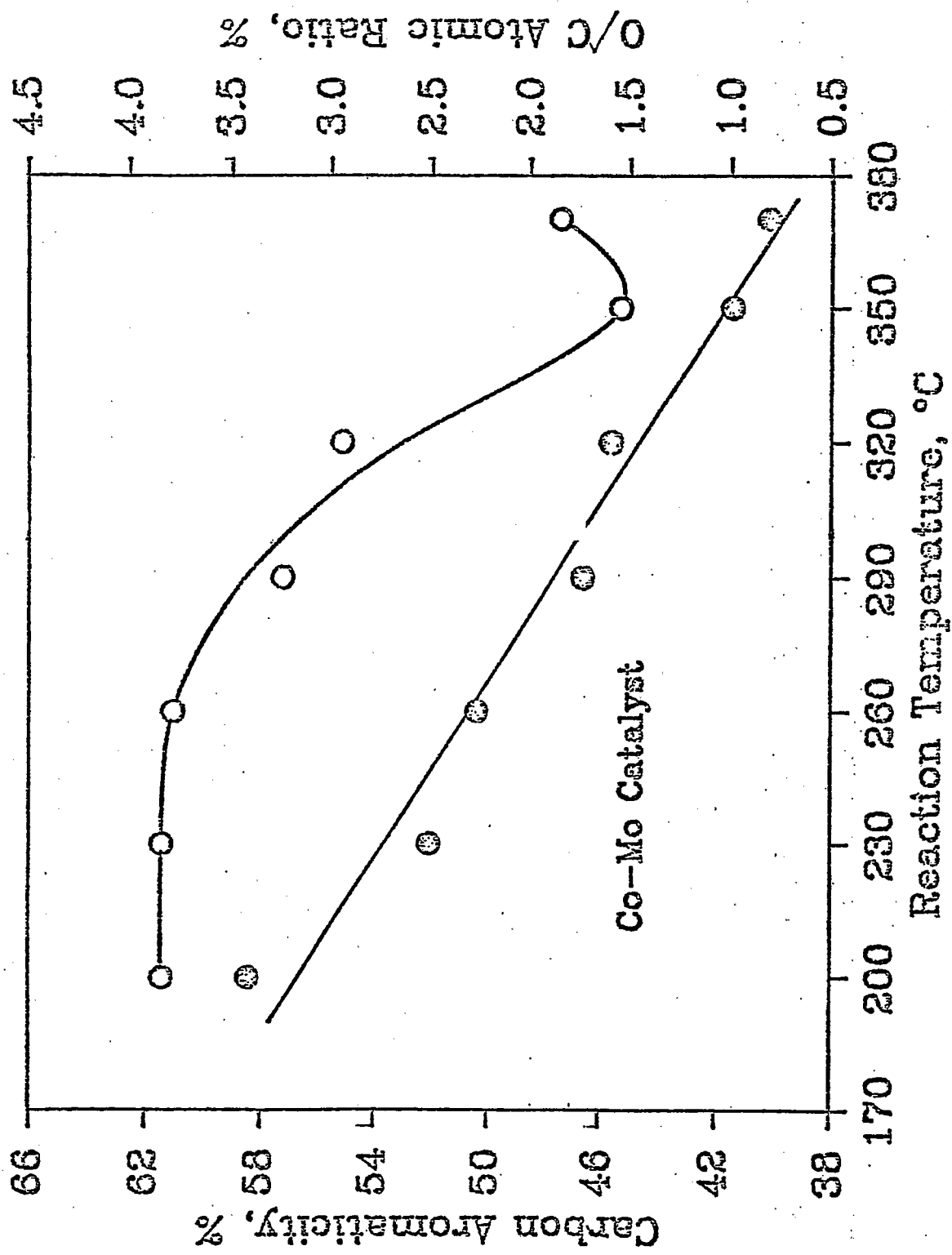


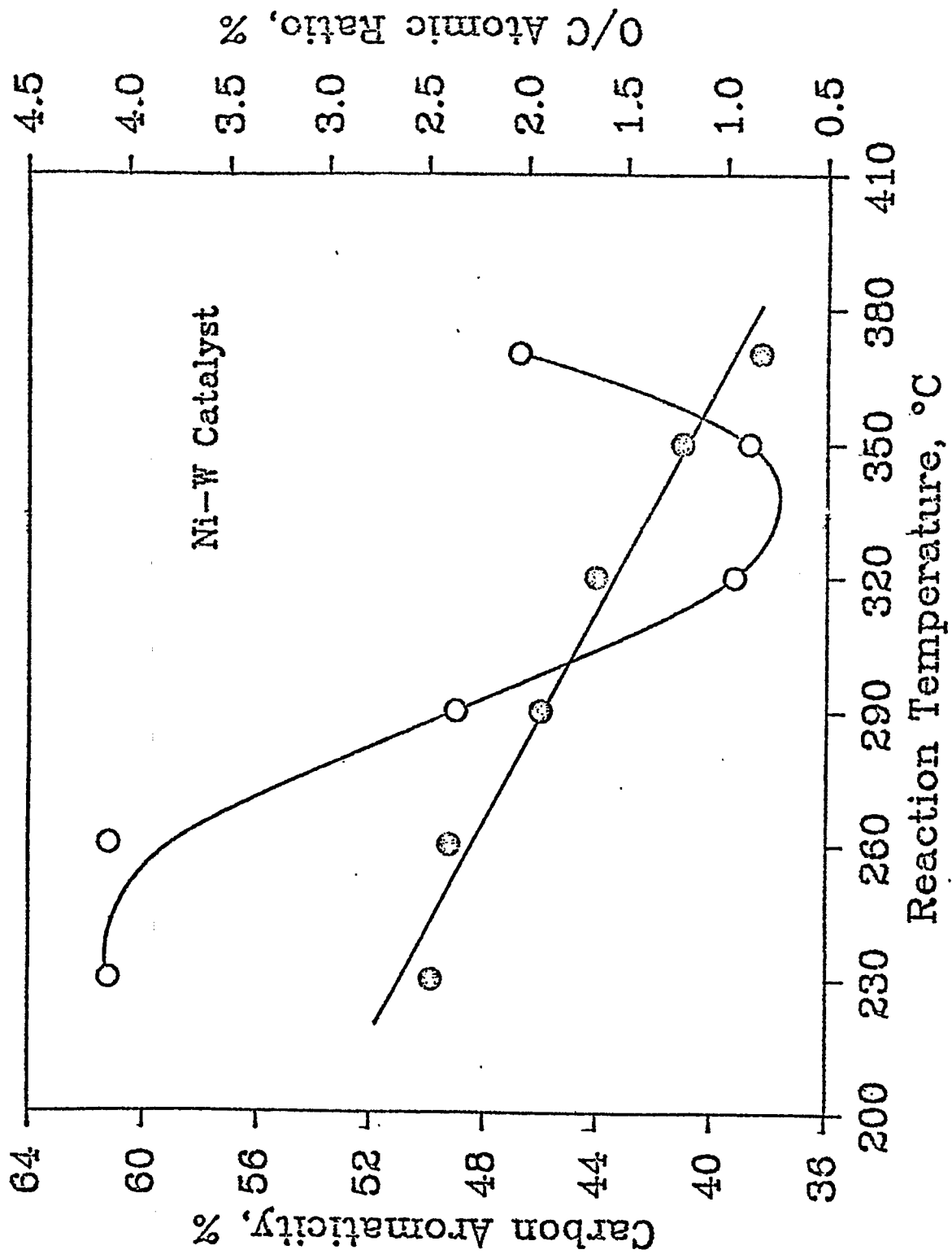












### Task 3

## Catalysis and Mechanism of Coal Liquefaction

### The Effect of Zinc Chloride on the Softening Temperature and Hydrogenolysis Activity of Coal

Faculty Advisor: D.M. Bodily  
Graduate Student: Tsejing Ray

#### Introduction

Metal halides such as  $ZnCl_2$  are well-known to be active catalysts for coal hydrogenation. Zinc chloride has been shown to be a very effective catalyst for coal hydrogenation in the entrained-flow reactor developed at the University of Utah.<sup>1,2</sup> Bell and co-workers<sup>3-5</sup> have studied the reactions of model compounds with  $ZnCl_2$  under conditions similar to those employed in coal hydrogenation. They observed cleavage of C-O and C-C bonds in the model compound and proposed that the active catalytic species is a Bronsted acid formed  $ZnCl_2$ .

Shibaoka, Russell and Bodily<sup>6</sup> proposed a model to explain the liquefaction of coal, based on microscopic examination of the solid products from metal halide catalyzed coal hydrogenation. The model involves a competition between hydrogenation and carbonization reactions. The hydrogenation process starts at the surface of vitrinite particles and progresses toward the center. The vitrinite is converted to a plastic material of lower reflectance, which is the source of oils, asphaltenes and preasphaltenes. Concurrently, carbonization occurs in the center of the particles, resulting in vesiculation and a higher reflectance material. The partially carbonized material can be hydrogenated at later stages, but at a lower rate than the original coal.

Thermal and/or catalytic bond rupture occurs during the liquefaction process. The initial products of the bond cleavage reactions may be stabilized by hydrogen addition, resulting in cleavage of bridges between aromatic ring systems and in dealkylation of aromatic rings. If the initial products of the reaction are not stabilized, they may polymerize to form semicoke-like material. This primary semicoke may be isotropic or exhibit a fine-grained anisotropic mosaic texture, depending on the rank of coal. The plastic material formed by stabilization of the initial products may be further hydrogenated or, under hydrogen deficient conditions, may form secondary semicoke. The secondary semicoke is of medium to coarse-grained anisotropic mosaic texture. Bodily and Shibaoka<sup>7</sup> used this model to explain the nature of the residues from hydrogenation in the short-residence, entrained-flow hydrogenation reactor. The role of the  $ZnCl_2$  catalyst is examined in this study.

#### Project Status

The results of the short-reaction time hydrogenolysis of Clear Creek, Utah coal impregnated with  $ZnCl_2$  in the previous report (Table 1 of Ref 8) were in error. The experiments have been repeated and the results are found in Table 1. An effect of  $ZnCl_2$  is not evident in the agglomeration

properties of the hydrogenolysis residues. The extraction and microscopic examination of the samples is not yet complete. The behavior of the Clear Creek coal (VM = 46.9 mafb) during hydrogenolysis at various temperatures was compared with that of a medium volatile bituminous (VM = 26.0 mafb). The medium volatile coal began to agglomerate between 405 and 464°C. Anisotropic regions were evident in the residues at 464°C. When 10% ZnCl<sub>2</sub> was impregnated on the coal, agglomeration was observed as low as 389°C and strong agglomeration and anisotropy were observed by 445°C.

### Future Work

The hydrogenolysis residues from Clear Creek coal will be extracted and examined by optical microscopy. Samples will be heated in inert atmospheres for comparison with those heated in hydrogen.

### References

1. R.E. Wood and W.H. Wiser, Ind. Eng. Chem., Proc. Design Devel., 15, 144 (1976).
2. J.M. Lytle, R.E. Wood and W.H. Wiser, Fuel, 59, 471 (1980):
3. D.P. Mobley and A.T. Bell, Fuel, 58, 661 (1979).
4. N.D. Taylor and A.T. Bell, Fuel, 59, 499 (1980).
5. D.P. Mobley and A.T. Bell, Fuel, 59, 507 (1980).
6. M. Shibaoka, N.J. Russel and D.M. Bodily, Fuel, 61, 201 (1982).
7. D.M. Bodily and M. Shibaoka, Fuel, submitted.
8. W.H. Wiser et al., DOE Contract No. DE-AC01-79ET14700, Quarterly Progress Report, Salt Lake City, Utah, July-Sept 1982, pp 10-11.

Table 1. Hydrogenolysis residues from Clear Creek, Utah coal.

<u>Reaction Temperature, °C</u>	<u>Catalyst</u>	<u>Agglomeration</u>
350	None	Free flowing
400	None	Free flowing
440	None	Free flowing
494	None	Some agglomeration
350	10% ZnCl <sub>2</sub>	Free flowing
400	10% ZnCl <sub>2</sub>	Free flowing
455	10% ZnCl <sub>2</sub>	Free flowing
520	10% ZnCl <sub>2</sub>	Some agglomeration

## Task 5

### The Mechanism of Pyrolysis of Bituminous Coal

Faculty Advisor: W.H. Wiser  
Graduate Student: J.K. Shigley

#### Introduction

In the present state of knowledge concerning the fundamental chemistry of coal liquefaction in the temperature range 375-550°C, the liquefaction reactions are initiated by thermal rupture of bonds in the bridges joining configurations in the coal, yielding free radicals. The different approaches to liquefaction, except for Fischer-Tropsch variations, represent ways of stabilizing the free radicals to produce molecules. The stabilization involving abstraction by the free radicals of hydrogen from the hydroaromatic structures of the coal is believed to be the predominant means of yielding liquid size molecules in the early stages of all coal liquefaction processes, except Fischer-Tropsch variations. The objective of this research is to understand the chemistry of this pyrolytic operation using model compounds which contain structures believed to be prominent in bituminous coals.

#### Project Status

Gas chromatographic/mass spectrometric analysis has been performed on the model compounds and the 400°C and 425°C 9-benzyl-1,2,3,4-tetrahydrocarbazole (9-BTHC) pyrolysis products. The GC/MS analysis of 9-BTHC and 9-benzyloxy-1,10-propanophenanthrene showed that these model compounds are satisfactorily pure (95+%). The GC/MS analysis of N-(naphthylmethyl)-5,6,7,8-tetrahydroquinolinium chloride proved to be much more difficult. Quinolinium salts are known to decompose on most gas chromatographic columns, and this proved to be true. This result made it impossible to analyze this model compound by GC/MS. An attempt was made to analyze this model compound utilizing direct probe mass spectrometry. This attempt also proved fruitless, as the model compound decomposed in the probe inlet. Attempts by lowering the probe inlet's temperature to limit or eliminate the compound's decomposition were not successful. No satisfactory GC/MS or MS analysis has been obtained for N-(naphthylmethyl)-5,6,7,8-tetrahydroquinolinium chloride.

The GC/MS analysis of the 9-BTHC pyrolysis products proved to be much more successful and beneficial. The total ion chromatogram of the 425°C pyrolysis products is shown in Figure 1. The identification of most of the major peaks was obtained by analyzing their mass spectra resulting from the GC/MS analysis. The data are tabulated in Table 1. Several of the peaks were unidentifiable either because no spectrum was obtained (#1995) or the data was not able to be analyzed.

After verifying the structures of the major pyrolysis products of 9-BTHC, pyrolysis experimentation was continued. The problems encountered with heavy product formation have been corrected. The 5mm sample tubes are prepared by

initially sealing clean 5 mm pyrex tubes on one end and then drying these tubes in a vacuum dessicator for at least 8 hours at 80°C. The tubes are removed from the dessicator and allowed to reach ambient conditions over a period of at least 1 hour. The weighed empty tubes are purged with high purity helium before loading with the 3-4 mg of sample. The weighed tube containing the sample is again purged with the high purity helium, before being connected to the vacuum. The sample tube is evacuated at room temperature and then is immersed in a dry ice/acetone bath still under vacuum. The sample tube is removed from the dry ice/acetone bath and are allowed to warm slowly to ambient temperature. The tube is then partially immersed in liquid nitrogen, so that the liquid nitrogen is at least 1 cm above the sample. The tube is then quickly sealed with an oxy torch. This procedure seems to have eliminated or at least minimized the formation of the heavy products.

Pyrolysis experiments for 9-BTHC at 375°C have been completed. The compiled data for these experiments are tabulated in Table 2. The data for each reaction time are the average of at least two experiments and in some cases of three experiments. The material balances are excellent with an average material balance of 96.7%. Relative amounts of the major pyrolysis products and the molar ratio of 9-BC/CARB are shown in Table 3. The ratio of 9-BC/CARB suggests that initially the free radicals produced by thermal are being stabilized by abstracting hydride radicals (H·) from the naphthenic portion of 9-BTHC. This ratio should eventually approach zero as the dehydrogenated model compound (9-BC) would undergo thermal cleavage, eventually producing carbazole and toluene, in the simplest scheme. Further experimentation must be conducted before these conclusions can be either substantiated or disproved.

The 375°C pyrolysis data were analyzed utilizing a standard integral kinetic order determination technique. The integral kinetic data are shown in Table 4, with the results of linear regression analysis at the bottom. The plots of the first and second order data are shown in Figures 2 and 3, respectively. The first order plot shows a definite concave downward curvature and the curve shown on the plot has been drawn free hand to best fit the data. The line on the second order plot is the result of the linear regression analysis and appears to be the best representation of the plotted data.

The results of the integral analysis strongly suggest that the disappearance of the model compound can best be described utilizing second order kinetics.

#### Future Work

Pyrolysis experiments on 9-BTHC will continue and hopefully be completed. The pyrolysis of 9-benzyloxy-1,10-propanophenanthrene will begin. The GC/MS analysis of the pyrolysis products of 9-BTHC will be performed again with special attention paid to the unidentified components of the previous analysis.

Table 1. 9-BTHC 425°C pyrolysis products GC/MS analysis data.

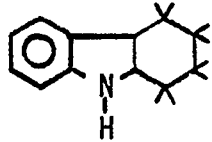
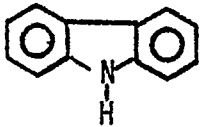
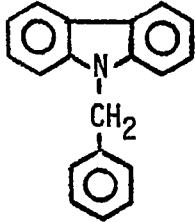
<u>Spectrum #</u>	<u>Molecular Ion Mass, g</u>	<u>Probable Structure</u>
1924	171.24	 1,2,3,4-tetrahydrocarbazole
1932	167.2	 Carbazole
1979	277.3	Unknown
1983	261.4	9-BTHC
1987	257.4	 9-benzylcarbazole
1995	Unknown	Unknown

Table 2. Pyrolysis of 9-benzy[1,2,3,4-tetrahydrocarbazole.

Temperature: 648°K (375°C)

Reaction Time, min	Initial mmoles of 9-BTHC	Tube Volume, cc	% Material Balance	Conversion of 9-BTHC
1.0	0.01467	0.7293	96.49	0.1565
3.0	0.01574	0.7207	95.66	0.2052
5.0	0.01282	0.7355	101.91	0.2234
8.0	0.01465	0.7934	97.19	0.2671
10.0	0.01984	0.7820	94.53	0.2971
15.0	0.01422	0.7657	95.03	0.3225
20.0	0.01655	0.7606	92.31	0.3723
25.0	0.01404	0.7493	99.84	0.3586
30.0	0.01349	0.7282	93.22	0.4157
45.0	0.01271	0.7527	105.66	0.4334
60.0	0.01295	0.7012	91.97	0.5185

Notes: 1. Tube Volume =  $\frac{\pi D^2 L}{4}$

2. % Material Balance =  $\left[ \frac{N(\text{THC}) + N(\text{CARB}) + N(\text{Unk}) + N_A + N(9\text{BC})}{N_{A0}} \right] \times 100$

3. Conversion =  $1 - \frac{N_A}{N_{A0}}$

where,

$N_A$  = millimoles of 9-BTHC

$N_{A0}$  = initial millimoles of 9-BTHC

Table 3. Pyrolysis of 9-BTHC molar ratios.

Reaction Time, min	Conversion of 9-BTHC	% Material Balance	Relative Amounts			
			THC	Carbazole	9-BC	
1.0	0.1565	96.49	0.0231	0.0260	1.492	57.5
3.0	0.2052	95.66	0.0716	0.0689	0.895	13.0
5.0	0.2234	101.91	0.0796	0.0526	0.714	13.6
8.0	0.2671	97.19	0.0934	0.0609	0.520	8.54
10.0	0.2971	94.53	0.104	0.0458	0.443	9.68
15.0	0.3225	95.03	0.103	0.0568	0.430	7.57
20.0	0.3723	92.31	0.152	0.0520	0.399	7.68
25.0	0.3586	99.84	0.170	0.0476	0.418	8.77
30.0	0.4157	93.22	0.205	0.0577	0.410	7.10
45.0	0.4334	105.66	0.292	0.855	0.504	5.89
60.0	0.5185	91.97	0.290	0.0685	0.324	4.73

Table 4. Pyrolysis of 9-benzyl-1,2,3,4-tetrahydrocarbazole overall reaction(s) order determination.

Temperature: 648<sup>o</sup>K (375<sup>o</sup>C)

Reaction Time, min	Kinetic Plots Ordinates	
	First Order $-\ln(1-X_A)$	Second Order $X_A/[C_{A0}(1-X_A)]$
1.0	0.1702	9.224
3.0	0.2297	11.824
5.0	0.2528	16.498
8.0	0.3107	19.737
10.0	0.3525	16.663
15.0	0.3894	25.632
20.0	0.4656	27.252
25.0	0.4442	29.837
30.0	0.5373	38.405
45.0	0.5680	45.308
60.0	0.7308	58.303

Plot	Y intercept	Slope	$r^2$
First Order $-\ln(1-X_A) = k_1 t$	0.2309	$8.611 \times 10^{-3}$	0.9375
Second Order $\frac{X_A}{C_{A0}(1-X_A)} = k_2 t$	11.045	0.7981	0.9799

where,  $k_1 [=] \text{mw}^{-1}$ ;  $k_2 [=] \frac{\text{cc}}{\text{mmole} \cdot \text{mw}}$

$X_A$  = conversion of 9-BTHC

$C_{A0}$  = initial concentration of 9-BTHC, mmole/cc

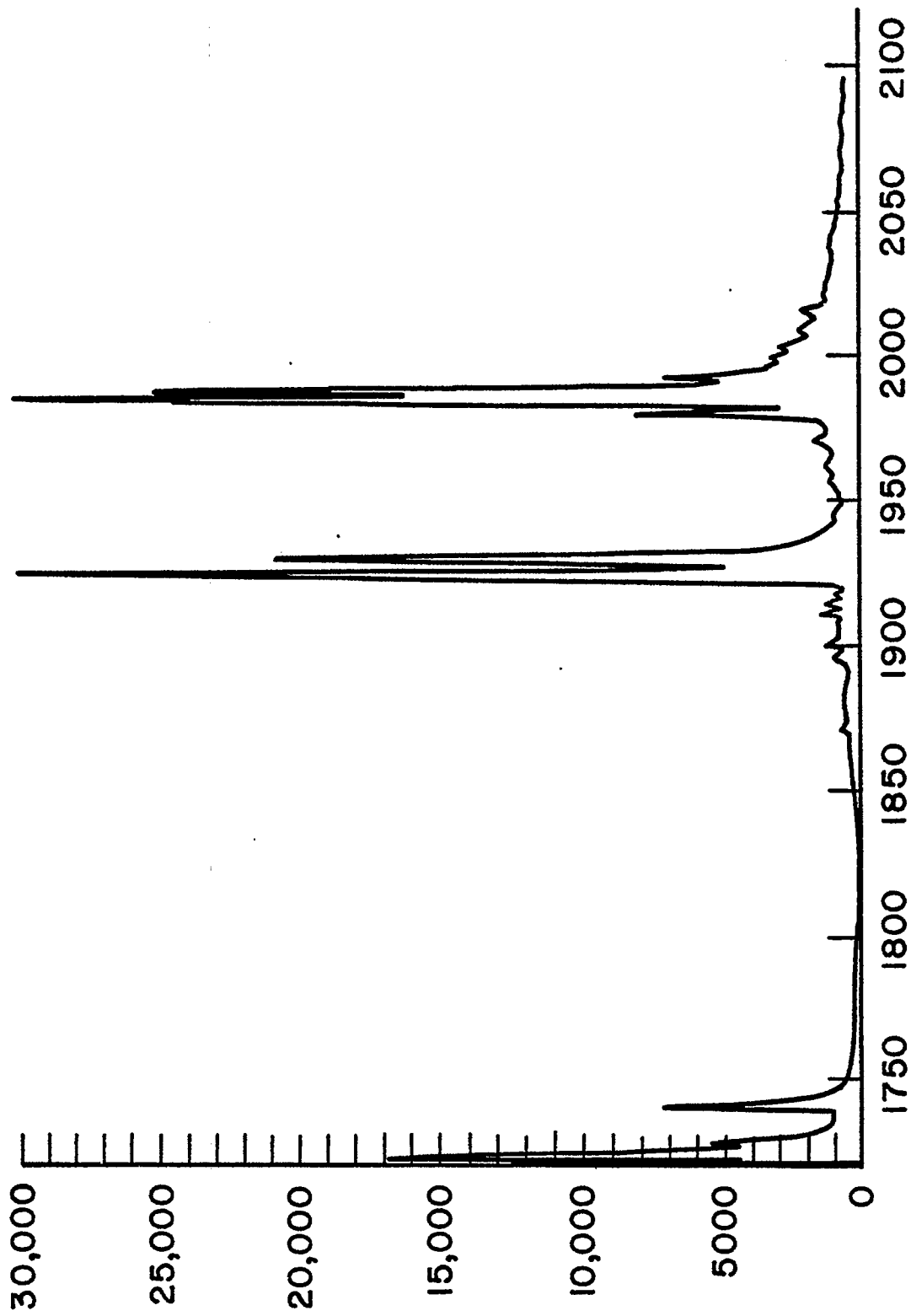


Figure 1. Total ion chromatogram of 9-BTHC 425°C pyrolysis products.

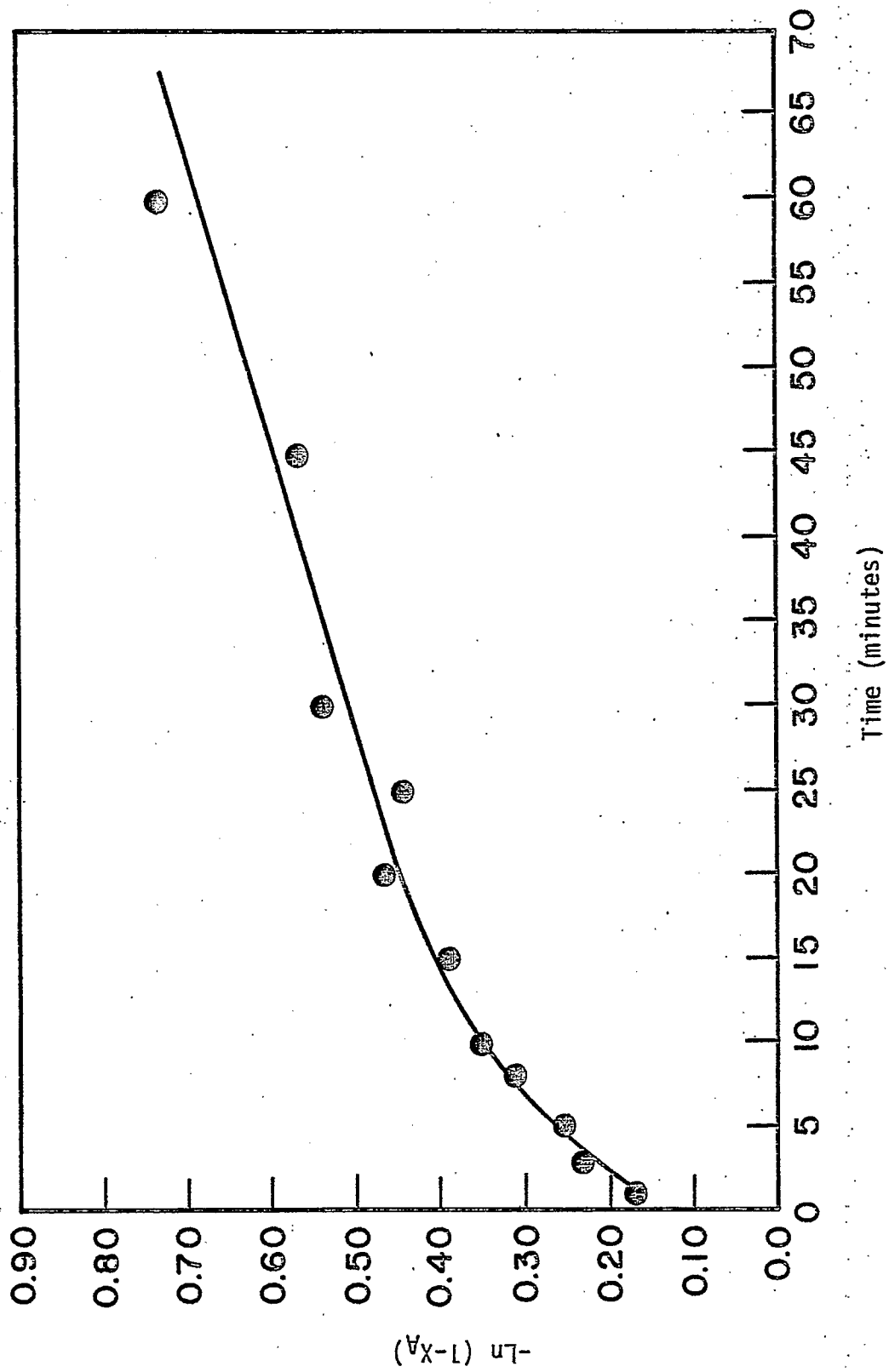


Figure 2. First order kinetics plot.

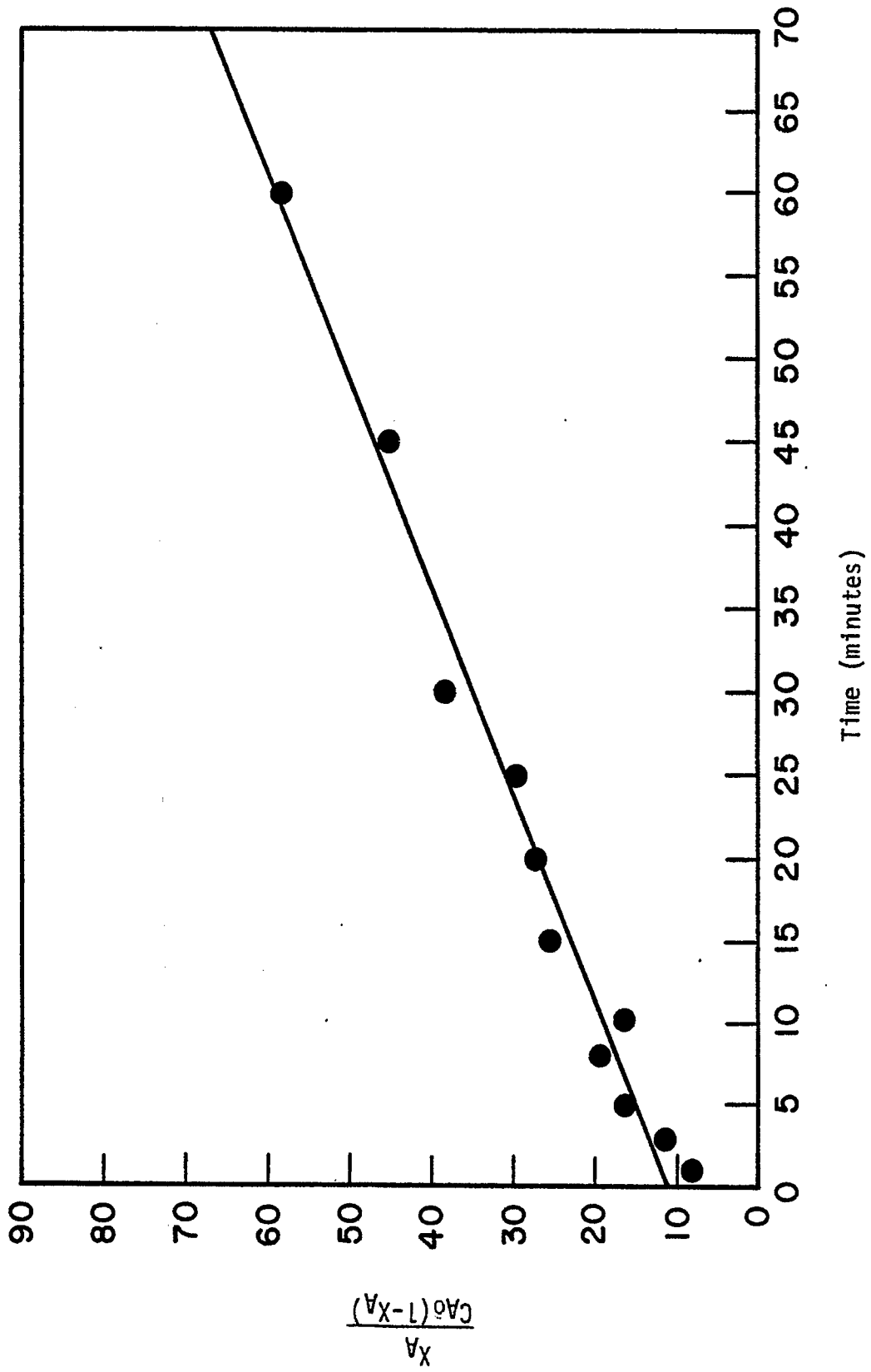


Figure 3. Second order kinetics plot.

## Task 6

### Catalytic Hydrogenation of CD Liquids and Related Polycyclic Aromatic Hydrocarbons

Faculty Advisor: J. Shabtai  
Research Associate: C. Russell

#### Introduction

The main objective of this research project is to develop a versatile process for controllable hydrotreating of highly aromatic coal liquids, viz., a process permitting production of naphthenic-aromatic feedstocks containing variable relative concentrations of hydroaromatic vs. aromatic ring structures. Such feedstocks, including the extreme case of a fully hydrogenated coal liquid, are suitable starting materials for catalytic cracking, as applied for preferential production of light liquid fuels. The overall objective of this project and of a parallel catalytic cracking study is, therefore, to develop and optimize a hydrotreating-catalytic cracking process sequence for conversion of coal liquids into conventional fuels.

The present project includes also a study of metal sulfide-catalyzed hydrogenation of model polycyclic arenes present in coal liquids, e.g., phenanthrene, pyrene, anthracene and triphenylene, as a function of catalyst type and experimental variables.<sup>1</sup> This part of the study provides basic information on the rate, mechanism and stereochemistry of hydrogenation of structurally distinct aromatic systems in the presence of sulfided catalysts.

#### Project Status

The systematic studies of the hydrogenation of chrysene and of an SRC-II distillate (b.p. 230-455°C) were extended to include an investigation of the kinetics of these reactions. Further, a study of the stereochemistry of hydrogenation of phenanthrene in the presence of a sulfided Ni-W/Al<sub>2</sub>O<sub>3</sub> was completed. The stereoisomeric composition of the perhydrophenanthrene product with this catalyst did not change significantly in the temperature range of 300-380°C and the hydrogen pressure range of 1500-2900 psig. It was as follows:

Perhydrophenanthrene Stereoisomer	Concentration, mol %
<u>Trans-anti-trans</u>	64
<u>Trans-anti-cis</u>	22
<u>Trans-syn-cis</u>	13
<u>Cis-syn-cis</u>	0.3

This composition is completely different from that of the product obtained from phenanthrene hydrogenation on Pt and other transition metals. For example, hydrogenation with a supported Ru catalyst yielded a perhydrophenanthrene product containing 85% of the cis-syn-cis stereoisomer, and only 15% of other stereoisomers. The observed fundamental difference in hydrogenation stereochemistry with sulfided vs. metal catalysts is ascribed to differences in the orientation of reaction intermediates on the surface of these two types of catalysts, as well as to differences in reaction mechanisms.<sup>1</sup>

#### Future Work

The study of the hydrogenation kinetics of a typical coal liquid (SRC-II middle-heavy distillate) and of a tetracyclic model compound, i.e., chrysene, will be continued and completed.

#### References

1. J. Shabtai, C. Russell, L. Veluswami and A.G. Oblad, paper in preparation.

## Task 7

### Denitrogenation and Deoxygenation of CD Liquids and Related N- and O- Containing Compounds

#### Hydrogenitrogenation of Coal-Derived Liquids and Related N-Containing Compounds

Faculty Advisor: J. Shabtai

Graduate Student: J. Yeh

#### Introduction

The main objective of this research project is to develop effective catalyst systems and processing conditions for hydrodenitrogenation (HDN) of coal-derived liquids (CDL) in a wide range of nitrogen contents and structural type composition. This is of particular importance in view of the higher concentration of nitrogen-containing compounds in CDL as compared to that in petroleum feedstocks. For a better understanding of denitrogenation processes, the project includes systematic denitrogenation studies not only of CDL but also of related model N-containing compounds found in such liquids, e.g., phenanthridine, 1,10-phenanthroline, carbazoles, acridines, etc., as a function of catalyst type and experimental variables. A part of the study is concerned with determination of the rate, mechanism and stereochemistry of HDN of structurally distinct N-containing aromatic systems in the presence of sulfided catalysts.

#### Project Status

It was found previously in Task 10 of this research project that the HDS/hydrogenation selectivity of sulfided catalysts changes markedly with catalyst composition and mode of preparation. In the present study the activities of a series of sulfided CoMo/ $\gamma$ -Al<sub>2</sub>O<sub>3</sub> and NiMo/ $\gamma$ -Al<sub>2</sub>O<sub>3</sub> catalysts for C-N hydrogenolysis vs. ring hydrogenation were determined, using 5,6-benzoquinoline (1) as a model compound. The hydrogen-HDN network for this compound is given in Figure 1, while the kinetic rate constants for the different steps of the reaction obtained with various catalysts are summarized in Table 1. The composition and methods of preparation of the catalysts are indicated in the footnotes of Table 1, while details are provided elsewhere.<sup>1</sup>

Kinetic rate constants (Table 1) were obtained for a reaction pressure of 2500 psig, and at a reaction temperature of 300°C. Comparison of  $k_1$  with the different catalysts indicates that the sulfided NiMo/ $\gamma$ -Al<sub>2</sub>O<sub>3</sub> catalyst IV has higher activity for ring hydrogenation of the pyridine moiety, as compared to the sulfided CoMo catalysts I-III. C-N hydrogenolysis of the first reaction intermediate, 1,2,3,4-tetrahydro-5,6-benzoquinoline (2) is a very slow reaction with all catalysts examined, although the CoMo catalysts I-III are somewhat more active for this step. Ring hydrogenation of 2, yielding two octahydrobenzoquinolines (3), is much faster than cleavage, and the NiMo catalyst IV is somewhat more active for this step than the CoMo catalysts I-III. Compound 3 is more susceptible to C-N hydrogenolysis (compared to 2), yielding the denitrogenated products 6. The CoMo catalysts I-III are found to be more active for this C-N hydrogenolysis step. Compound 3 undergoes also

competing ring hydrogenation to yield perhydro-5,6-benzoquinoline 4, which is ultimately denitrogenated to 7.

The following conclusions could be reached:

- (a) The NiMo catalyst IV shows higher ring hydrogenation activity in the stepwise reaction of 1.
- (b) The CoMo catalysts I-III show higher C(aromatic)-N hydrogenolysis activity compared to the NiMo catalyst IV.
- (c) The NiMo catalyst IV shows higher C(aliphatic)-N hydrogenolysis activity compared to the CoMo catalysts I-III.

#### Future Work

HDN studies with CDL and model compounds will be continued. The HDN kinetics of an SRC-II distillate will be investigated.

#### References

1. G. Muralidhar, F.E. Massoth and J. Shabtai, submitted for publication (J. Catalysis).

Table 1

Catalysts (No.) <sup>a</sup>	Rate Constants <sup>b</sup>							
	k <sub>1</sub>	k <sub>2</sub>	k <sub>3</sub>	k <sub>4</sub>	k <sub>5</sub>	k <sub>6</sub>	k <sub>7</sub>	k <sub>8</sub>
3Co8Mo/ $\gamma$ -Al <sub>2</sub> O <sub>3</sub> (I) <sup>c</sup>	0.891	0.009	0.835	--	0.052	0.072	--	0.476
(Step)3Co8Mo/ $\gamma$ -Al <sub>2</sub> O <sub>3</sub> (II) <sup>d</sup> 1	1.52	0.012	0.994	0.303	0.055	0.067	0.178	0.647
6Co8Mo/ $\gamma$ -Al <sub>2</sub> O <sub>3</sub> (III)	1.92	0.011	1.03	0.314	0.069	0.075	0.369	0.370
3Ni8Mo/ $\gamma$ -Al <sub>2</sub> O <sub>3</sub> (IV)	7.83	0.003	1.16	--	0.040	0.074	(>0.4) <sup>e</sup>	0.894

<sup>a</sup>Concentration levels are 8% by wt of Mo in catalysts 1-5, 3% by wt of Co in catalyst 1 and 2; 6% by wt of Co in catalyst 3; and 3% by wt of Ni in catalyst 4. All catalysts were presulfided before use.

<sup>b</sup>Unit is: hr<sup>-1</sup>.

<sup>c</sup>Prepared by a standard impregnation procedure. 1

<sup>d</sup>Prepared by stepwise addition of Co to Mo-impregnated  $\gamma$ -Al<sub>2</sub>O<sub>3</sub>. 1

<sup>e</sup>Some difficulties were encountered on accurate determination of this constant.

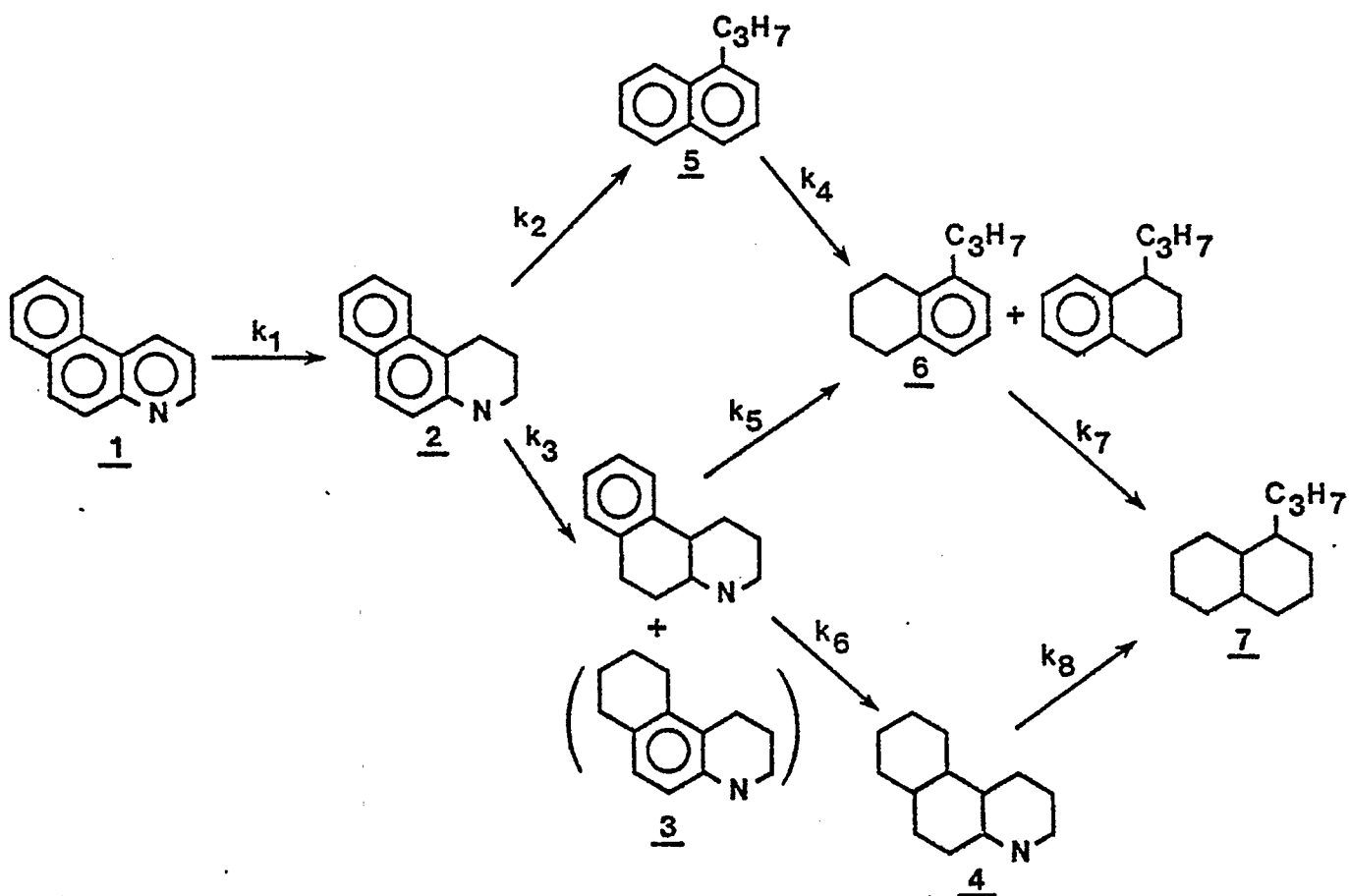


Figure 1. Hydrogenation-HDN of 5,6-benzoquinoline.

## Task 8

### Catalytic Cracking of Hydrogenated Coal-Derived Liquids and Related Compounds

Faculty Advisors: J. Shabtai  
A.G. Oblad  
Graduate Student: John McCauley

#### Introduction

Hydrogenation followed by catalytic cracking provides a feasible process sequence for conversion of coal liquids into conventional fuels. Such a sequence has certain advantages in comparison with a hydrocracking-catalytic reforming scheme.

The present project is concerned with the following interrelated subjects: (1) systematic catalytic cracking studies of polycyclic naphthenes and naphthenoaromatics found in hydrogenated coal liquids and (2) systematic catalytic cracking studies of hydrotreated coal-derived liquids.

#### Project Status

Systematic catalytic cracking studies, using newly synthesized cross-linked smectite (CLS) molecular sieves,<sup>1,2</sup> are being continued. The cracking activities of Ce<sup>3+</sup>- and La<sup>3+</sup>-exchanged cross-linked montmorillonites (Ce-CLM and La-CLM, respectively) were compared with that of CeY-type zeolite. Cumene, 1,3-diisopropylbenzene, 1,3,5-triisopropylbenzene, and 1,3,5-tri-*t*-butylbenzene, having critical molecular diameters in the range of 6.8 - 9.4 Å and critical molecular "thickness" in the range of 5.3 - 6.6 Å, were used as model feedstocks. For cumene cracking the activities of the Ce-CLM and La-CLM catalysts in the temperature range of 300-450°C were similar with that of CeY-zeolite, due to free intrasorption of this compound in the intracrystalline channel system of both types of catalysts. However, with gradual increase in the critical molecular diameter and thickness of the alkylbenzene reactant, the larger-pore CLM catalysts showed increasingly higher relative activities compared to that of the CeY-zeolite. Thus, for 1,3,5-tri-*t*-butylbenzene the activity of a partially cross-linked Ce-CLM catalyst was found to be more than one order of magnitude higher than that of CeY-type zeolite. Cracking studies with CLM catalysts, using polycyclic naphthenes and naphthenoaromatics are continuing.

#### Future Work

The above indicated studies will be continued.

#### References

1. J. Shabtai, U.S. Patent 4,238,364 (1980).
2. J. Shabtai, R. Lazar and A.G. Oblad, Proc. 7th International Congress on Catalysis, Tokyo, Japan, 1980, pp 828-840.

## Task 9

### Hydropyrolysis (Thermal Hydrocracking) of CD Liquids

Faculty Advisors: J.S. Shabtai  
A.G. Oblad  
Graduate Student: Y. Wen

#### Introduction

This project is concerned with a systematic investigation of hydro-pyrolysis (thermal hydrocracking) as an alternative processing concept for upgrading of heavy coal-derived liquids (CDL) into light liquid products. The high efficiency and versatility of hydro-pyrolysis has been indicated in previous studies with heavy CDL feedstocks and with model compounds.<sup>1-3</sup> The present project is an extension of this previous work for the purpose of (a) further developing and enlarging the scope of the hydro-pyrolytic process, and (b) optimizing the operating conditions for different types of feedstocks, e.g., coal liquids from different liquefaction processes, partially hydrotreated coal liquids, and relevant model compounds. The project includes systematic studies of reaction kinetics, product composition, and coking tendencies, as a function of operating variables. The work with model compounds provides necessary data for further elucidation of mechanistic aspects of the hydro-pyrolysis process.

#### Project Status

The hydro-pyrolysis reactions of tetralin as a function of temperature and pressure were investigated. Table 1 and Figures 1-3 summarize the change in product composition as a function of hydrogen pressure (between 750-2250 psig), keeping a constant reaction temperature (550°C). As seen, the total tetralin conversion at this temperature increases only slightly with increase in pressure (from 21.3% at 750 psig to 26.6% at 2250 psig). The product consists mostly of liquids and solids, and the extent of gas formation is very low (1.4-3.2% by wt). Ethane is the main gaseous product, and its concentration increases with increase in pressure, viz., at 750 psig it is 63 mol % and at 2250 psig it is 72 mol % of the total gas product (Figure 1). The  $C_2H_6/C_2H_4$  ratio increases from 3.5 at 750 psig to 11.1 at 2250 psig. Other gas products, viz., methane, propylene, propane and n-butane, are formed in small amounts only. The liquid products consist of ethylbenzene, n-butylbenzene, o-diethylbenzene, o-ethylstyrene, decalin, 1,2-dihydronaphthalene and naphthalene. The product composition and its change with pressure indicates the occurrence of two competing reactions, i.e., (a) hydrogenation-dehydrogenation reactions leading to naphthalene, 1,2-dihydronaphthalene and decalin; and (b) cleavage reactions of the hydroaromatic ring in tetralin resulting in alkylbenzenes.

The change in composition of the alkylbenzene products as a function of pressure, at 550°C, is given in Figure 2. As seen, the extent of cleavage reactions increases with increase in pressure. However, the main reaction of tetralin at 550°C is dehydrogenation to naphthalene. The extent of dehydrogenation at this temperature decreases only moderately with increase in pressure (Figure 3). The cleavage/dehydrogenation selectivity for tetralin hydro-pyrolysis increases only at higher temperatures (575-600°C) while

applying at the same time a hydrogen pressure  $\geq 1800$  psig (see details in next report).

The formation of products indicated in Table 1 can be rationalized in terms of the free radical mechanism indicated in Scheme 1.

#### Future Work

The study of tetralin hydrolysis as a function of operating conditions will be completed.

#### References

1. J. Shabtai, R. Ramakrishnan and A.G. Oblad, Advances in Chemistry, No. 183, Thermal Hydrocarbon Chemistry, Amer. Chem. Soc., 1979, pp 297-328.
2. R. Ramakrishnan, Ph.D. Thesis, University of Utah, Salt Lake City, Utah, 1978.
3. A.G. Oblad, J. Shabtai and R. Ramakrishnan, U.S. Patent 4,298,457 (1981).

Table 1.  
Change in Product Composition from Hydropyrolysis  
of Tetralin (1) as a Function of Hydrogen Pressure <sup>a-d</sup>.

Hydrogen pressure (psig)	750	1000	1250	1500	1750	2000	2250
H <sub>2</sub> / <u>1</u> mol ratio	4.1	5.5	6.8	8.2	9.5	10.9	12.2
Conversion (mol%)	21.3	21.3	22.2	25.5	26.5	26.4	26.6
Product distribution (wt%)							
Gas	1.4	1.8	2.0	2.3	2.8	3.2	3.2
Liquids (plus solids)	98.6	98.2	98.0	97.7	97.2	96.8	96.8
Product Component (mol%) <sup>e</sup> :							
Methane	0.6	0.8	0.8	0.9	1.3	1.2	1.2
Ethane	3.9	5.2	6.0	7.0	9.1	10.0	10.0
Ethylene	1.1	1.2	1.2	0.8	0.8	0.9	0.9
Propane	0.2	0.3	0.3	0.6	0.8	1.0	1.1
Propylene	0.4	0.4	0.4	0.5	0.5	0.6	0.6
n-Butane	0	0	0	0	0	0.1	0.1
Ethylbenzene	4.2	5.0	5.5	7.4	8.7	8.7	9.4
n-Butylbenzene	1.3	1.9	2.8	4.4	5.6	6.4	7.4
o-Diethylbenzene	2.0	2.2	2.2	2.2	2.0	2.0	2.0
o-Ethylstyrene	6.8	7.6	8.3	9.2	9.8	9.5	9.7
Decalin	0.6	0.6	0.6	0.6	0.6	0.6	0.7
1,2-Dihydronaphthalene	4.7	4.4	4.0	3.7	3.3	3.3	3.3
Naphthalene	80.3	78.3	76.6	72.6	69.9	69.5	67.5

<sup>a</sup>Reaction temp., 550°C; <sup>b</sup>Residence time, 30 sec.; <sup>c</sup>LHSV=3.1 hr<sup>-1</sup>;  
<sup>d</sup>Feedstock pumping rate = 5 ml/min; <sup>e</sup>Mol/100 mol reacted tetralin (1).

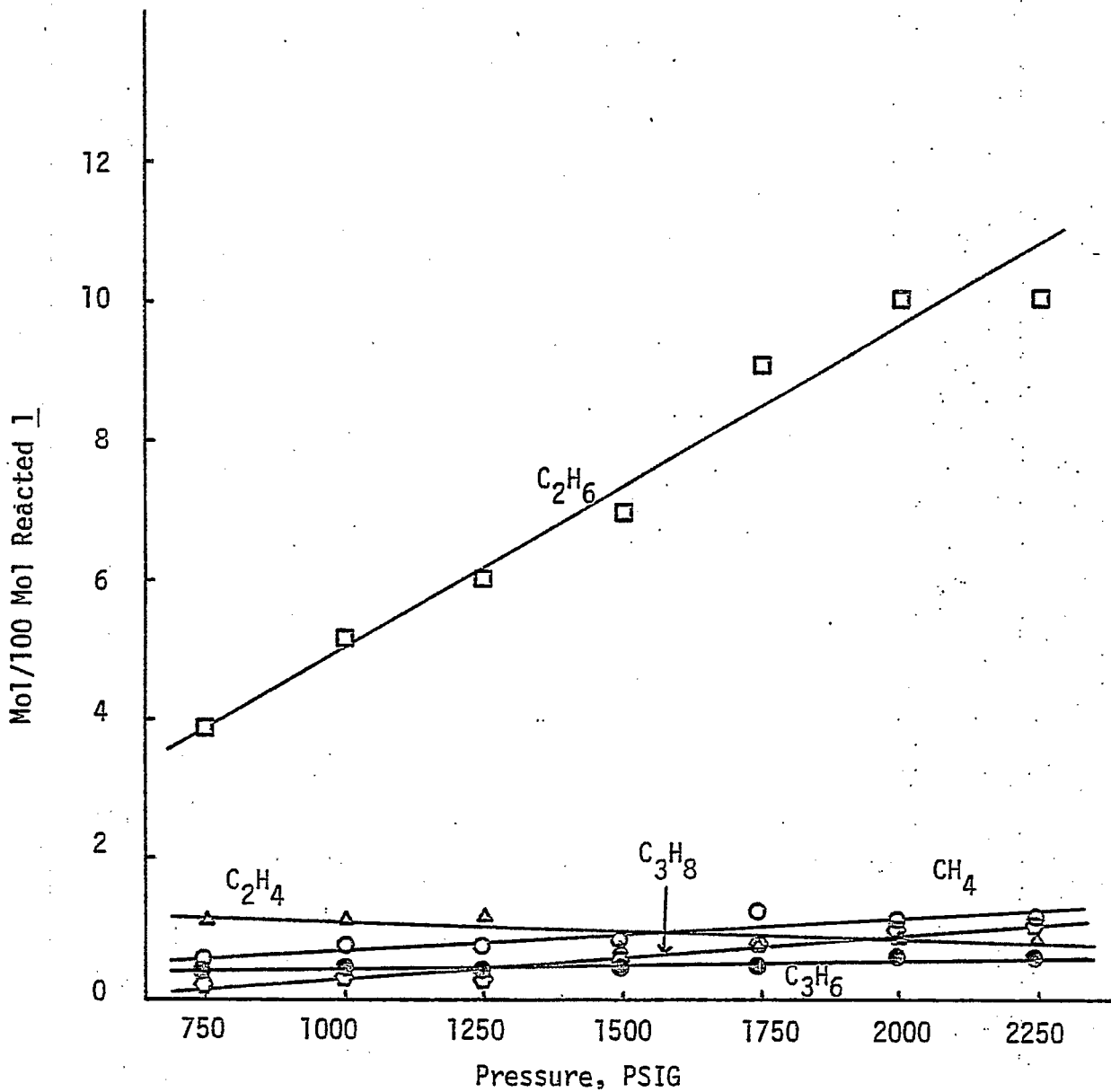


Fig 1. Change in composition of the gas product from hydrolysis of tetralin (1) as a function of hydrogen pressure; temperature: 550°C; LHSV: 3.1 hr<sup>-1</sup>.

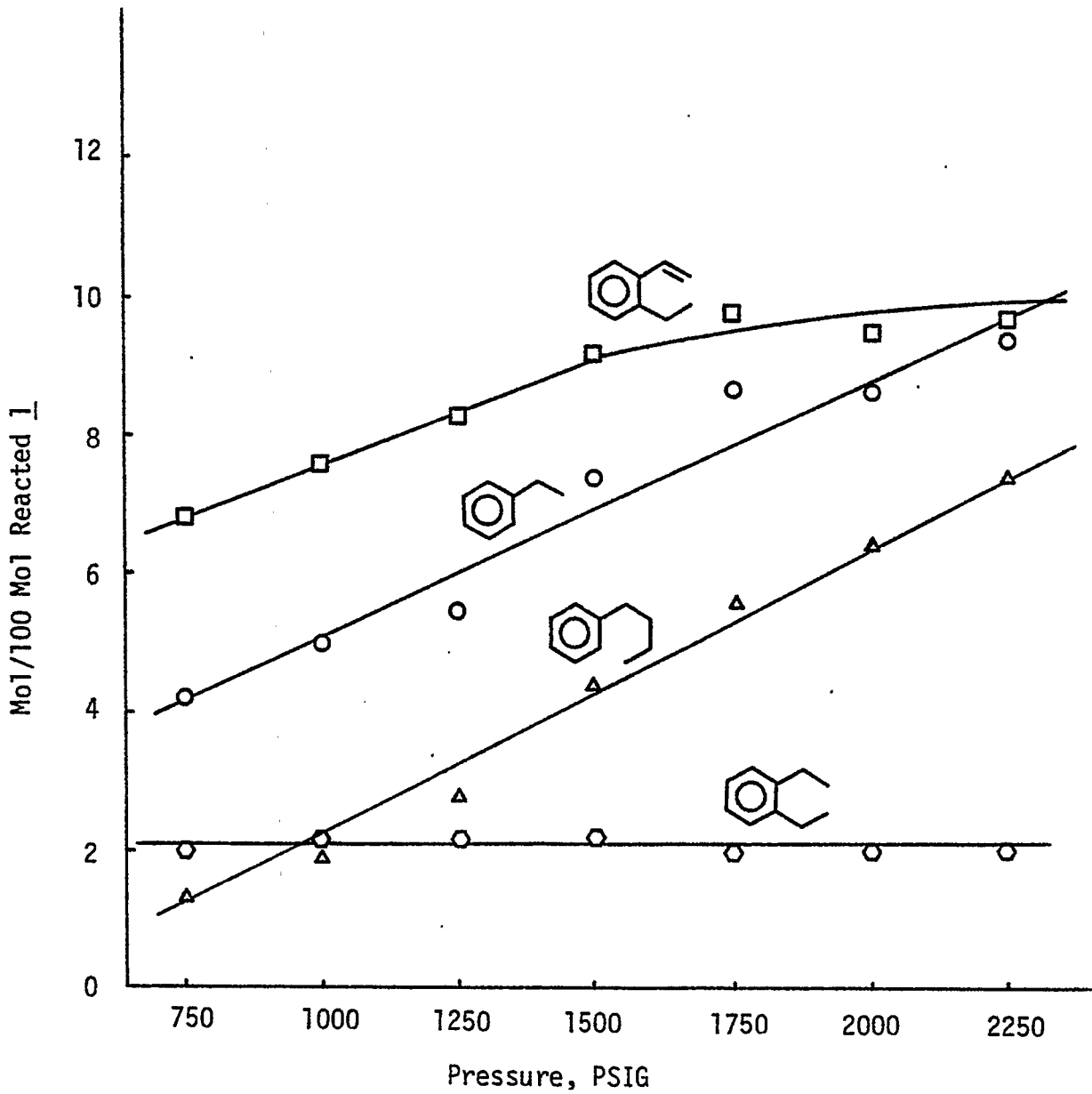


Fig 2. Change in composition of the alkylbenzene product from hydropyrolysis of tetralin (1) as a function of hydrogen pressure; temperature: 550°C; LHSV: 3.1 hr<sup>-1</sup>.

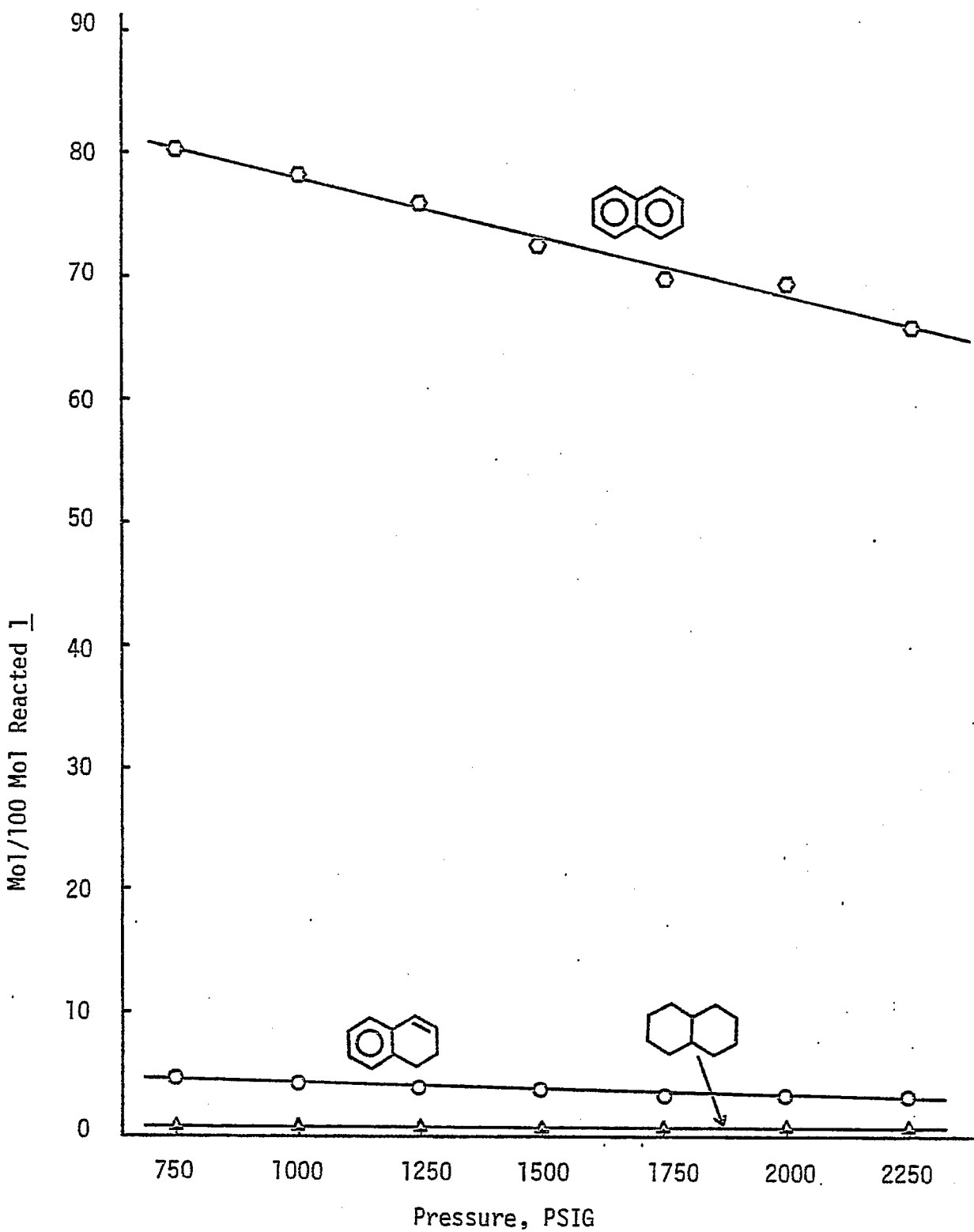


Fig 3. Change in composition of hydrogenation-dehydrogenation products from hydropyrolysis of tetralin (I) as a function of hydrogen pressure; temperature: 550°C; LHSV: 3.1 hr<sup>-1</sup>.



Systematic Structural Activity Study of Supported  
Sulfided Catalysts for Coal Liquids Upgrading

Faculty Advisors: F.E. Massoth  
J. Shabtai  
Post-Doctoral Fellow: Y. Liu  
N.K. Nag  
Graduate Student: K. Baluswamy

Introduction

The objective of this research is to develop an insight into the basic properties of supported sulfide catalysts and to determine how these relate to coal liquids upgrading. The proposed program involves a fundamental study of the relationship between the surface-structural properties of various supported sulfide catalysts and their catalytic activities for various types of reactions. Thus, there are two clearly defined and closely related areas of investigation, viz., (1) catalyst characterization, especially of the sulfided and reaction states and (2) elucidation of the mode of interaction between catalyst surfaces and organic substrates of different types. The study of subject (1) will provide basic data on sulfided catalyst structure and functionality, and would allow the development of catalyst surface models. Subject (2), on the other hand, involves systematic studies of model reactions on sulfide catalysts, and the utilization of data obtained for development of molecular level surface reaction models correlating the geometry (and topography) of catalyst surfaces with the steric conformational structure of adsorbed organic reactants. The overall objective of the project is to provide fundamental data needed for design of specific and more effective catalysts for upgrading of coal liquids.

Atmospheric activity tests using model compounds representative of hydrodesulfurization (thiophene), hydrogenation (hexene) and cracking (isooctene) were employed to assay changes in the catalytic functions of various supported CoMo catalysts. It was found that hydrodesulfurization (HDS) and hydrogenation (HYD) activities were generally unaffected by the type of alumina used or by the cobalt salt used in the preparation; whereas, cracking (CKG) activity varied considerably. Increase in Co or Ni content at a fixed Mo content of 8% resulted in considerably higher promotion of HDS activity than HYD activity. Addition of additives at 1/2% level to the standard CoMo/Al<sub>2</sub>O<sub>3</sub> catalyst generally increased HDS and CKG for acidic additives and decreased these functions for basic additives, HYD being unaffected. At 5% level, the additives decreased all functions, basic additives decreasing activities more severely. In a series of catalysts employing silica-alumina as the support, the HDS and hydrogenation functions decreased with increasing silica content, while cracking went through a maximum in activity. Catalysts prepared by supporting CoMo on TiO<sub>2</sub>, SiO<sub>2</sub>·MgO and carbon showed low activities, except for high cracking activity for the two former catalysts.

Oxide precursors of CoMo and Mo catalysts supported on various silica-aluminas evaluated by ESCA showed that support-active component interaction decreased with increase of silica in the support. It was also found that cobalt did not influence the Mo dispersion. On alumina, the Mo phase was found to be dispersed in essentially a monoatomic form.

Several catalysts, which were evaluated in the atmospheric pressure test unit, were subsequently tested at elevated pressure (34 atm) using dibenzothiophene (HDS), naphthalene (HYD) and indole (HDN). The high pressure runs were carried out sequentially in the order indicated to assess the separate catalytic functionalities. Repeat runs of HDS and HYD after HDN gave appreciably lower activities for HDS and HYD which was found to be due to strongly adsorbed residues containing nitrogen.

### Project Status

A summary of catalyst activity test results carried out at elevated pressure on a number of catalysts previously prepared and evaluated at atmospheric pressure is presented in Table 1. Conversions for HDS of benzothiophene, HYD of naphthalene and HDN of indole are given at fixed run conditions. Reproducibility of results on a different charge of the same catalyst was generally good. The relative activities are qualitatively in agreement with the previous results at atmospheric pressure, with respect to general ranking of catalyst activities, but lack quantitative correlation.

Comparisons of HDS activity with HYD and with HDN activities are shown in Figure 1. The lack of linear relationships and the scatter of the data imply that different sites on the catalysts are involved in HDS. Figure 2 shows the relationship between HDN and HYD activities. The much better linear fit would seem to indicate that HYD and HDN use the same sites. It should be mentioned that the HDN conversion as calculated in our data treatment method is related to the first C-N bond breaking step<sup>1</sup> (and not to a prehydrogenation step of the N-ring); thus, it would seem doubtful that the reaction of C-N splitting and aromatic ring HYD would occur on the same site. Indeed, evidence for differences in the nature of these sites has already been reported with respect to response to added H<sub>2</sub>S, viz., HYD decreased whereas HDN increased with increase in H<sub>2</sub>S in the feed.<sup>2</sup>

Activity of HDS of dibenzothiophene has been reported to correlate with O<sub>2</sub> adsorption.<sup>3,4</sup> We have previously reported no such correlation with thiophene at atmospheric pressure.<sup>5</sup> Correlation of our HDS dibenzothiophene data with O<sub>2</sub> data previously obtained also show a poor fit, as seen in Figure 3. Equally poor correlations were obtained for HYD and HDN. We conclude from the scatter but overall linearity of these plots that O<sub>2</sub> chemisorption is related to the general state of dispersion of the active Mo phase, but not to any specific active site, a conclusion reached earlier from the low pressure results.<sup>5</sup>

Because of the poor quantitative relationship between the high pressure and low pressure activities for the same catalysts, additional experiments on four catalysts were made at low and high pressure in the high pressure apparatus. For each catalyst, the following sequence

was carried out after sulfiding the catalyst: (1) at atmospheric pressure, thiophene HDS and hexene HYD were run in sequence; (2) the system was then pressurized to 500 psi and benzothiophene HDS and naphthalene HYD run in sequence; (3) finally, the pressure was reduced back to atmospheric and step (1) repeated. This procedure would assure that the low pressure and high pressure results were obtained on the same catalyst in the same reactor, and establish whether any catalyst deactivation occurred during the high pressure runs.

The low pressure conversions after the high pressure run were about the same as before the high pressure run, indicating no catalyst deactivation occurred as a result of the high pressure run. The general trend in conversions was the same for both the low and high pressure runs for HDS and HYD. Figure 4 shows a direct correlation for HDS between low and high pressure conversions. A less satisfactory linear correlation exists for HYD conversions. These results indicate that low pressure testing of catalysts for HDS and HYD can be expected to reasonably reflect catalytic activities under high pressure reaction conditions, at least with respect to model compound studies. The reason for the poorer correlation between the high pressure results and those obtained previously at low pressure is not known at present.

#### Future Work

A series of Ni-W catalysts will be tested at elevated pressure. The stirred-tank reactor will be assembled and used to test several catalysts for comparison with the fixed-bed reactor results at elevated pressure.

#### References

1. W.H. Wiser, F.E. Massoth, J. Shabtai, G. Muralidhar and Y. Liu, DOE Contract No. DE-AC01-79ET14700, Quarterly Progress Report, Salt Lake City, Utah, April-June 1982.
2. W.H. Wiser, F.E. Massoth, J. Shabtai, Y. Liu and K. Baluswamy, ibid., July-Sept 1982.
3. S.J. Tauster, T.A. Pecoraro and R. Chianelli, J. Catal., 63, 515 (1980).
4. S.J. Tauster and J.L. Riley, ibid., 67, 250 (1981).
5. W.H. Wiser, F.E. Massoth and W. Zmierczak, DOE Contract No. DE-AC01-79ET14700, Quarterly Progress Report, Salt Lake City, Utah, Oct-Dec 1981.

Table 1. Conversions for different Co-Mo catalysts at standard conditions.<sup>a</sup>

Catalyst No.	Run	Support <sup>b</sup>	Conversion, %		
			HDS	HYD	HDN
1	R 12	$\gamma$ -Al <sub>2</sub> O <sub>3</sub>	62.5	60.2	52.8
	R 18		65.3	59.0	49.5
	R 107		65.3	60.5	- -
2	R 10	10% SiO <sub>2</sub> -Al <sub>2</sub> O <sub>3</sub>	55.5	48.0	54.5
	R 17		66.7	60.7	54.0
	R 105		57.5	51.5	- -
3	R 11	25% SiO <sub>2</sub> -Al <sub>2</sub> O <sub>3</sub>	62.5	54.0	46.5
	R 106		57.5	53.5	- -
4	R 13	75% SiO <sub>2</sub> -Al <sub>2</sub> O <sub>3</sub>	17.0	49.0	21.7
5	R 9	SiO <sub>2</sub>	5.5	7.0	9.5
6	R 16	75% SiO <sub>2</sub> -MgO	38.0	28.0	20.0
8	R 15	CoMo/5% ZnAl <sub>2</sub> O <sub>3</sub>	67.1	64.8	54.0
9	R 14	5% Zn/CoMo-Al <sub>2</sub> O <sub>3</sub>	29.0	42.0	37.0
10	R 7	American Cyanamid	65.0	53.0	51.5
11	R 6	Topsoe B	87.5	57.0	61.0
12	R 4	Ketjenfine	72.5	49.5	51.0
13	R 19	1% Co-Mo/Al <sub>2</sub> O <sub>3</sub>	42.2	57.2	49.5
14	R 20	6% Co-Mo/Al <sub>2</sub> O <sub>3</sub>	87.3	68.5	62.5

<sup>a</sup>Standard conditions: 0.5 g Cat  
500 psi  
277°C for HDS and HYD  
350°C for HDN

<sup>b</sup>All catalysts contained 8% Mo and 3% Co, except 13 and 14.

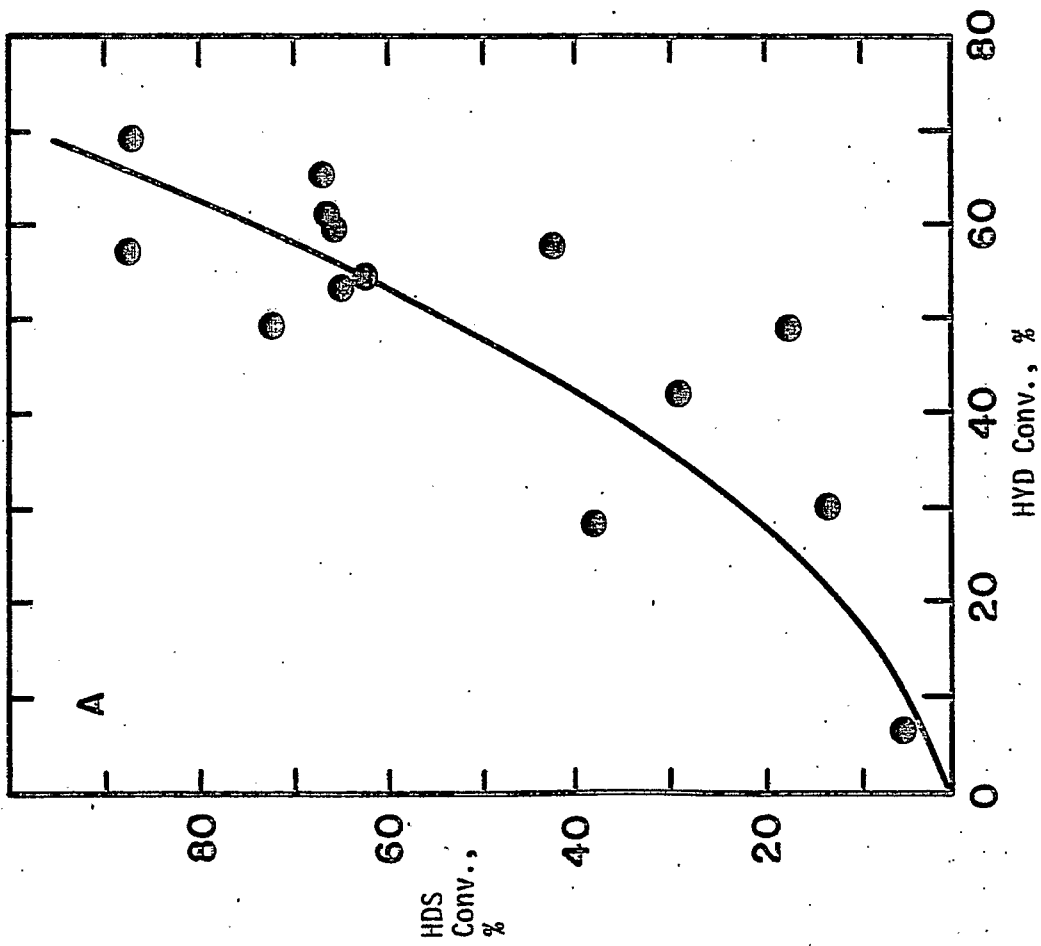
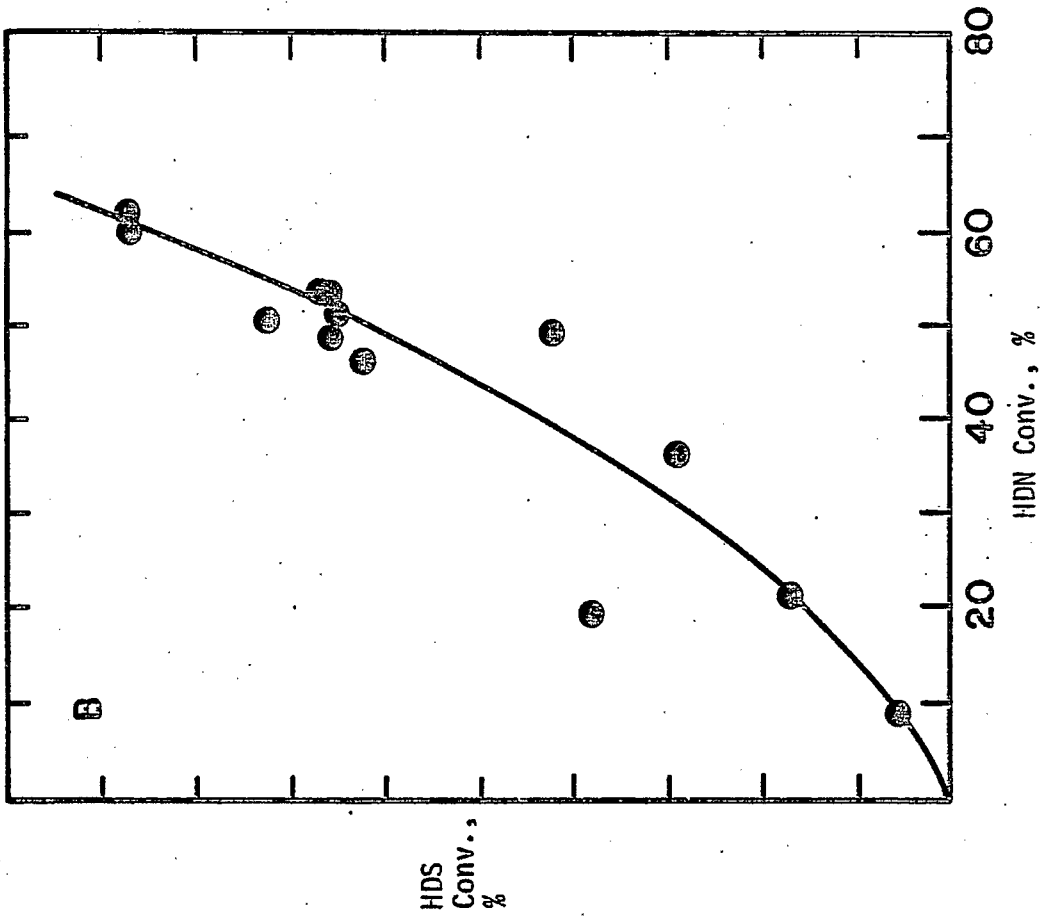


Figure 1. HDS conversion vs. (A) HYD conversion and (B) HDN conversion for various catalysts.

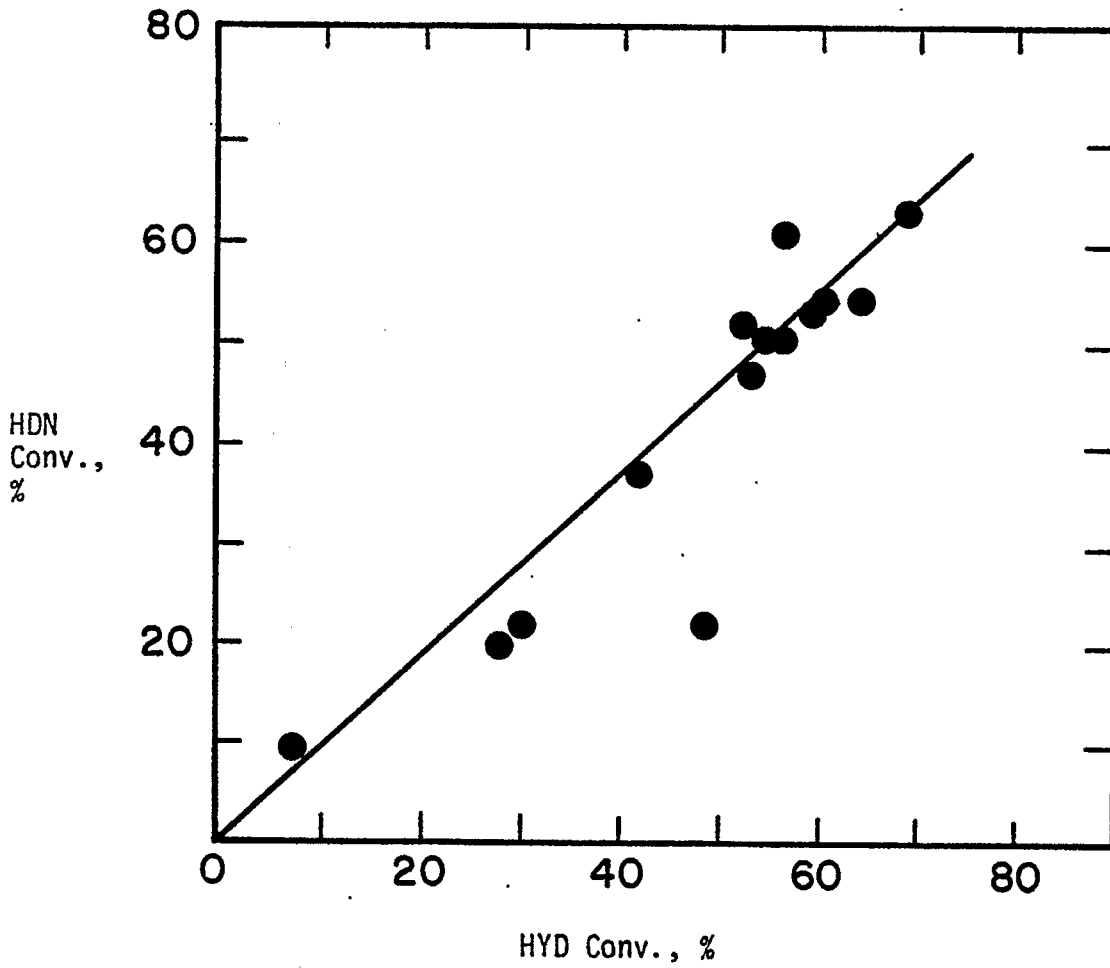


Figure 2. HDN conversion vs. HYD conversion for various catalysts.

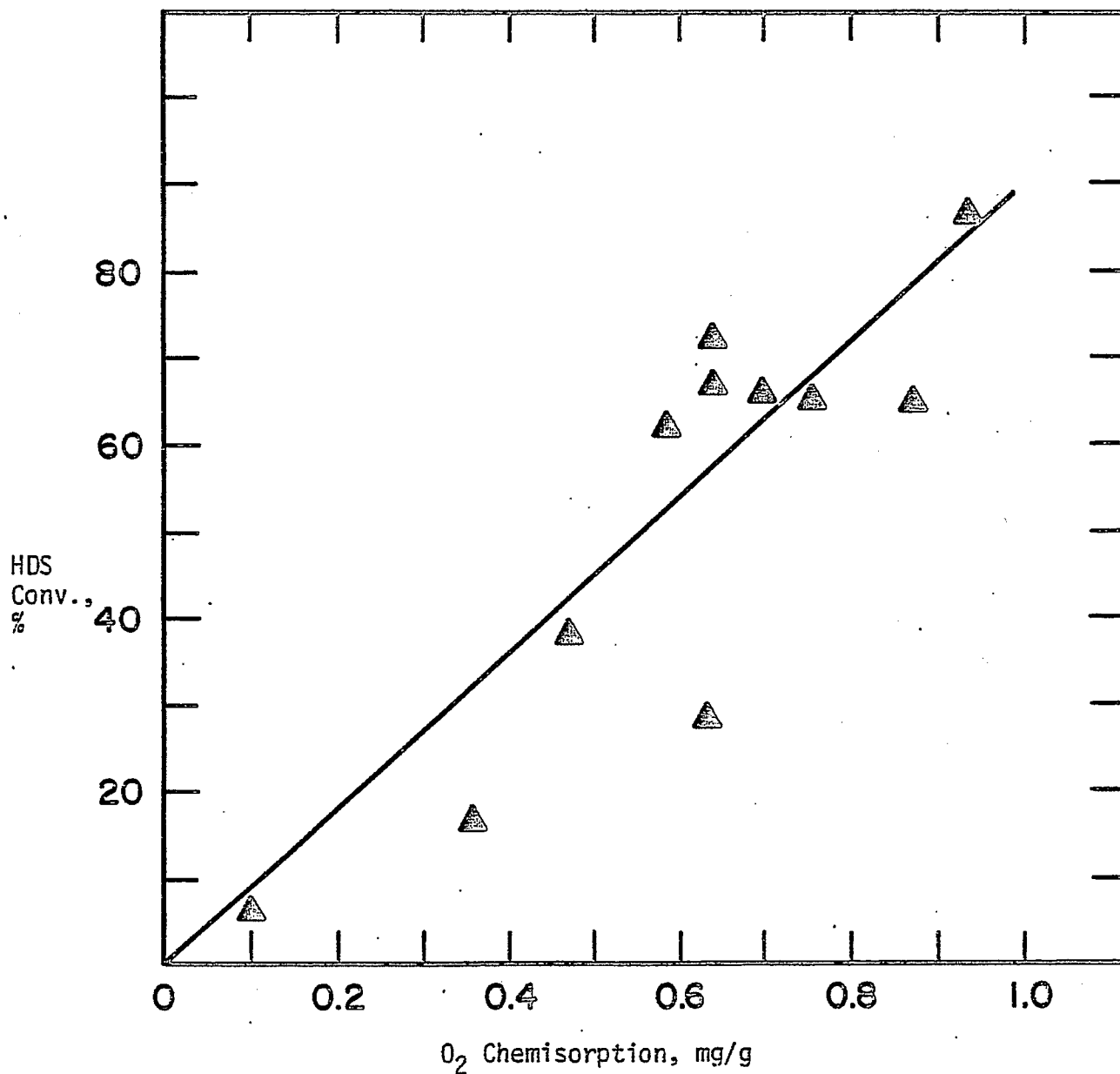


Figure 3. Correlation between HDS conversion and O<sub>2</sub> chemisorption.

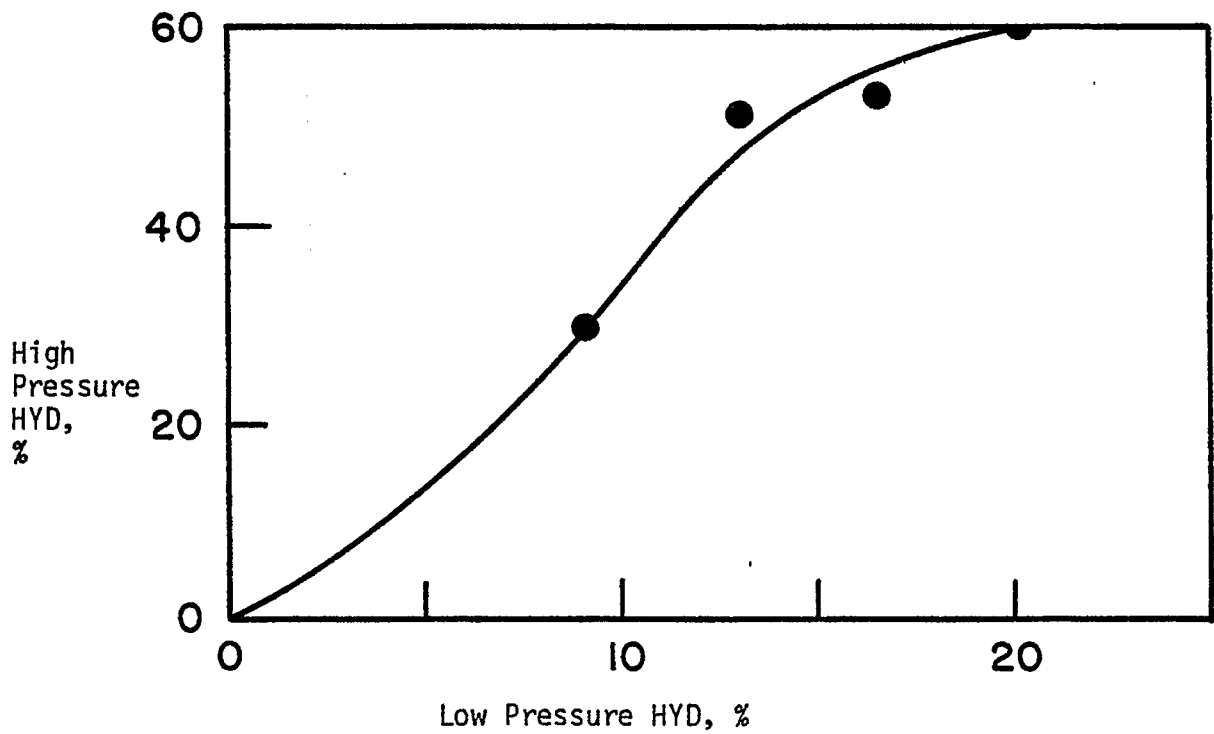
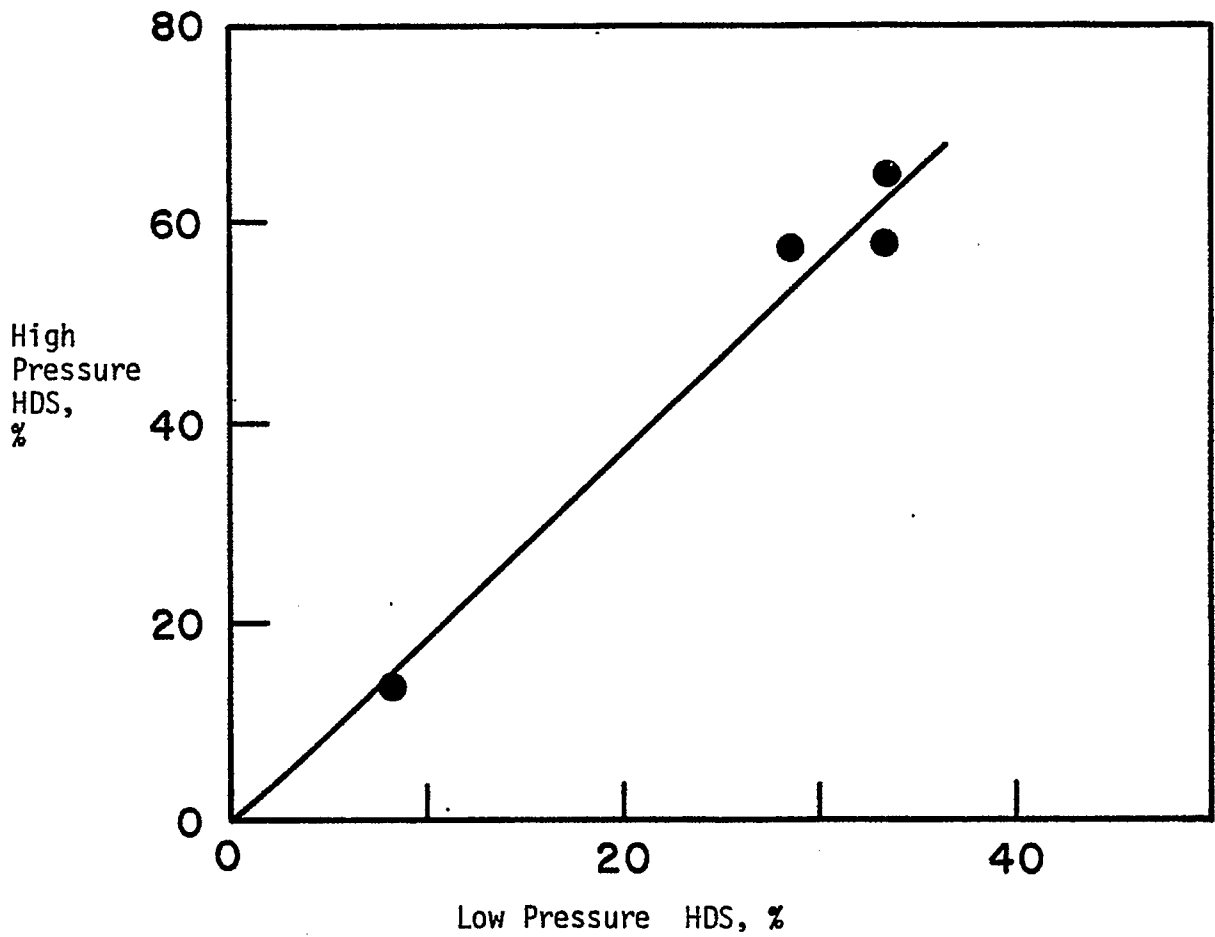


Figure 4. Relation between high and low pressure conversions for HDS and HYD.

Basic Study of the Effects of Poisons on the  
Activity of Upgrading Catalysts

Faculty Advisor: F.E. Massoth  
Post-Doctoral Fellow: J. Miciukiewicz

Introduction

The importance of cobalt-molybdena catalysts for hydrotreating and hydrodesulfurization of petroleum feedstocks is well-known. These catalysts are also being studied for hydrodesulfurization and liquefaction of coal slurries and coal-derived liquids. However, such complex feedstocks result in rapid deactivation of the catalysts. To gain an insight into the deactivation mechanism, the detailed kinetics of reactions of model compounds representative of heteroatom hydrogenolysis and hydrogenation are compared before and after addition of various poisons and coke precursors. The studies are carried out using a constant stirred microbalance reactor, which enables simultaneous measurement of catalyst weight change and activity. Supplementary studies are made to gain additional insight into the effect of poisons on the active catalyst sites. Finally, catalysts aged in an actual coal pilot plant run are studied to compare with laboratory studies.

Previous work on this project has shown that catalyst poisoning by pyridine or coke results in loss of active sites for benzothiophene HDS, but that the remaining unpoisoned sites retain their original activity. Pyridine appeared to be site selective in poisoning effect whereas coke was nonspecific. Furthermore, at least two HDS sites were indicated from the pyridine poisoning studies.

Poisoning of a CoMo/Al<sub>2</sub>O<sub>3</sub> catalyst with several nitrogen-containing compounds gave the following order of deactivation of hexene hydrogenation: quinoline > pyridine > indole > aniline. Thiophene hydrodesulfurization was deactivated more than hexene hydrogenation, but was less sensitive to the type of poison adsorbed. Poisoning with 2,6-dimethyl pyridine gave opposite results, hydrogenation being deactivated more than hydrodesulfurization, showing that steric and inductive effects are important in the effect of specific poisons on catalyst deactivation.

Project Status

Work has continued on the effects of N-compound poisoning on thiophene hydrodesulfurization (HDS) and 1-hexene hydrogenation (HYD) activities of a commercial CoMo/Al<sub>2</sub>O<sub>3</sub> catalyst.

It was reported earlier<sup>1</sup> that 2,6-lutidine (2,6-dimethyl pyridine) adsorbed at low concentrations on the CoMo/Al<sub>2</sub>O<sub>3</sub> catalyst gave an increase in HDS activity rather than the decrease expected from a poison, while at the same time hexene HYD was decreased. All other N-poisons studied resulted in decreases in both HDS and HYD activity.<sup>2</sup> To confirm this unusual result, poisoning studies with 2,6-lutidine were repeated. Also, the isomer 3,5-lutidine was studied to determine whether this

particular structure was unique or steric effects were operative. The experimental technique has been described in a previous report.<sup>1</sup>

The results of these poisoning experiments are given in Figure 1. Again the enhancement in HDS activity at low concentrations of adsorbed 2,6-lutidine were obtained, confirming earlier results. Of significance, 3,5-lutidine did not give the same response, showing deactivation of the HDS activity, as did pyridine. The deactivation response of the latter two N-compounds are identical within experimental error. As before, 2,6-lutidine showed rapid deactivation of HYD activity, opposite from its effect on HDS, and in agreement with earlier results. Deactivation with 3,5-lutidine and pyridine was somewhat less than with 2,6-lutidine, and the two former N-poisons gave essentially similar responses.

Adsorption isotherms for the three N-poisons are given in Figure 2. Also shown are similar isotherms for a  $\gamma$ -Al<sub>2</sub>O<sub>3</sub> support for two of the poisons. It is obvious that the majority of the adsorbed species occur on the sulfided CoMo phase rather than the catalyst support. The amount adsorbed follows the order: 3,5-lutidine > pyridine > 2,6-lutidine. This is in line with the higher basic strength of substituted ring structures with respect to 3,5-lutidine, but not for 2,6-lutidine. Compounds of the pyridine type can adsorb in two ways:<sup>3</sup> (1) perpendicular to the surface with  $\sigma$ -bonding through the N atom and (2) parallel to the surface with  $\pi$ -bonding of the ring. Bonding of the former type is considerably stronger than the latter, e.g., no poisoning of HDS activity was found with benzene. The low adsorption of the 2,6-lutidine is probably due to steric hindrance of the methyl groups adjacent to the N atom, preventing appreciable  $\gamma$ -bonding and leading to predominantly weaker  $\pi$ -bonding.

Analysis of the adsorption isotherms of Figure 2 revealed that they do not obey a Langmuir isotherm, but rather a Freundlich isotherm. The former isotherm is based on energetically identical adsorption sites, whereas the latter assumes a distribution of strengths of adsorption sites. It is therefore concluded that the adsorption sites of the catalyst are heterogenous.

To explain the deactivation effects observed in Figure 1, we propose adsorption of the N-compounds to occur on different strengths of active sites and in different modes of adsorption. The active sites are considered to be acidic in nature, consisting of vacancies (Lewis acid sites) on the MoS<sub>2</sub> surface arising from missing S atoms.<sup>4</sup> There is much evidence that the active sites for HDS of thiophene are geometrically different from those for HYD of olefins.<sup>4</sup> Strong poisons can adsorb at these sites, blocking access of reactants to these sites, and lower catalytic activity. The  $\sigma$ -bonded poisons are expected to be more strongly adsorbed than  $\pi$ -bonded poisons in this respect.

Considering first the HYD deactivation results, deactivation from 2,6-lutidine is not any less than from 3,5-lutidine or pyridine, and is in fact somewhat greater (Figure 1). Steric effects due to the methyl groups adjacent to the N-atom in 2,6-lutidine obviously do not come into play here. Therefore, adsorption on a HYD site may be via  $\pi$ -bonding (no steric effect expected) or via  $\sigma$ -bonding on a site of appropriate geometry that the methyl groups of 2,6-lutidine do not interfere with adsorption. To a first approximation, the three N-poisons should show identical poisoning deactivation with respect to amount adsorbed if they

are  $\pi$ -bonded regardless of strength of adsorption, and 3,5-lutidine and pyridine show such a response, but 2,6-lutidine does not. The stronger response of the latter could be due to some perpendicular  $\sigma$ -bonded adsorption, with partial overlap of the methyl groups on another adjacent HYD site. Thus, the same number of molecules adsorbed will cover somewhat more HYD sites with 2,6-lutidine than the others, accounting for greater deactivation. Since the increased deactivation effect is not pronounced, either both types of adsorption occur, or many adjacent HYD sites are not present.

For the case of HDS deactivation, the opposite effect is observed, viz., 2,6-lutidine shows less deactivation than the other N-compounds. Here, we propose that adsorption on the HDS site is sterically hindered by the methyl groups of 2,6-lutidine, and that adsorption must occur in a parallel configuration through  $\pi$ -bonding. Evidence of steric effects associated with HDS sites comes from the much lower HDS activity of 2,5-thiophene as compared to thiophene.<sup>5</sup> It is only speculation at this time as to the cause of the promotion of HDS activity at low levels of adsorption of 2,6-lutidine. If adsorption on a site adjacent to the HDS site (this may be a HYD site or another different site) is stronger than the relatively weak  $\pi$ -bonding on the HDS site, at low concentration, the N-molecule will be preferentially adsorbed on this adjacent site to the HDS site. The neighboring adsorbed molecule could then cause an inductive electronic effect on the HDS site, increasing its intrinsic activity for thiophene HDS. Alternatively, it could cause an increase in  $H_2$  adsorption, again increasing the thiophene activity. Whatever the cause, at higher levels of 2,6-lutidine, rapid deactivation occurs. Now, there are sufficient molecules available to adsorb directly on the HDS site and the deactivation curve approaches that of the other poisons. That this promotional effect does not occur with 3,5-lutidine or pyridine is likely due to strong  $\sigma$ -type adsorption (no steric effect expected) of these poisons on the HDS sites, leading to immediate deactivation even at low levels of poison on the catalyst.

### Future Work

A poisoning test with 2,6-lutidine using a laboratory prepared CoMo catalyst on pure  $\gamma$ - $Al_2O_3$  will be made to determine if the HDS enhancement observed with the commercial catalyst is due to an impurity or is indigenous to the active Mo sulfide phase. Kinetic studies of HDS and HYD on fresh, aged and regenerated catalysts which had been used in an H-coal PDU test will be started.

### References

1. W.H. Wiser and F.E. Massoth, DOE Contract No. DE-AC01-79ET14700, Quarterly Progress Report, Salt Lake City, Utah, April-June 1982.
2. ibid., July-Sept 1982.
3. M.J. Ledoux, P.E. Puger and G. Maire, J. Catal., 76, 285 (1982).
4. F.E. Massoth and G. Muralidhar, paper presented at Fourth Climax Intern. Conf. Chemistry and Uses of Molybdenum, Golden, Colorado, August 1982.

5. C.N. Satterfield, M. Modell and J.A. Wilkens, Ind. Eng. Chem., Proc. Des. Devel., 19, 154 (1980).

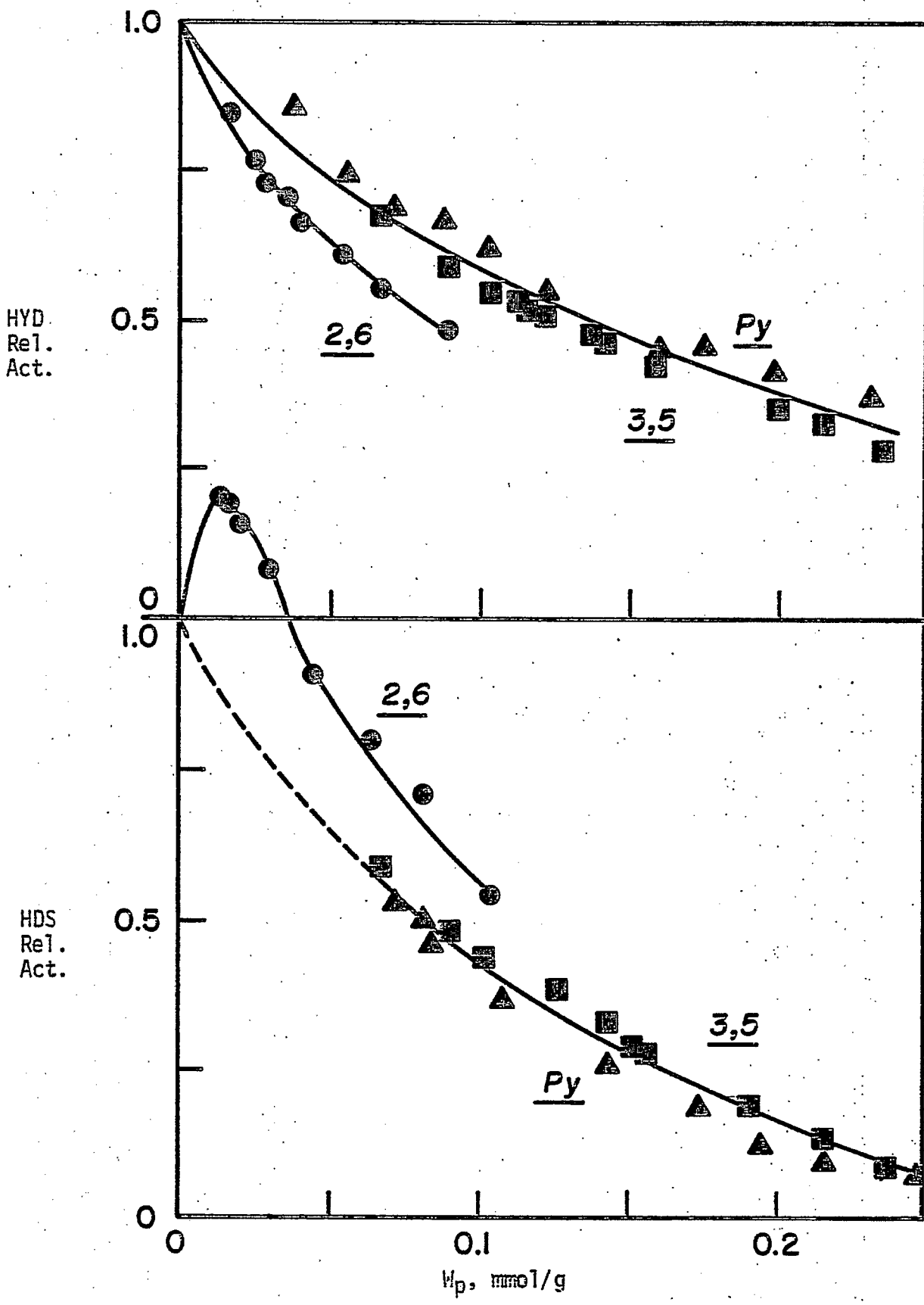


Figure 1. Relative HYD and HDS activity vs. amount of N-poison on catalyst. ● 2,6-lutidine, ■ 3,5-lutidine, ▲ pyridine.

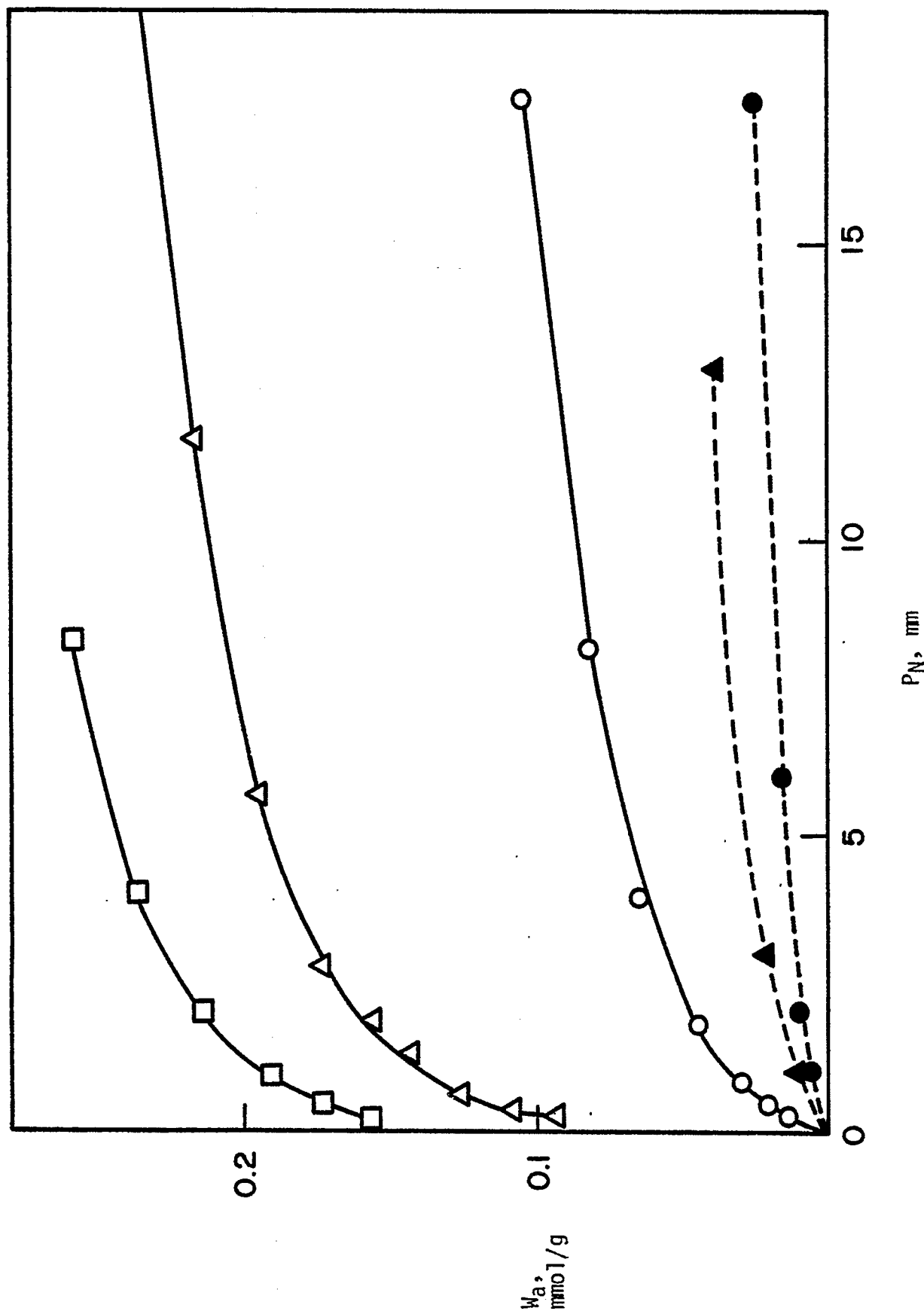


Figure 2. Adsorption isotherms for N-poisons on catalyst (open) and  $\gamma\text{-Al}_2\text{O}_3$  (solid).  
 □ 3,5 lutidine,  $\Delta$  2,6 lutidine, ○ 3,5 lutidine on  $\gamma\text{-Al}_2\text{O}_3$ , ● 2,6 lutidine on  $\gamma\text{-Al}_2\text{O}_3$ .

Diffusion of Polyaromatic Compounds in  
Amorphous Catalysts Supports

Faculty Advisor: F.E. Massoth  
Post-Doctoral Fellow: G. Seo

Introduction

This project involves accessing diffusional resistance within amorphous-type catalysts. Of primary concern is the question of whether the larger multiring hydroaromatics found in coal-derived liquids will have adequate accessibility to the active sites within the pores of typical processing catalysts. When molecular dimensions approach pore size diameters, the effectiveness of a particular catalyst is reduced owing to significant mass transfer resistance. An extreme case occurs when molecular and pore size are equivalent and pores below this size are physically inaccessible.

The project objective can be achieved through a systematic study of the effect of molecular size on sorptive diffusion rates relative to pore geometry. Conceptually, the diffusion of model aromatic compounds is carried out using a stirred batch reactor. The preferential uptake of the aromatic from the aliphatic solvent is measured using a UV spectrometer. Adsorption isotherms are determined to supplement the diffusion studies.

Four aromatic solutes ranging from 7 to 19 Å and four aluminas (representative of catalyst supports) having average pore sizes of 50 to 150 Å have been studied. The solutes were dissolved in cyclohexane solvent for ambient temperature studies. n-Dodecane was employed as solvent for high temperature studies because of its lower vapor pressure. Uptake experiments demonstrate that the slow step in the adsorption process was intraparticle diffusion. Equilibrium adsorption isotherms of the various solutes for the different aluminas in cyclohexane solvent were all nonlinear and well represented by Freundlich equations. Effective diffusivities were determined from the uptake data by applying a pore diffusion model incorporating a Freundlich isotherm. At higher temperature, reproducible adsorption isotherms were not obtained due to impurities in the dodecane. Effective diffusivities were calculated from the uptake data assuming a linear isotherm.

The effective diffusivities were found to be less than those for free pore diffusion, the ratio giving a measure of the restrictive effect due to pores. This restrictive factor was shown to decrease with increasing ratio of solute molecular diameter to alumina pore diameter. At ambient conditions, empirical correlations between the restrictive factor and the ratio of molecular to pore diameter were obtained, which agreed well with literature results for other systems.

No significant effect of pressure on effective diffusivities of solutes was observed up to 70 atm of hydrogen or helium. But the effect of temperature on effective diffusivities was significant. The increase in effective diffusivity was appreciably greater than predicted by the increase in bulk diffusivity for this temperature range. This difference indicates that pore diffusion is an activated process. Even at elevated temperature, the effective diffusivities to the free-solution diffusivities of the same cross-sectional area ( $D_e/D_{b\epsilon}$ ) were all less than unity, indicating that the mobility of the solutes in alumina is less than their mobility in free solution of same cross-sectional area.

### Project Status

The diffusion of coronene and tetraphenylporphine into three aluminas at elevated temperature was studied during this period. As there was an appearance of chemical reaction of tetraphenylporphine at 90°C during the diffusion experiment, at present the upper temperature was confined to 60°C. The increase in effective diffusivities of coronene and tetraphenylporphine into the aluminas with temperature was greater than the increase expected from bulk diffusion. The ratios of  $D_e/D_{b\epsilon}$ , indicating the mobility of the solutes in alumina to that in free solution of the same cross-sectional area, also increased as shown in Tables 1 and 2. The activation energy for diffusion increased with decrease in the pore size of the alumina.

Ratios of  $D_e/D_{b\epsilon}$  were previously correlated with a restrictive factor,  $F(\lambda)^1$ , viz.,

$$\frac{D_e}{D_{b\epsilon}} = \frac{F(\lambda)}{\tau_0} \quad (1)$$

where  $D_e$  is the effective diffusivity,  $D_b$  is bulk diffusivity,  $\epsilon$  is porosity,  $\lambda$  is the ratio of molecular diameter of diffusate to pore diameter, and  $\tau_0$  is the tortuosity of alumina when  $\lambda$  approaches zero. From a semi-logarithmic plot of  $D_e/D_{b\epsilon}$  versus  $\lambda$ , a straight line equation was derived for alumina at ambient temperature,<sup>1</sup> which had the form:

$$\ln\left(\frac{D_e}{D_{b\epsilon}}\right) = -4.5\lambda - 0.23 \quad (2)$$

Semi-logarithmic plots of  $D_e/D_{b\epsilon}$  versus  $\lambda$  for the present data (Tables 1 and 2) are shown in Figure 1. Even though the points show scatter, the logarithm of the group parameter  $D_e/D_{b\epsilon}$  decreased approximately linearly with increasing  $\lambda$  at each temperature. The slopes determined from least square analyses are 10 at 25°C, 7.9 at 40°C and 4.1 at 60°C. Thus, the slopes decrease with increasing temperature, indicating that the restrictive effect becomes less prominent as temperature increases. Thus, pore restriction is not only a function of  $\lambda$  but also of temperature.

Steric hindrance and hydrodynamic drag were suggested as possible causes of pore restriction for diffusion of solutes into small pores. Steric hindrance is determined by the ratio of physical size, and hydrodynamic drag is due to the forces between the wall and the diffusing molecule. At high temperature, the diffusing molecule has a larger kinetic energy and the interaction between the wall and the diffusate is decreased, e.g., the hydrodynamic drag is reduced at high temperature.

The effective diffusivities decreased markedly in dodecane solvent compared to cyclohexane, as shown in Table 3. This decrease might be due to a blocking effect of the large dodecane molecule.<sup>2</sup> The effect of the solvent on effective diffusivities can be compared by using the restrictive coefficient equation, as shown in Figure 2. In cyclohexane solvent, the coefficient is 4.5 and in dodecane it is 10, indicating the large dodecane solvent molecule reduced the diffusion rate of the solutes. To find a quantitative expression for the solvent effect, additional experimental results using several solvents of different molecular size will be required.

At present, the experimental results are scattered and are not enough to derive a quantitative expression for the temperature and solvent effects. It is convenient to express temperature and solvent effects on effective diffusivities in terms of the restrictive coefficient.

#### Future Work

Additional diffusion experiments of naphthalene and octaethylporphine in aluminas will be carried out at higher temperature. The diffusion in decane and hexadecane solvent will be studied for comparison of solvent effects.

#### References

1. A. Chantong, Ph.D. Thesis, University of Utah, Salt Lake City, Utah, 1982.
2. J. Caro, M. Bulow and J. Karger, AICHE J., 26, 1044 (1980).

Table 1. Effect of temperature on effective diffusivities of Coronene in alumina C, M and L.

Alumina	Temperature, °C	$D_b \times 10^6$ <sup>a</sup> cm <sup>2</sup> /s	$D_e \times 10^6$ <sup>b</sup> cm <sup>2</sup> /s	$D_e/D_b$ <sup>c</sup>	$E_a$ <sup>c</sup> kcal/mole
C	25	6.7	2.4	0.46	5.8
	40	8.9	4.8	0.69	
	60	12.5	6.7	0.69	
M	25	6.7	1.1	0.23	8.6
	40	8.9	3.1	0.49	
	60	12.5	5.1	0.58	
L	25	6.7	0.63	0.15	9.3
	40	8.9	1.2	0.21	
	60	12.5	3.2	0.40	

<sup>a</sup> $D_b$  is bulk diffusivity estimated from Wilke-Chang equation.

<sup>b</sup> $D_e$  is effective diffusivity in dodecane solvent.

<sup>c</sup>Values determined using Arrhenius plots.

Table 2. Effect of temperature on effective diffusivities of tetraphenylporphine in Alumina C and M.

Alumina	Temperature, °C	$D_b \times 10^6$ <sup>a</sup> cm <sup>2</sup> /s	$D_e \times 10^6$ <sup>b</sup> cm <sup>2</sup> /s	$D_e/D_b$	$E_a$ <sup>c</sup> kcal/mole
C	25	4.0	0.81	0.25	6.9
	40	5.4	1.4	0.32	
	60	7.5	2.7	0.46	
M	25	4.0	0.15	0.05	13
	40	5.4	0.48	0.13	
	60	7.5	1.5	0.28	

<sup>a</sup> $D_b$  is bulk diffusivity estimated from Wilke-Chang equation.

<sup>b</sup> $D_e$  is effective diffusivity in dodecane solvent.

<sup>c</sup>Values determined using Arrhenius plots.

Table 3. Comparison of effective diffusivities of coronene and tetraphenylporphine into aluminas in cyclohexane and dodecane solvent at 25°C.

Solute	Alumina	$D_e \times 10^6$ , cm <sup>2</sup> /s	
		Cyclohexane <sup>a</sup>	dodecane <sup>b</sup>
Coronene	C	4.1	2.4
	M	2.4	1.1
	L	2.1	0.63
Tetraphenylporphine	C	1.6	0.81
	M	0.66	0.15

<sup>a</sup>Reference 1.

<sup>b</sup>Present data.

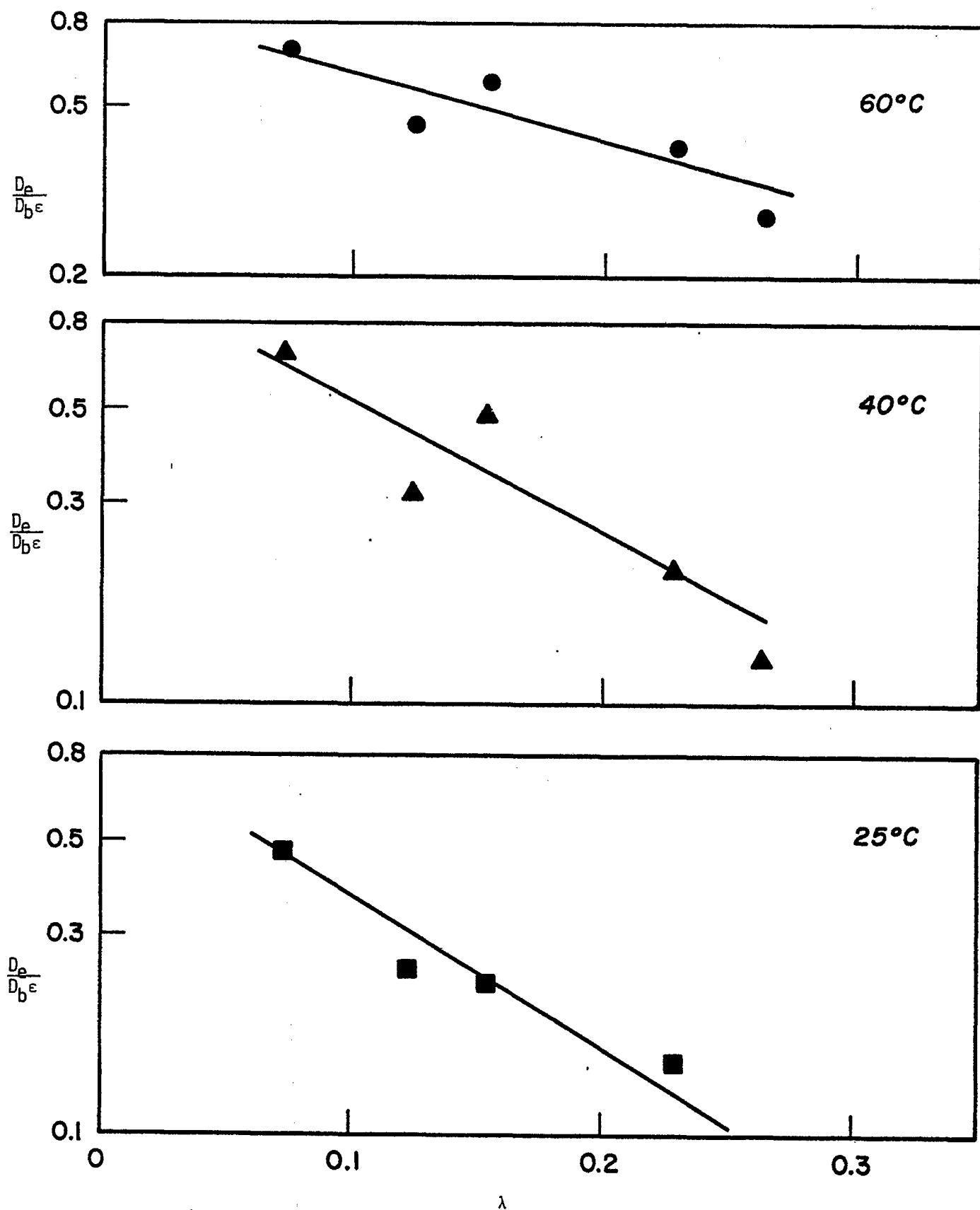


Figure 1. Semi-logarithmic plots of  $D_e/D_b\epsilon$  versus  $\lambda$  at 25°C (■), 40°C (▲) and 60°C (●).

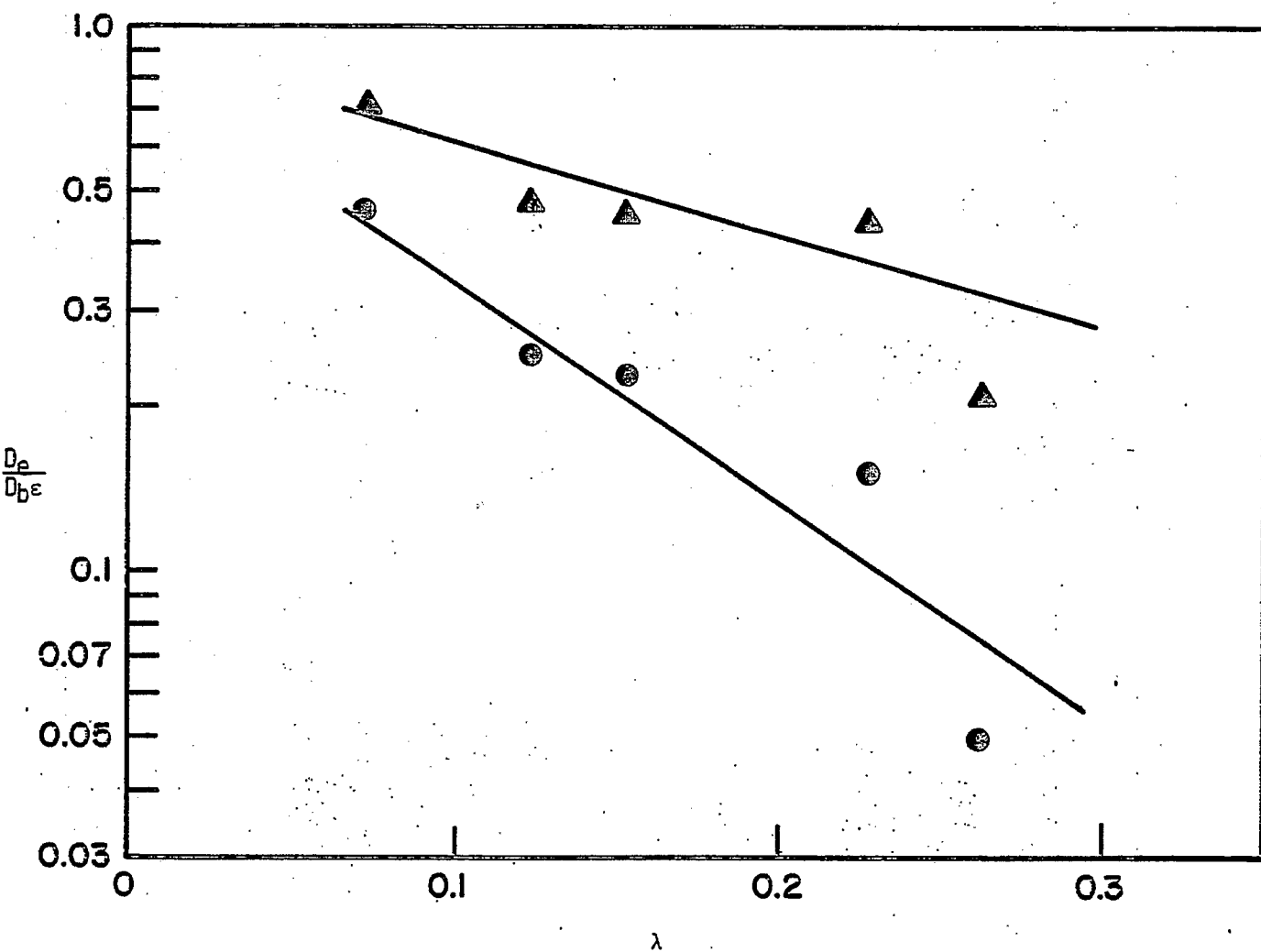


Figure 2. Semi-logarithmic plots  $D_e/D_{be}$  versus  $\lambda$  in cyclohexane<sup>I</sup> ( $\blacktriangle$ ) and dodecane ( $\bullet$ ) solvents at 25°C.

## Catalyst Research and Development

Faculty Advisor: F.V. Hanson  
Graduate Students: C.S. Kim  
K.R. Chen

### Introduction

The objectives of this project are to develop a preparation technique for a Raney type catalyst (particularly Raney iron-manganese), to establish catalyst characterization techniques, and to determine the optimum process variables for the maximum production of gasoline boiling range hydrocarbons, low molecular weight olefins and BTX via hydrogenation of carbon monoxide. A detailed discussion of the objectives was presented in a previous report.<sup>1</sup>

An electric heating furnace was built to prepare the Al-Fe and Al-Fe-Mn alloys. Several samples of aluminum alloys were prepared and an optimum preparation technique was developed.

A stirred-tank reactor was fabricated to activate the alloys in an aqueous solution of sodium hydroxide at different activation conditions and is working satisfactorily.

A high pressure fixed-bed reactor system has been built to determine the catalyst composition and activation variables which will optimize the catalyst activity and selectivity. The same reactor will be used for the process variable investigation.

A thermogravimetric analysis technique was used to determine an optimum reduction temperature. The optimum temperature was 400°C for precipitated catalysts and 375°C for Raney catalysts. All the catalysts were reduced under a hydrogen gas stream at the optimum temperature for 5 hours, just prior to the activity test in the fixed-bed.

A series of exploratory runs were made to determine a proper range of process variables for a standard catalyst screening test. The catalysts were tested at the following conditions in the fixed-bed reactor: pressure, 200 psig; space velocity, 3.0 cc/g-cat-sec; H<sub>2</sub>/CO, 2.0; temperature, 423 to 473 K. Raney Fe and Raney Fe-Mn catalysts showed higher catalytic activity than the precipitated Fe and Fe-Mn catalysts, respectively, by two to four times, while the product selectivity of Raney catalyst was quite comparable to each corresponding precipitated type catalyst. However, Fe-Mn catalysts (Raney and coprecipitated type) showed higher olefin selectivity, especially C<sub>2</sub>-C<sub>4</sub> olefins, compared to Fe catalyst of both types. At the same preparation conditions, a high temperature leaching (above 323 K) and a high NaOH concentration (20%) leaching yielded Raney catalysts with the highest catalytic activity.

The composition of Raney catalysts has been determined by Atomic Absorption. The BET surface area of Raney Fe catalysts ranged from 26 to 54 m<sup>2</sup>/g, while the surface area of Raney Fe-Mn catalysts ranged from 64 to 116 m<sup>2</sup>/g.

The phases in the Raney catalysts have been identified by X-ray diffraction. A major phase in all the Raney catalyst was  $\alpha$ -Fe. Magnetite was found from Raney catalysts prepared at 363 K and unreacted aluminum alloy phases were found from catalysts prepared below 323 K.

### Project Status

Electron probe microanalysis has been completed for Al-Fe (50/50 wt %) and Al-Fe-Mn (59/38/3 wt %) alloys. The above two alloys were homogenized by heating at 1173 K for 2 days in evacuated quartz tubes. Standard metallographic techniques were used to prepare specimens for the optical micrograph and probe analysis as described in the previous report.

An optical micrograph of the Al-Fe alloy etched with 20 volume % sulfuric acid at 70°C is presented in Figure 1. Two regions with different shades are shown in the micrograph, indicating the presence of two different metal phases. Microprobe analysis indicated that the dark regions had compositions of  $Fe_2Al_5$  whereas the white regions had composition of  $FeAl_2$ . The probe analysis confirmed the presence of two phases,  $FeAl_2$  and  $Fe_2Al_5$ , consistent with the phase diagram of binary Al-Fe alloy at the composition of Al/Fe = 50/50 wt %.

The surface of an unetched Al-Fe-Mn (59/38/3 wt %) alloy, homogenized at 1173 K for 2 days, was scanned by microprobe. The composition of the alloy was found to be uniform, indicating there was only a single phase and the absence of any second phase. The composition of the alloy corresponded to (Fe, Mn)  $Al_3$ .

From Figure 1 it can be seen that the grain size of  $FeAl_2$  phases is about 400 micron maximum. It is blade-shaped and some remaining dendrite structure can be seen.

The major phase in the Raney Fe and Raney Fe-Mn catalysts was  $\alpha$ -Fe as indicated in the previous report.<sup>3</sup> The crystallite size of the  $\alpha$ -Fe was estimated by X-ray line broadening technique. The experimental technique was the same as the one used for X-ray diffraction of the catalyst for phase identification. The catalyst sample was scanned from 10 to 80° (2 $\theta$ ) at a scanning speed of 1/20°/min (2 $\theta$ ). An  $\alpha$ -quartz powder was used as a standard to estimate instrumental line broadening. The crystallite size was estimated using the Warren's equation (1)<sup>4</sup> and Scherrer's Equation (2)<sup>5</sup> as follows:

$$B^2 (\text{true}) = B^2 (\text{experimental}) - B^2 (\text{instrumental}) \quad (1)$$

$$L = \frac{k\lambda}{B \cos \theta} \quad (2)$$

where B: line broadening of diffraction peak at half maximum intensity, 1/2.I max (radians)

k: shape factor, equal to 0.9

$\theta$ : diffraction angle (radian)

$\lambda$ : wavelength of X-ray (Å)

L: crystallite size (Å)

Although the Scherrer's Equation (2) is not regarded as being accurate in determining a crystallite size, it gives a relatively accurate measure of

the crystallite size, especially for a group of catalysts prepared by the same procedures. Since the Al-Fe and Al-Fe-Mn alloys both have intense reflections near the diffraction peak of  $\alpha$ -Fe at (110) plane, the above estimation could not be made for the catalysts which contained some remaining alloy phases due to the overlapping of the diffraction peaks. This was the case for catalysts prepared below 323 K or prepared with low concentrations of NaOH solution (less than 20%).

Table 1 lists the crystallite sizes determined. From Table 1 it can be seen that a high temperature leaching (363 K) yielded a catalyst with a large crystallite size compared to the one prepared at a low temperature (323 K) if all other preparation conditions (leaching mode and NaOH concentration) were the same. The effect of the leaching temperature on the crystallite size was the most pronounced in the case of Raney Fe prepared by alloy addition method. A mere difference of 40 K in the leaching temperature resulted in a difference in crystallite size by about two times.

This trend between the leaching temperature and the crystallite size was quite consistent with observations made by Robertson and Anderson,<sup>5</sup> who found that a low temperature leaching yielded a Raney nickel catalyst with small crystals.

The BET surface area of the Raney Fe and Fe-Mn catalysts was correlated with the crystallite size of  $\alpha$ -Fe by Equation (3) suggested by Allred et al.<sup>7</sup> as follows:

$$\zeta = \frac{kf10^4}{Ld} \quad (3)$$

where  $\zeta$ : BET surface area ( $\text{m}^2/\text{g}$ )

k: geometric factor, equal to 6 for spherical or cubic crystallites

f: fraction of crystallite surface available for gas adsorption

d: density ( $\text{g}/\text{cm}^3$ )

L: mean size of crystallite ( $\text{\AA}$ )

Table 1 lists the BET surface area and the reciprocal of the crystallite size of  $\alpha$ -Fe in the Raney catalysts. Figure 2 shows that a linear relationship exists between the two parameters. The f-value was calculated from the slope of the line in Figure 2, using  $k=6$  and  $d=7.86$  for body-centered cubic crystals of  $\alpha$ -Fe. The real density of  $\alpha$ -Fe in the Raney catalysts must be somewhat lower than the value used in the calculation 7.86. The f-value obtained was 0.74, which was quite close to 0.65 for the Raney nickel catalyst with face-centered cubic structures of nickel, obtained by Robertson and Anderson.<sup>6</sup>

The catalytic activity and selectivity of Raney Fe and Raney Fe-Mn catalysts have been tested in a fixed-bed reactor and reported in previous reports.<sup>8,9</sup> The kinetic parameters, such as activation energy and pre-exponential factors, have been determined using a first order kinetic equation as described in the previous report.

Table 2 lists relative activities of the Raney Fe catalysts obtained by comparing the first order rate constants for Raney Fe catalysts with the rate constant for the precipitated Fe catalyst. The rate constant was obtained by back calculation from a best-fitting Arrhenius plot for each catalyst, using a least-square method.

The relative activities were obtained by taking the rate constant for precipitated Fe catalyst at each temperature as 1.0. The relative activities in the parentheses are the relative activity values of the precipitated Fe catalyst at each temperature obtained by taking the rate constant at 423 K as 1.0.

Table 2 shows that the relative activity of a catalyst increased with increasing temperature when the activation energy of the catalyst was higher than that of the precipitated Fe catalyst, 26 kcal/mol, and vice versa. The most noticeable increase was found with the R-Fe-A50 (Raney Fe, prepared by alloy addition at 50°C) catalyst for which the activation energy was the highest. All the Raney Fe catalysts were more active than the precipitated Fe catalyst except for the R-Fe-C90 (10%) catalyst (Raney Fe, prepared by addition of 10% NaOH solution).

When comparing the activities of Raney Fe catalysts, prepared at different leaching temperature, the activities of Raney Fe catalyst, prepared at a low leaching temperature (25°C) were lower than the activities of the catalysts prepared at higher temperatures (50°C and 90°C), irrespective of the preparation mode, alloy or caustic addition. At the same leaching temperature the 10% NaOH solution leaching resulted in a catalyst with lower activity than the 20% solution leaching as can be seen from the data of R-Fe-C90 and R-Fe-C90 (10%) catalysts.

No reasonable correlation could be established between the BET surface areas and the relative activities of the Raney Fe catalysts. A correlation could have been developed by determining the number of active sites for the reaction on each catalyst from selective chemisorption of CO and H<sub>2</sub>.

A detailed product selectivity data for Raney Fe catalysts were included in a previous report.<sup>8</sup> The product selectivities for the Raney Fe catalysts were quite comparable to the selectivities for the precipitated Fe catalyst.

Figure 3 shows the change of C<sub>2</sub>-C<sub>4</sub> hydrocarbon olefin/paraffin ratio with reaction temperature. The C<sub>2</sub>-C<sub>4</sub> O/P ratio decreased with increasing temperature. No noticeable difference in C<sub>2</sub>-C<sub>4</sub> O/P ratio was found between different Fe catalysts, irrespective of preparation mode and catalyst type, especially at a high temperature, 453 K. The C<sub>2</sub>-C<sub>4</sub> O/P ratio at 453 K ranged from 1.0 to 1.5.

Figure 4 shows the variation of O/P ratio of each hydrocarbon C<sub>2</sub>, C<sub>3</sub> and C<sub>4</sub> with temperature in the case of R-Fe-A90 catalyst (Raney Fe, prepared by alloy addition at 90°C).

The C<sub>2</sub> O/P ratio decreased markedly with increasing temperature, while C<sub>3</sub> and C<sub>4</sub> O/P ratios remained constant or decreased moderately. The resultant total C<sub>2</sub>-C<sub>4</sub> O/P ratio decreased with increasing temperature, mainly due to the sharp decrease of the C<sub>2</sub> O/P ratio. All other Fe catalysts exhibited similar trends.

Table 3 lists the kinetic parameters and relative activities of Raney Fe-Mn catalysts. All the Raney Fe-Mn catalysts were more active than the coprecipitated Fe-Mn catalyst by 2 to 4 times at the reaction conditions under study. A similar trend was found between catalyst activity and preparation condition (leaching temperature and NaOH concentration) as has been explained previously for the Raney Fe catalysts.

The product selectivities of Raney Fe-Mn catalysts were comparable to the selectivity of coprecipitated Fe-Mn catalysts as can be seen in the previous reports.<sup>8</sup> However, there was a noticeable difference in the C<sub>2</sub>-C<sub>4</sub> O/P ratio between Raney Fe and Raney Fe-Mn catalysts.

Figure 5 shows the variation of C<sub>2</sub>-C<sub>4</sub> O/P ratios of Raney Fe-Mn catalysts with temperature. The C<sub>2</sub>-C<sub>4</sub> O/P ratios remained quite constant or slightly increased with increasing temperature. The C<sub>2</sub>-C<sub>4</sub> O/P ratios of Raney Fe-Mn catalysts ranged from 1.8 to 2.5 at 453 K, which is about two times the C<sub>2</sub>-C<sub>4</sub> O/P ratios of Raney Fe catalysts at the same reaction condition. Figure 6 shows the variation of the O/P ratio of each C<sub>2</sub>, C<sub>3</sub> and C<sub>4</sub> hydrocarbon with temperature for R-FeMn-C90 catalyst (Raney Fe-Mn, caustic addition at 90°C).

The C<sub>2</sub> O/P ratio decreased (Figure 6) with increasing temperature, while the C<sub>3</sub> and C<sub>4</sub> O/P ratios increased markedly. The resultant C<sub>2</sub>-C<sub>4</sub> O/P ratio increased moderately with increasing temperature.

A correlation between the activation energy and the pre-exponential factor for the Raney Fe and Raney Fe-Mn catalysts is presented in Figure 7. A linear relationship exists between the two kinetic parameters, lnA and E<sub>a</sub>. The slope of the line is 1/RT, from which the isokinetic temperature can be obtained.<sup>9</sup> At the isokinetic temperature, 442 K, the reaction rates on all the catalysts become the same. Above the isokinetic temperature a catalyst with a higher activation energy has a higher k value (rate constant) or higher catalytic activity, while below that temperature the reaction rate of a catalyst with a lower activation energy becomes higher.

### Future Work

Mr. C.S. Kim is preparing his Ph.D thesis and Mr. K.R. Chen is completing the process variable experiments with the Raney Fe/Mn catalysts. Immediate future work will include a statistically designed process variable study of CO hydrogenation over a Raney Fe-Mn catalyst and the completion of the leaching kinetics for Al-Fe and Al-Fe-Mn alloy. Long range future work will include a detailed kinetic study of CO hydrogenation and a selective chemisorption study.

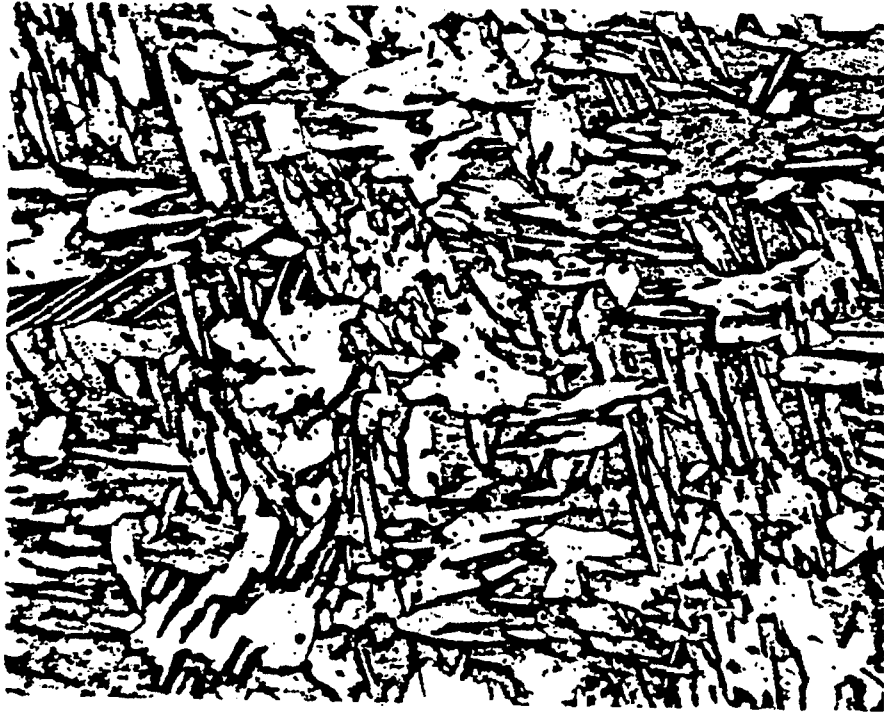
### References

1. W.H. Wiser, F.V. Hanson and C.S. Kim, DOE Contract No. DE-AC01-79ET 14700, Quarterly Progress Report, Salt Lake City, Utah, Oct-Dec 1979.
2. ibid., July - Sept 1981.
3. ibid., Jan - Mar 1982.

4. B.C. Warren, J. Appl. Phys., 12, 375 (1941).
5. P. Scherrer, Goettinger Nachr., 2, 98 (1918).
6. S.D. Robertson and R.B. Anderson, J. Catal., 23, 286 (1971).
7. V.D. Allred, S.R. Buxton and J.P. McBride, J. Phys. Chem., 61, 117 (1957).
8. W.H. Wiser, F.V. Hanson and C.S. Kim, DOE Contract No. DE-AC01-79 ET 14700, Quarterly Progress Report, Salt Lake City, Utah, Apr-June 1982.
9. M. Boudart, "Kinetics of Chemical Processes," Prentice Hall, Inc. New Jersey, 1968, p. 181.

Figure 1. Optical micrograph of Al-Fe alloy. Sample etched with 20 vol %  $H_2SO_4$  solution at  $70^{\circ}C$  for 30 sec.

200 X



400X

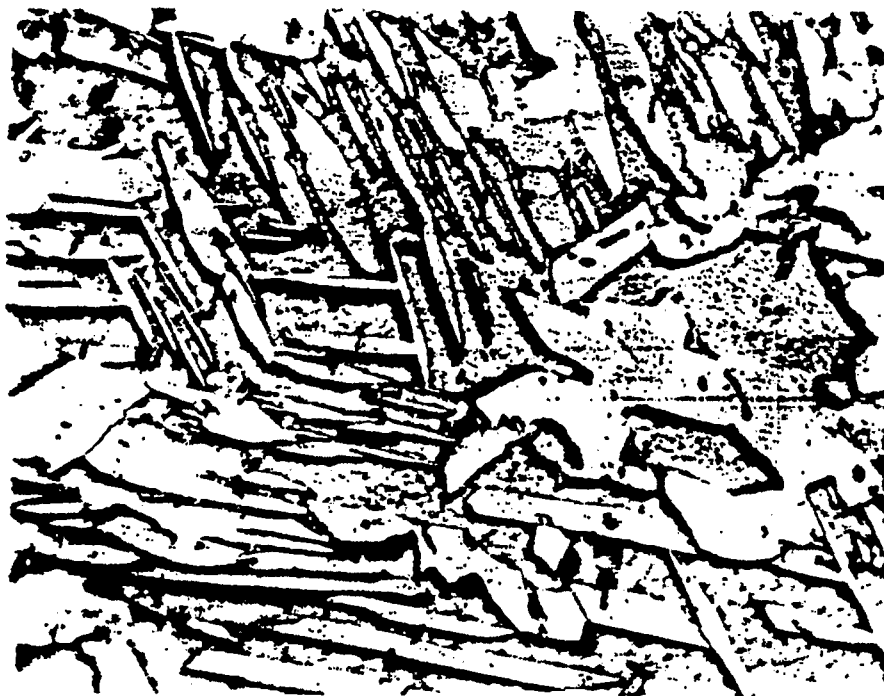


Figure 2. Correlation of surface area and crystallite size.

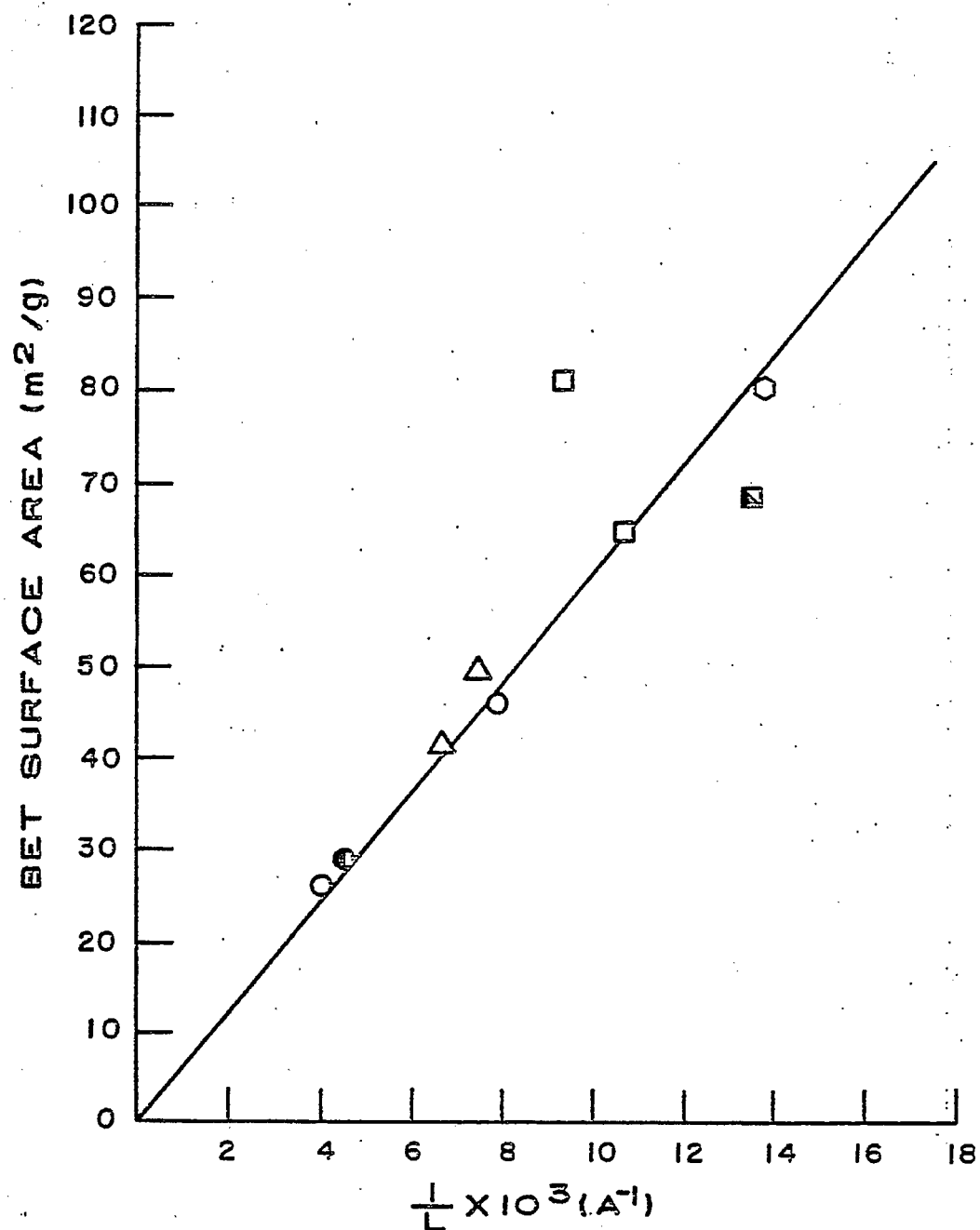


Figure 3. C<sub>2</sub>-C<sub>4</sub> O/P ratio for Raney Fe catalyst. Pressure: 1378 KPa (200 psig), H<sub>2</sub>/CO: 2.0, SV: 3.0 cm<sup>3</sup> g<sup>-1</sup>s<sup>-1</sup>.

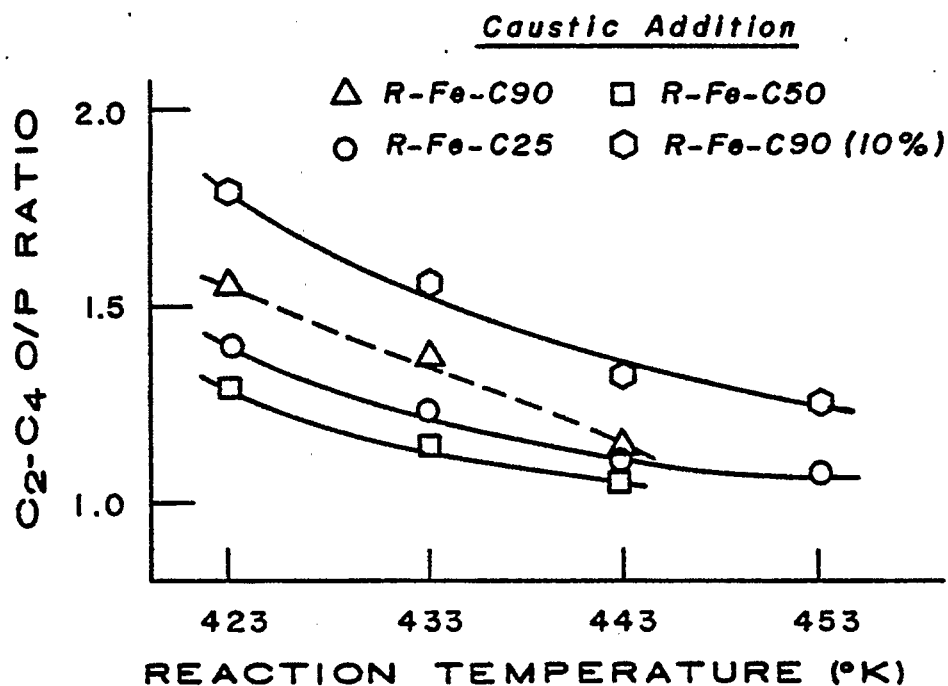
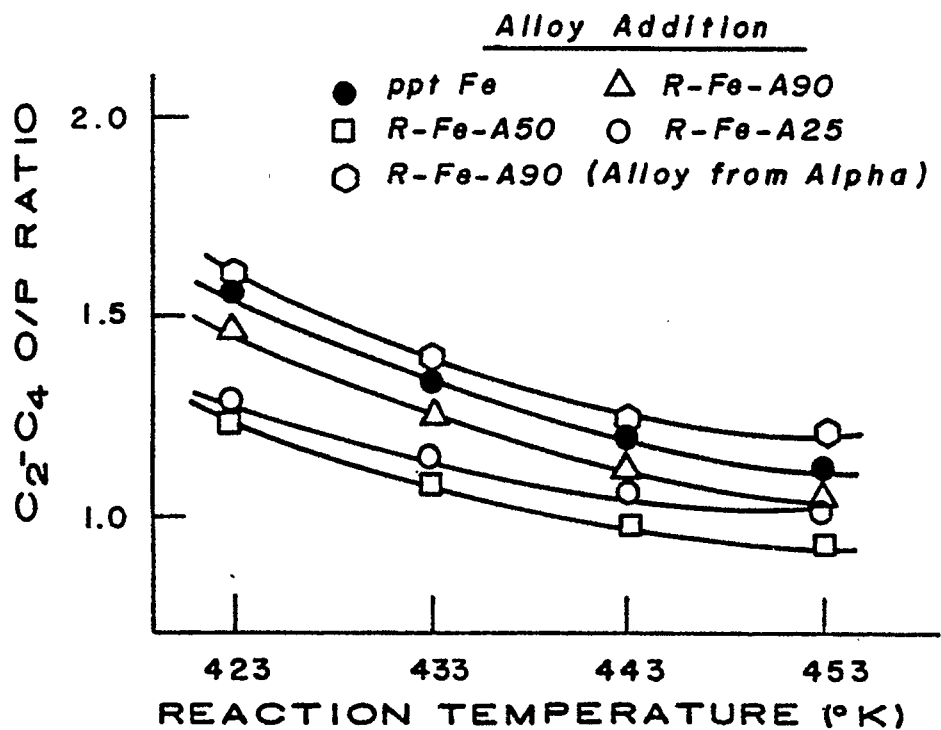


Figure 4. Variation of olefin selectivity with temperature.  
Catalyst: R-Fe-A90, Pressure: 1378 KPa (200 psig)  
SV:  $3.0 \text{ cm}^3\text{g}^{-1}\text{s}^{-1}$ ,  $\text{H}_2/\text{CO}$ : 2.0

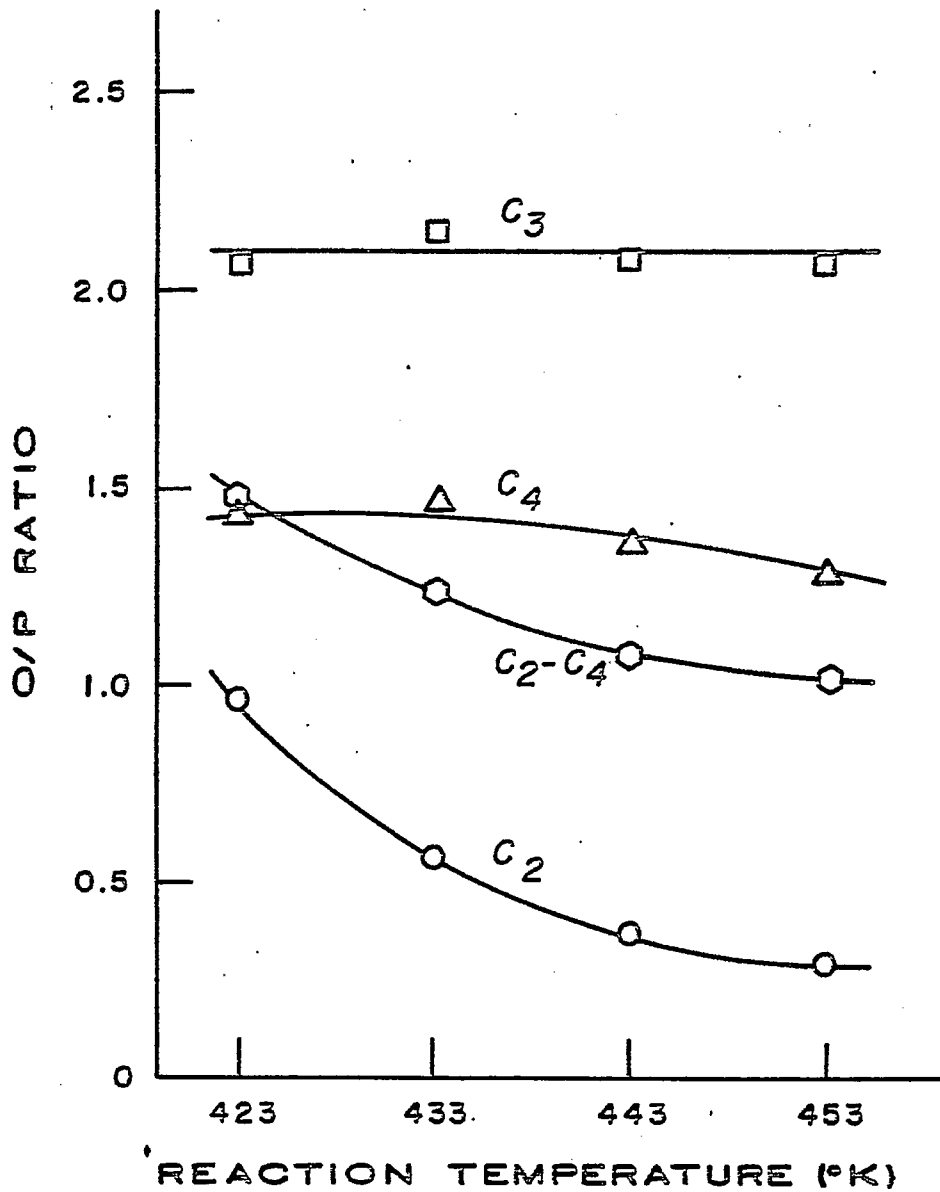


Figure 5. C<sub>2</sub>-C<sub>4</sub> O/P ratio for Raney Fe-Mn catalysts.  
 Pressure: 1378 KPa (200 psig), H<sub>2</sub>/CO: 2.0, SV: 3.0 cm<sup>3</sup> g<sup>-1</sup> s<sup>-1</sup>

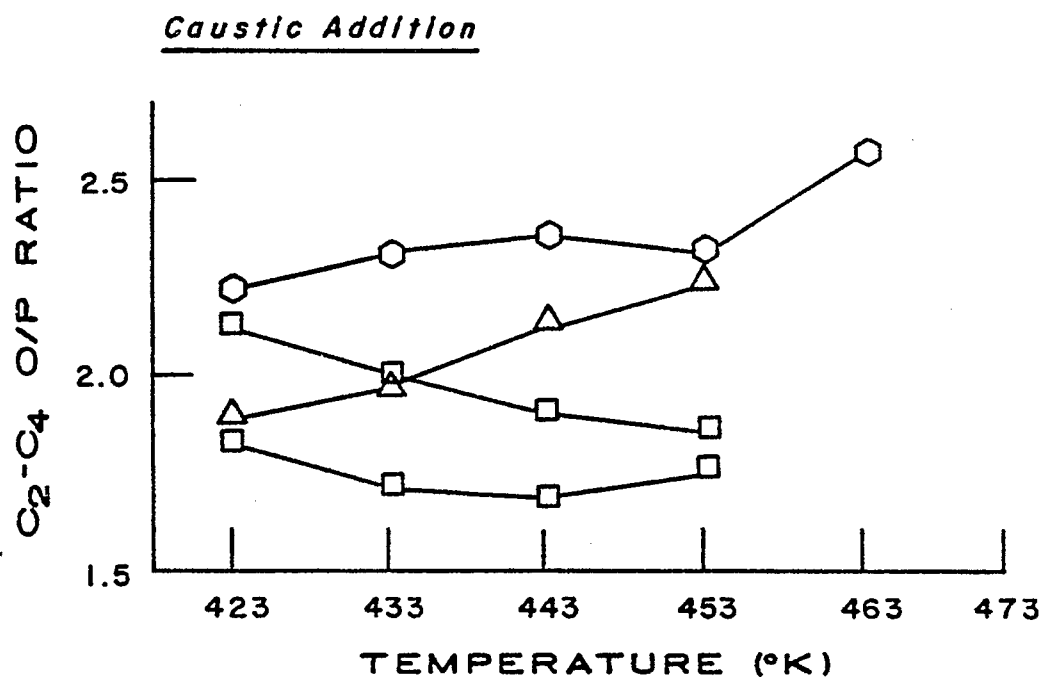
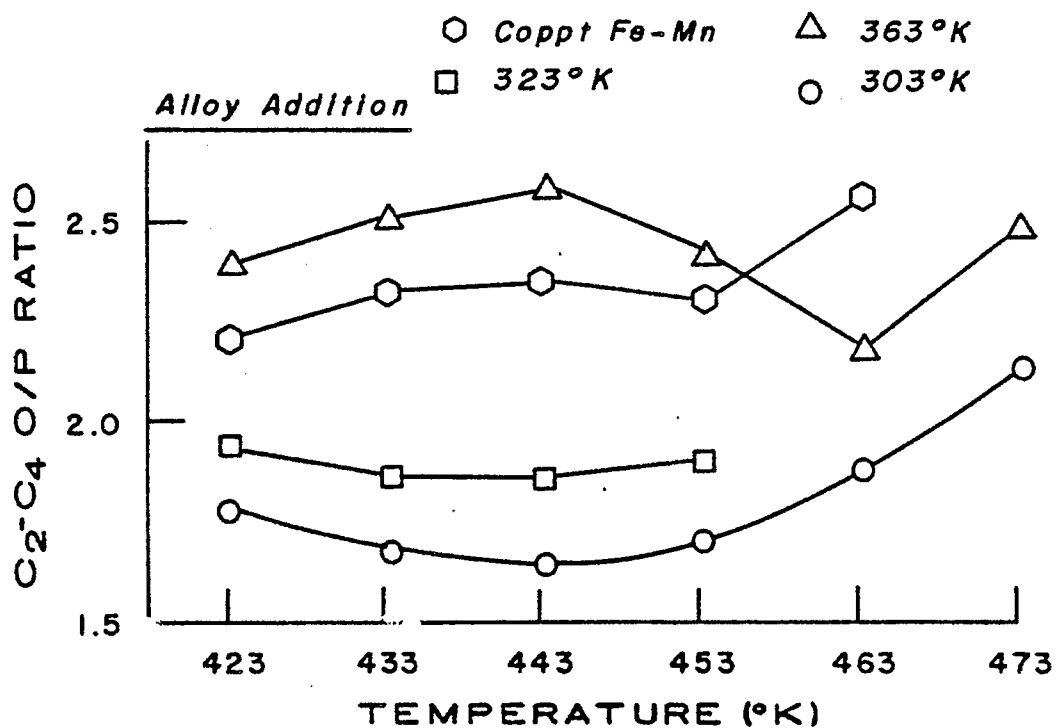


Figure 6. Variation of olefin selectivity with temperature.  
Catalyst: R-FeMn-C90, Pressure: 1378 KPa (200 psig),  
 $H_2/CO$ : 2.0, SV:  $3.0 \text{ cm}^3 \text{ g}^{-1} \text{ s}^{-1}$

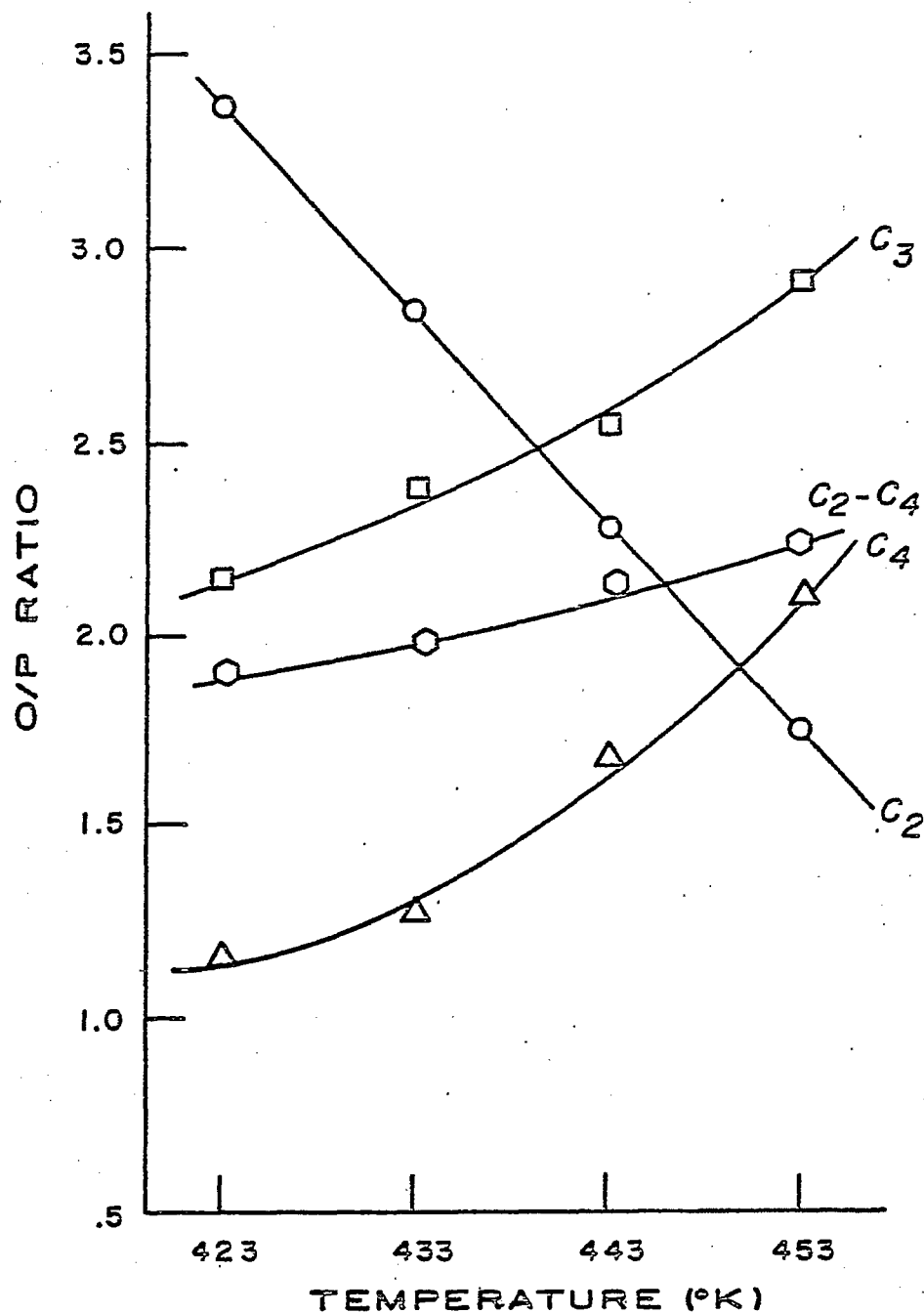


Figure 7. Isokinetic temperature.

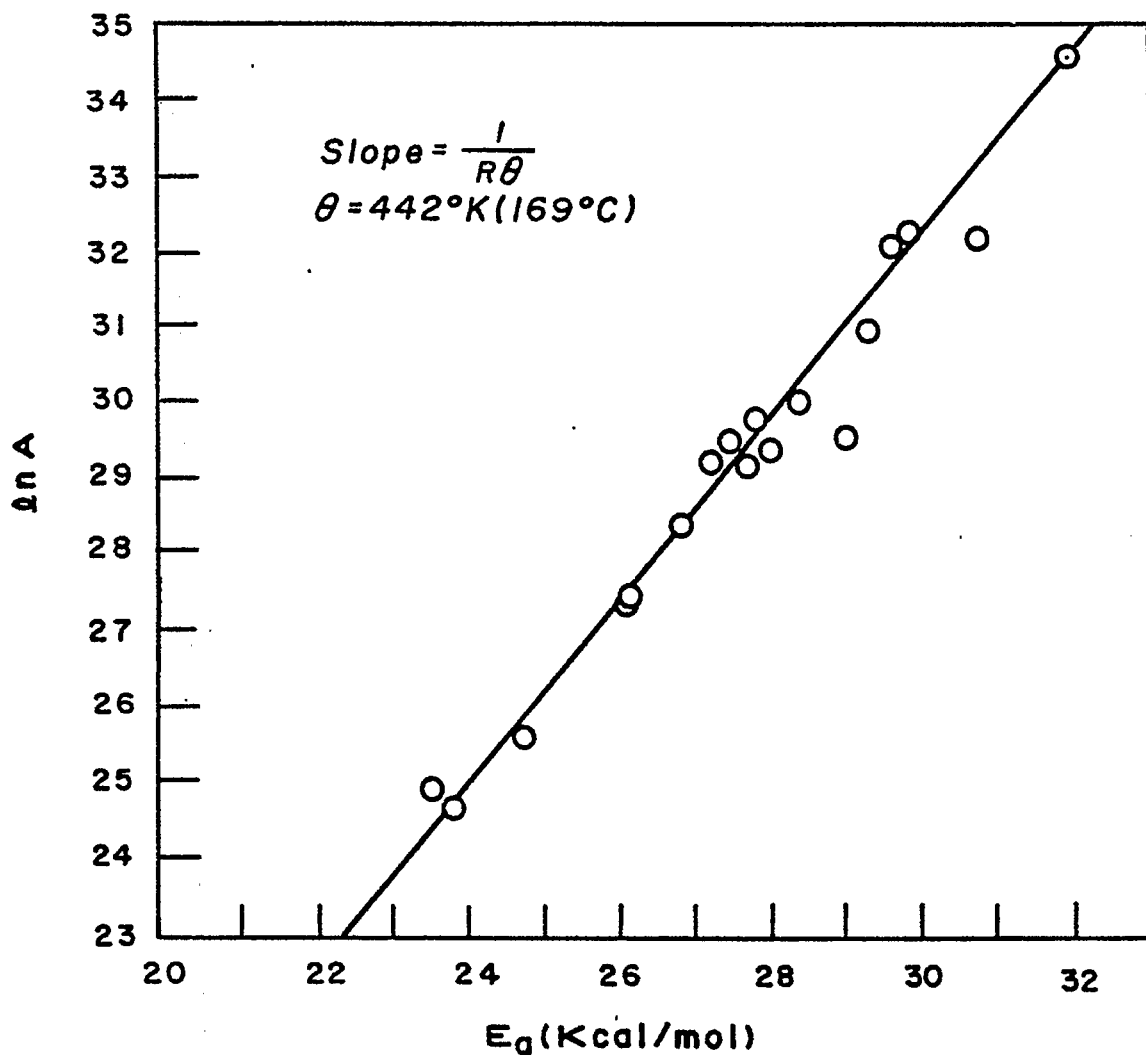


Table 1. Surface area and crystallite size.

<u>Catalyst</u>	<u>L, Crystallite Size (Å)</u>	<u>1/L x 10<sup>3</sup> (Å<sup>-1</sup>)</u>	<u>BET Area (in<sup>2</sup>/g)</u>
R-Fe-A50	126	7.93	46
R-Fe-A90	252	3.97	26
R-Fe-A90 <sup>a</sup>	222	4.50	29
R-Fe-C50	149	6.73	41
R-Fe-C90	134	7.46	49
R-FeMn-A50	93	10.77	64
R-FeMn-A90	107	9.36	81
R-FeMn-A50 <sup>a</sup>	74	13.57	68
R-FeMn-C50	74	13.57	78

<sup>a</sup>Alloy from alpha products.

Table 2. Kinetic parameters and relative activity of Raney Fe catalysts.

Catalyst Type	$E_a$ (Kcal/mol)	A	Relative Activity					
			423 K	433 K	443 K	453 K	463 K	473 K
ppt Fe	26.0	$6.9 \times 10^{11}$	(1.0) 1.0	(2.1) 1.0	(4.17) 1.0	(7.7) 1.0	(14.5) 1.0	(26.4) 1.0
R-Fe-C90	29.8	$9.8 \times 10^{13}$	1.63	1.81	2.00	2.20	2.40	2.62
R-Fe-C50	29.6	$7.8 \times 10^{13}$	1.64	1.81	1.99	2.17	2.37	2.57
R-Fe-C25	27.2	$4.5 \times 10^{12}$	1.61	1.66	1.71	1.76	1.81	1.86
R-Fe-C90 (10%)	24.7	$1.2 \times 10^{11}$	0.90	0.87	0.84	0.81	0.78	0.76
R-Fe-A90	27.4	$5.9 \times 10^{12}$	1.65	1.72	1.78	1.84	1.91	1.97
R-Fe-A50	31.9	$9.6 \times 10^{14}$	1.27	1.49	1.74	2.01	2.32	2.65
R-Fe-A25	27.8	$8.1 \times 10^{12}$	1.32	1.39	1.45	1.52	1.59	1.66
R-Fe-A90 <sup>a</sup>	23.5	$7.0 \times 10^{10}$	2.08	1.94	1.81	1.70	1.60	1.51

<sup>a</sup>Alloy from alpha products.

Table 3. Kinetic parameters and relative activity of Raney Fe-Mn catalysts.

Catalyst Type	$E_a$ (kcal/mol)	A	Relative Activity					
			423 K	433 K	443 K	453 K	463 K	473 K
Coppt Fe-Mn	29.0	$5.7 \times 10^{12}$	(1.0) 1.0	(2.2) 1.0	(4.8) 1.0	(9.8) 1.0	(19.7) 1.0	(38.5) 1.0
R-FeMn-A30	23.8	$4.7 \times 10^{10}$	3.98	3.44	3.00	2.64	2.33	2.07
R-FeMn-A50	28.0	$5.3 \times 10^{12}$	2.89	2.81	2.74	2.68	2.61	2.56
R-FeMn-A90	23.6	$2.6 \times 10^{13}$	3.24	3.25	3.28	3.30	3.32	3.35
R-FeMn-A50 (10%)	30.7	$9.1 \times 10^{13}$	2.12	2.21	2.31	2.41	2.51	2.61
R-FeMn-C50	26.1	$8.0 \times 10^{11}$	4.43	4.07	3.78	3.52	3.28	3.07
R-FeMn-C50	28.4	$9.9 \times 10^{12}$	3.41	3.34	3.29	3.25	3.20	3.16
R-FeMn-C90	26.8	$1.9 \times 10^{12}$	4.41	4.14	3.91	3.70	3.51	3.34

## Task 13

### Catalyst Research and Development Synthesis of Light Hydrocarbons from CO and H<sub>2</sub>

Faculty Advisor: F.V. Hanson

Graduate Student: Y.S. Tsai

#### Introduction

The production of low molecular weight olefins (C<sub>2</sub>-C<sub>4</sub>) from the hydrogenation of carbon monoxide has been investigated over unsupported iron-manganese catalysts. The results from the preliminary tests which were performed in a bench-scale fixed-bed reactor system showed that the unsupported iron-manganese catalysts were very selective in the production of C<sub>2</sub>-C<sub>4</sub> olefins. Data from the screening tests of the sixteen iron-manganese catalysts indicated that a catalyst composed of 2 parts of manganese per 100 parts of iron was the most selective. The effects of the process variables were also studied. The results essentially agreed with those reported in the literature.

The hydrogenation of carbon monoxide is a highly exothermic reaction and the CO conversion is usually kept below 10 percent to prevent hot spots in the catalyst bed due to the nature of the heat transfer limitations in the fixed-bed reactor. The dense bed packing mode is frequently used in catalyst evaluation studies. When this method is used a temperature rise within the catalyst bed will still occur even though the conversion level is maintained at less than 10%. This phenomena may cause a shift in the catalyst activity and selectivity for the production of C<sub>2</sub>-C<sub>4</sub> olefins and the data obtained may not necessarily reflect the catalyst performance at the observed reactor temperature. The dilution of the catalyst bed is an effective method often used to reduce the temperature rise. Therefore, the effect of catalyst dilution has been determined using Denstone 57 (an inert ceramic) as the diluent. The reactor temperature profiles and the catalyst activity and selectivity were determined to assess the effects of catalyst dilution in the hydrogenation of carbon monoxide.

#### Project Status

A single batch of a coprecipitated iron-manganese catalyst (YST-4: 3.0 Mn/100 Fe) was used in this investigation. The inert/catalyst dilution ratios discussed in this report are volume ratios. The reactor was loaded with the appropriate mixture of YST-4 and Denstone 57 according to the procedures outlined in previous reports. The catalysts were reduced in-situ and the activity and selectivity were determined at a set of standard conditions. The standard evaluation conditions were as follows:

Reactor Temperature	483 ~ 498 K (210 ~ 225°C)
Reactor Pressure	kPa (200 psig)
H <sub>2</sub> /CO Ratio	2/1
Reactant Space Velocity	1.0 cm <sup>3</sup> s <sup>-1</sup> (g cat) <sup>-1</sup>

The catalyst bed temperature profiles (temperature as function of bed depth) for the different dilution ratios and reaction temperatures are presented in Figures 1 through 6. The dense bed packing mode (i.e., no diluent) exhibited no detectable temperature rise at 1.5 mole % CO conversion (catalyst bed temperature 463 K (190°C) (Figure 1). However, at 6.7 mole % CO conversion (catalyst bed inlet temperature 486 K (213°C) the observed temperature rise was approximately 7 K (Figure 1). Dilution of the catalyst with Denstone 57 (1/1, 2/1 and 3/1 Denstone/catalyst) did not appreciably alter the magnitude of the temperature rise when CO conversions were maintained in the range from 6.5 - 7.5 mole %, however, the inlet catalyst bed temperature had to be increased several degrees to achieve the desired conversion (Figures 2, 3 and 4). At a Denstone/catalyst dilution ratio of 4/1, the temperature rise was suppressed and the observed catalyst bed temperature profile appeared to be more uniform, however, end-effect heat losses from the reactor-furnace system significantly affected the profile (Figure 5). Heat loss effects were minimized by reducing the catalyst charge to the reactor from 8.0 g and 4.0 g. At a Denstone/catalyst dilution ratio of 4/1 with 4.0 g of catalyst, the catalyst bed temperature profile was nearly isothermal at a CO conversion of 7.3 mole % (Figure 6). Thus it was concluded that the observed catalyst bed temperature profile can be maintained nearly isothermal at a Denstone/catalyst ratio of 4/1 when the CO conversion is kept below 7.5 mole % provided the catalyst bed is located in the reactor zone from 4 inches to 10 inches (i.e., a catalyst charge of 4.0 g).

The effect of catalyst dilution on the activity and selectivity were also determined in the CO conversion range 6.5 - 7.5 mole %. The data from these experiments are presented in Table 1. The dense bed packing mode produced a higher yield of CO<sub>2</sub> and CH<sub>4</sub> and a lower yield of C<sub>2</sub>-C<sub>4</sub> and C<sub>5</sub><sup>+</sup> hydrocarbons than was generally observed with the diluted bed packing mode. The increased CO<sub>2</sub> yield may be related to the higher temperature rise at the hot spot in the dense bed mode which could shift the selectivity in favor of the CO disproportionation reaction and accelerate the deposition of coke on the catalyst. The olefin/paraffin ratio of the C<sub>2</sub>-C<sub>4</sub> hydrocarbons was significantly lower for the dense bed packing mode. The yields and selectivities were quite similar for all the diluted bed packing mode experiments above a packing ratio of 1/1. Based on these experiments all future experiments will be conducted with a Denstone/catalyst ratio of 4/1 and a catalyst charge of 4.0 g.

#### Future Work

The optimum catalyst pretreatment for the maximum production of C<sub>2</sub>-C<sub>4</sub> olefins will be investigated. The catalyst characterization studies will be initiated. The literature survey concerning the CO hydrogenation as well as the heat and mass transfer calculations for the fixed-bed reactor will be continued.

Table 1. Effects of the catalyst bed dilution on the catalyst activity and selectivity.

Dilution Ratio	CO Conversion (%)	Selectivities					O/P in C <sub>2</sub> -C <sub>4</sub>
		C <sub>02</sub>	C <sub>1</sub>	C <sub>2</sub> -C <sub>4</sub>	C <sub>5</sub> <sup>+</sup>	ROH	
0 (a)	6.7	15.9	22.5	42.3	13.8	5.5	1.81
1/1 (a)	7.3	11.1	19.4	45.8	18.6	5.1	2.52
2/1 (a)	7.0	13.7	18.4	46.5	18.3	3.1	2.83
3/1 (a)	6.5	9.6	19.7	46.6	18.2	5.9	2.63
4/1 (a)	7.2	11.1	19.2	46.2	19.3	4.2	2.57
4/1 (b)	7.3	10.6	19.3	46.6	19.1	4.4	2.55

(a) Weight of the catalyst used: 8.0 g.

(b) Weight of the catalyst used: 4.8 g.

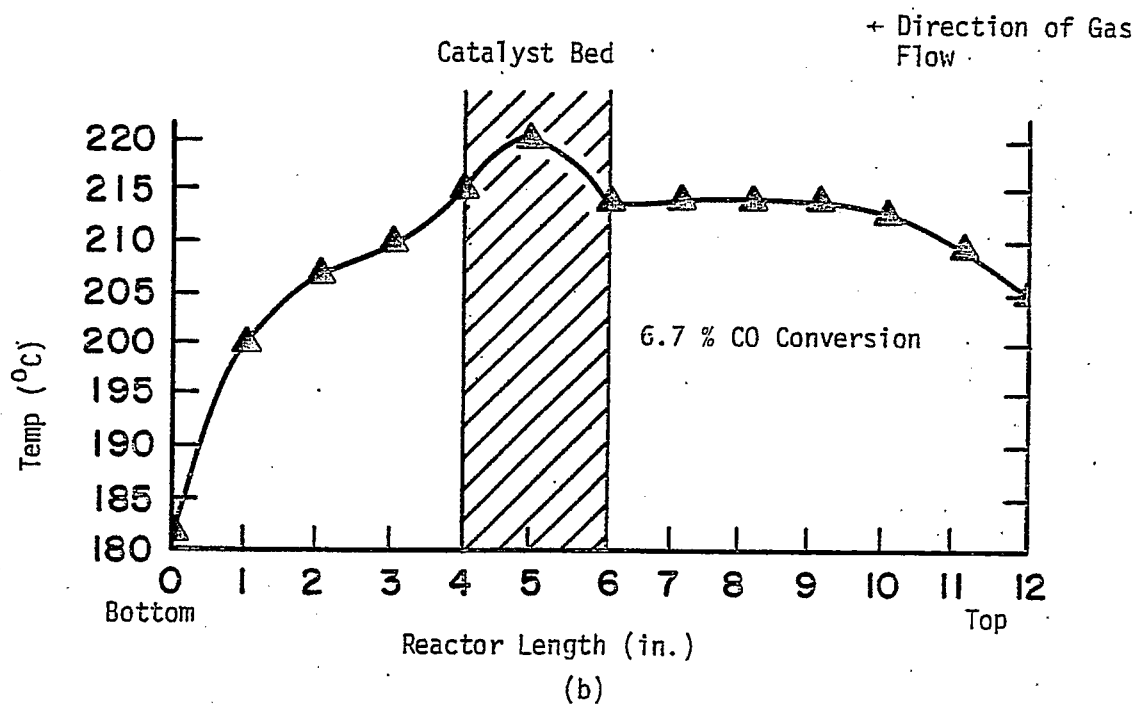
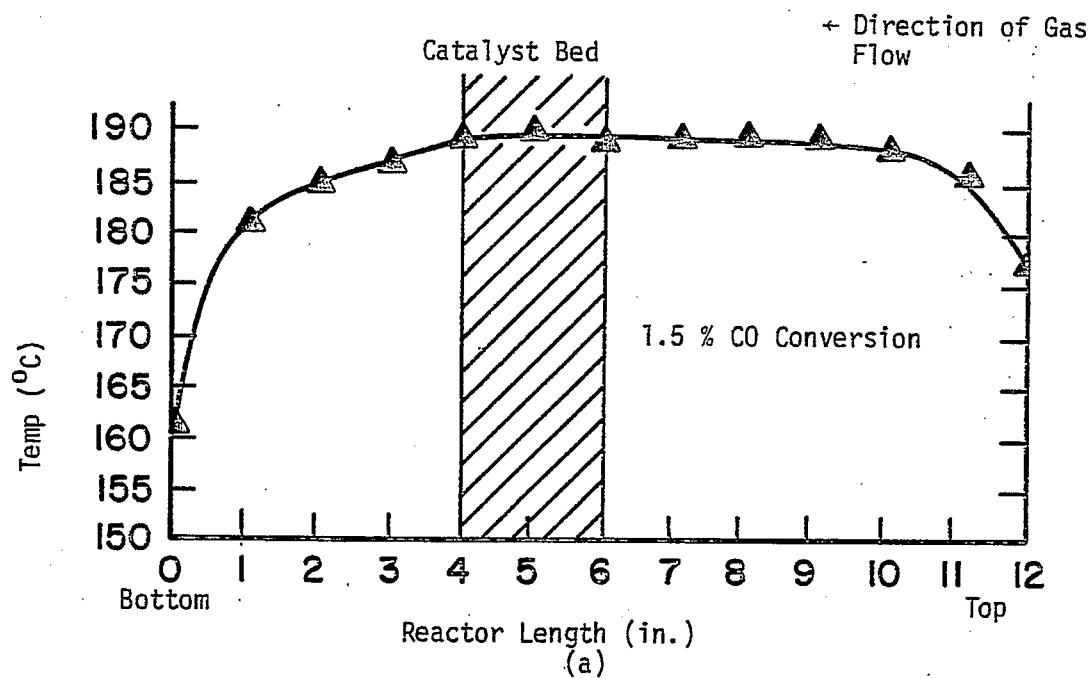


Figure 1. Temperature profiles in the dense fixed-bed reactor: (a) 1.5% CO conversion; (b) 6.7% CO conversion (YST-4 catalyst, 8.0 g used).

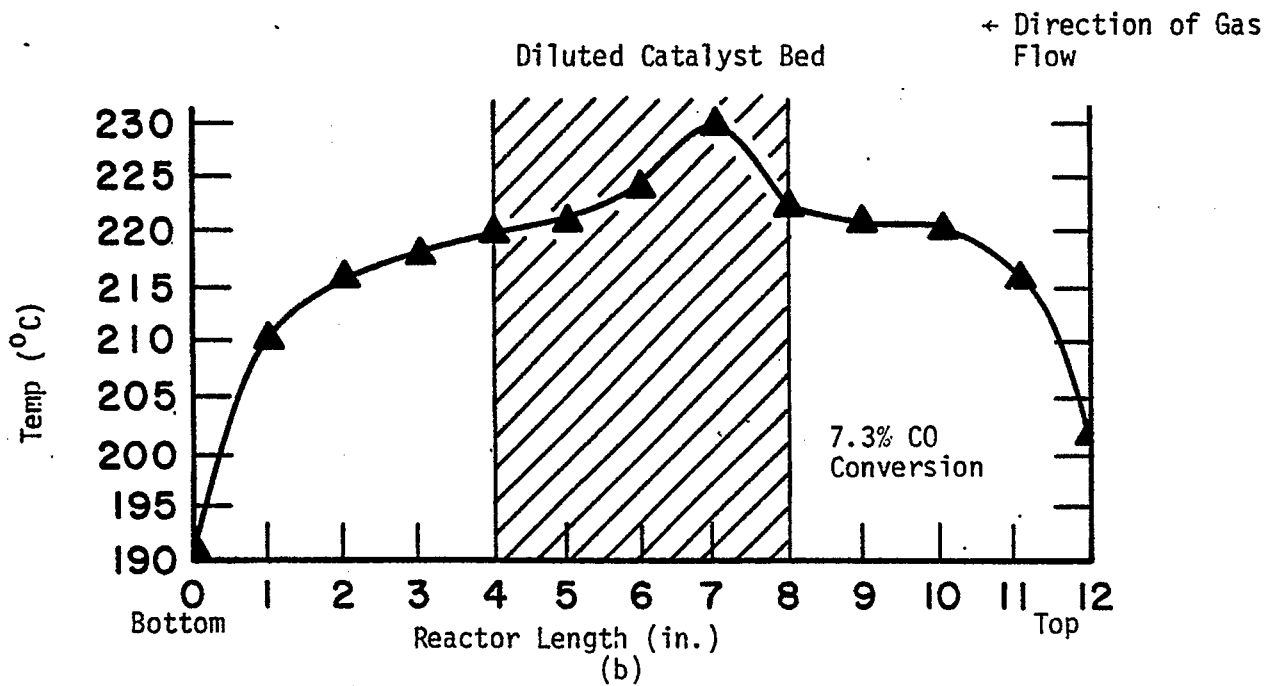
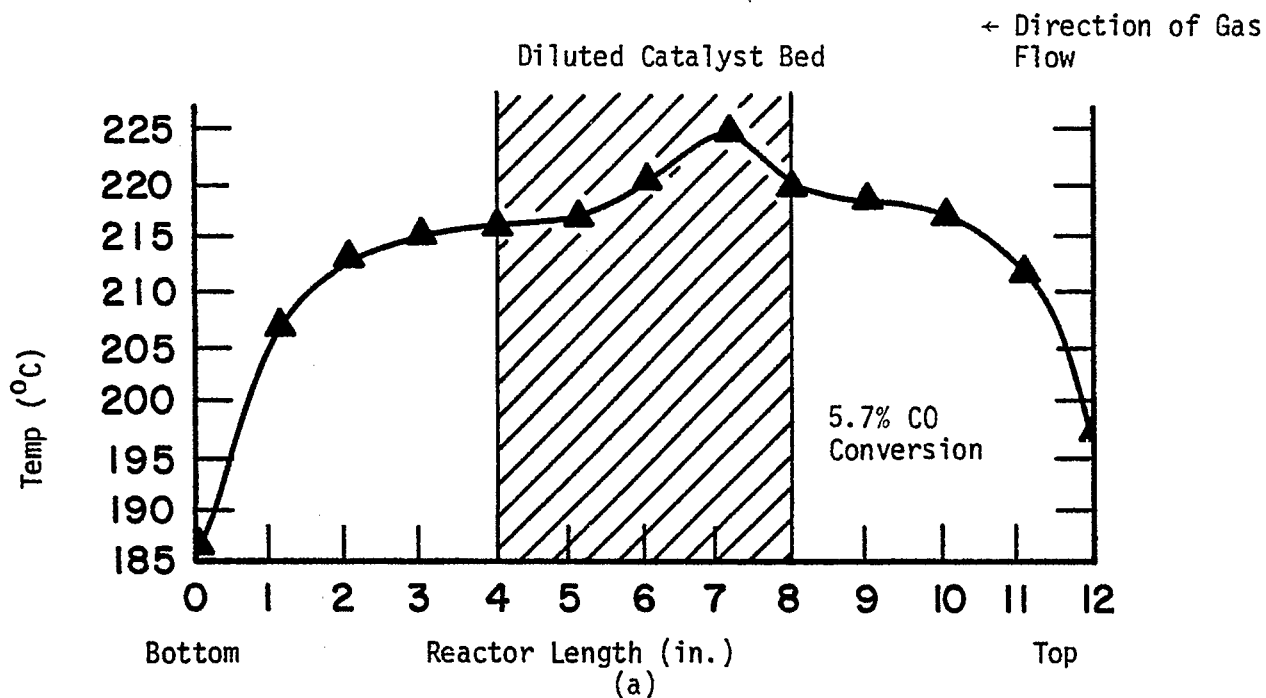


Figure 2. Temperature profiles in the diluted fixed-bed reactor: (a) 5.7% CO conversion; (b) 7.3% CO conversion (YST-4 catalyst, 8.0 g used, volumetric dilution ratio: Denstone 57/catalyst = 1/1).

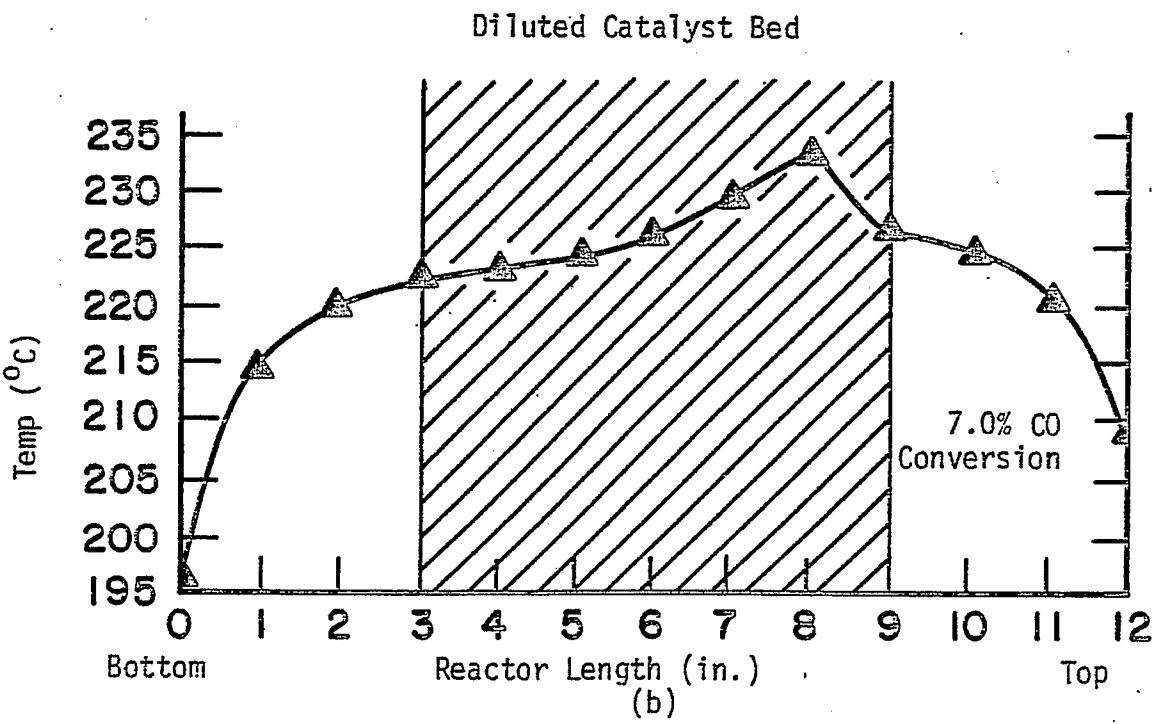
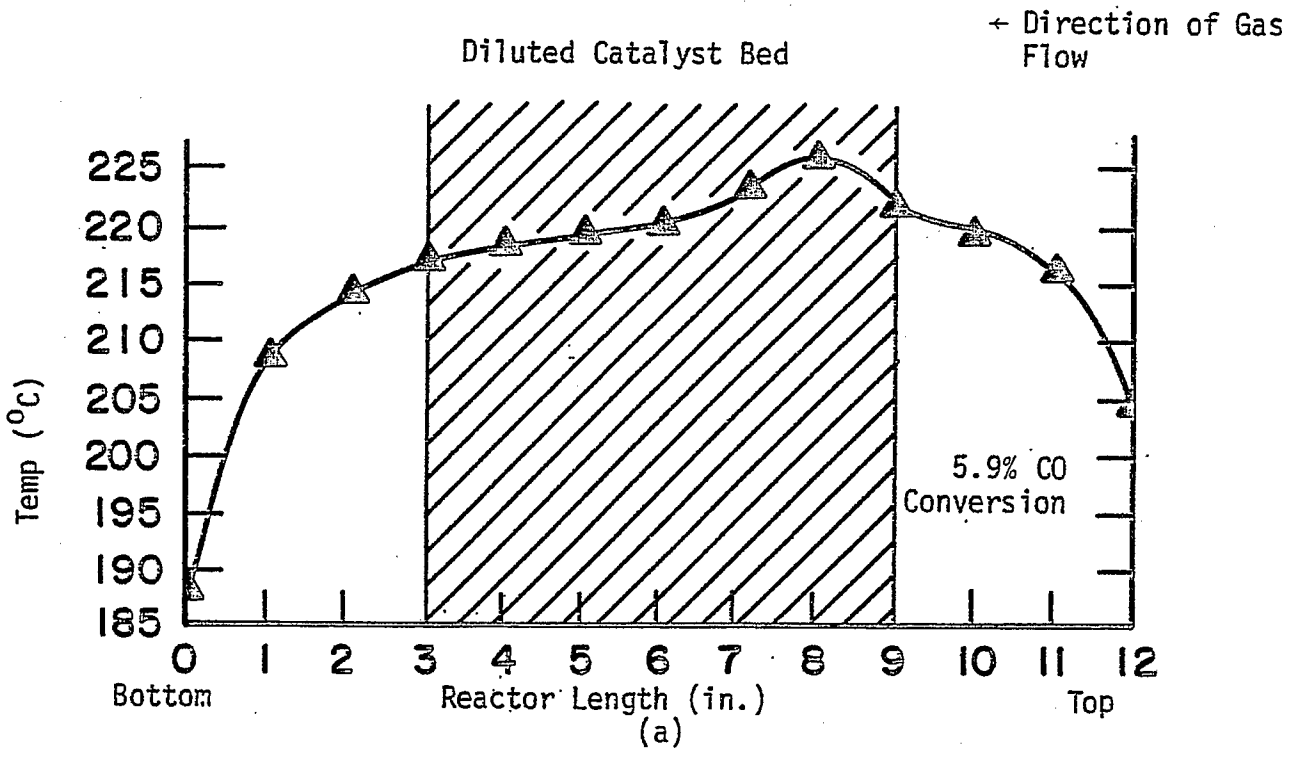


Figure 3. Temperature profiles in the diluted fixed-bed reactor: (a) 5.9% CO conversion; (b) 7.0% CO conversion (YST-4 catalyst, 8.0 g used, volumetric dilution ratio: Denstone 57/catalyst = 2/1).

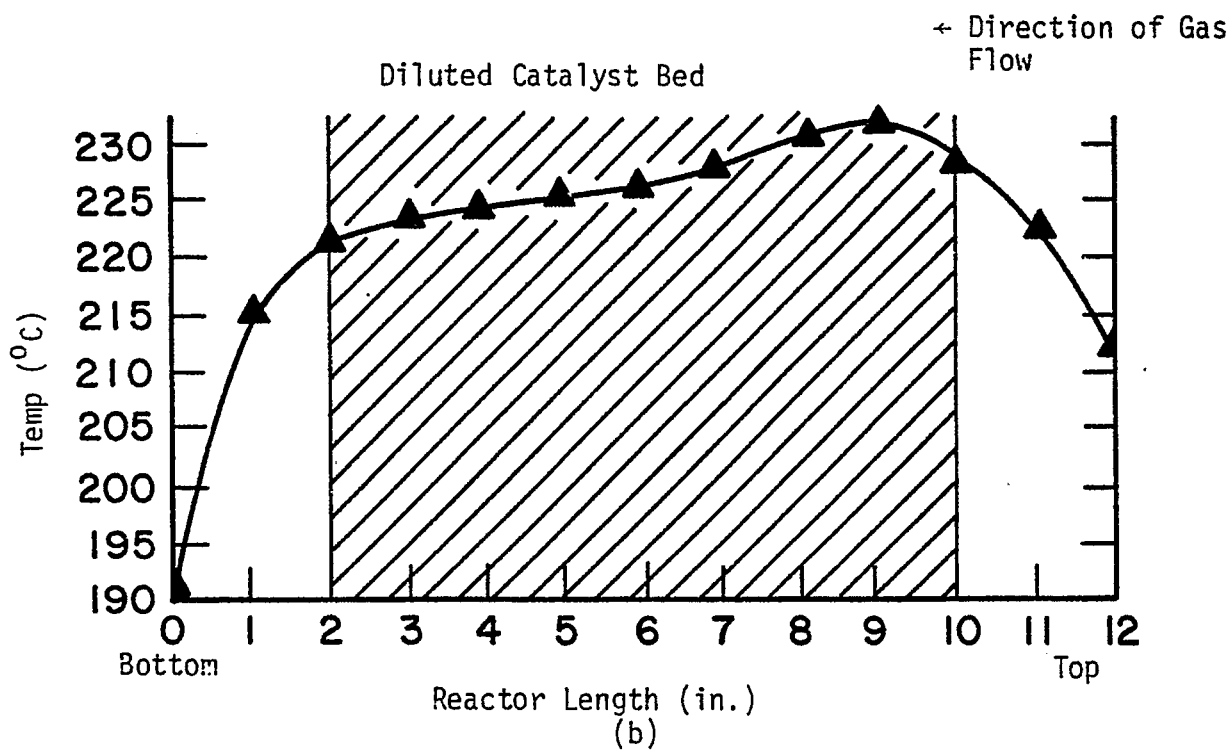
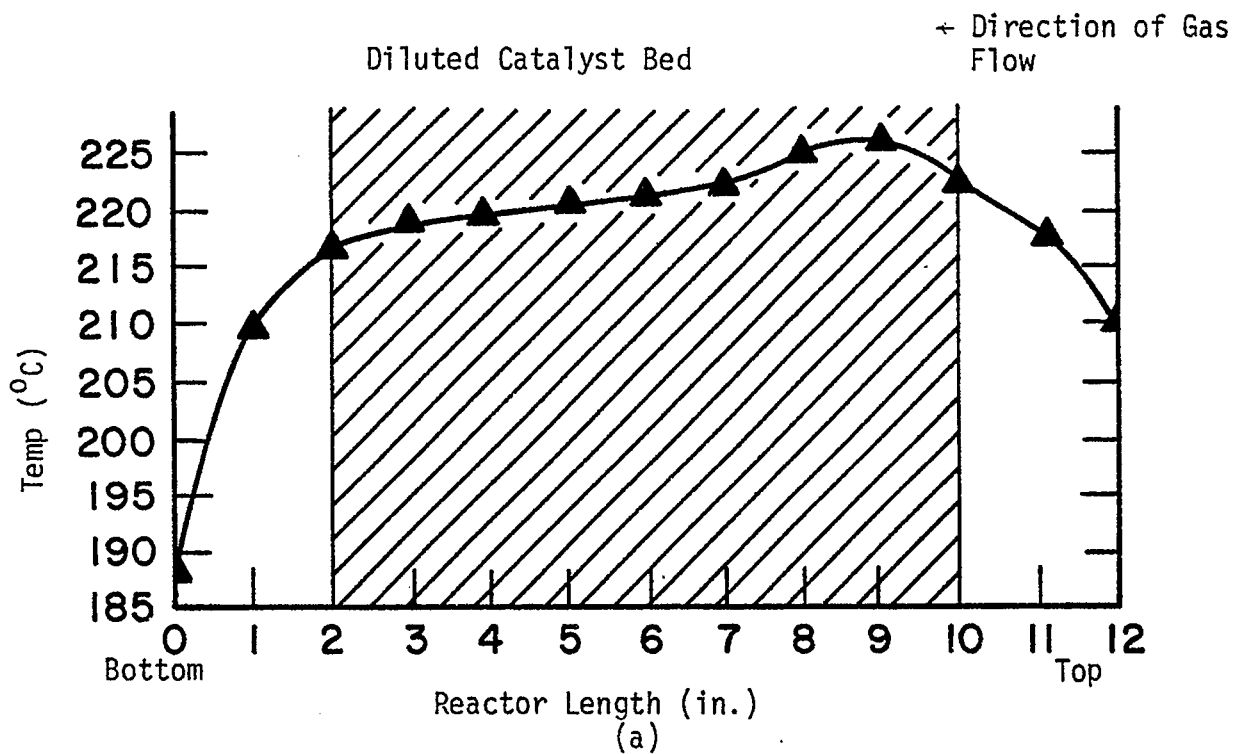


Figure 4. Temperature profiles in the diluted fixed-bed reactor: (a) 6.5% CO conversion; (b) 8.2% CO conversion (YST-4 catalyst, 8.0 g used, volumetric dilution ratio: Denstone 57/catalyst = 3/1).

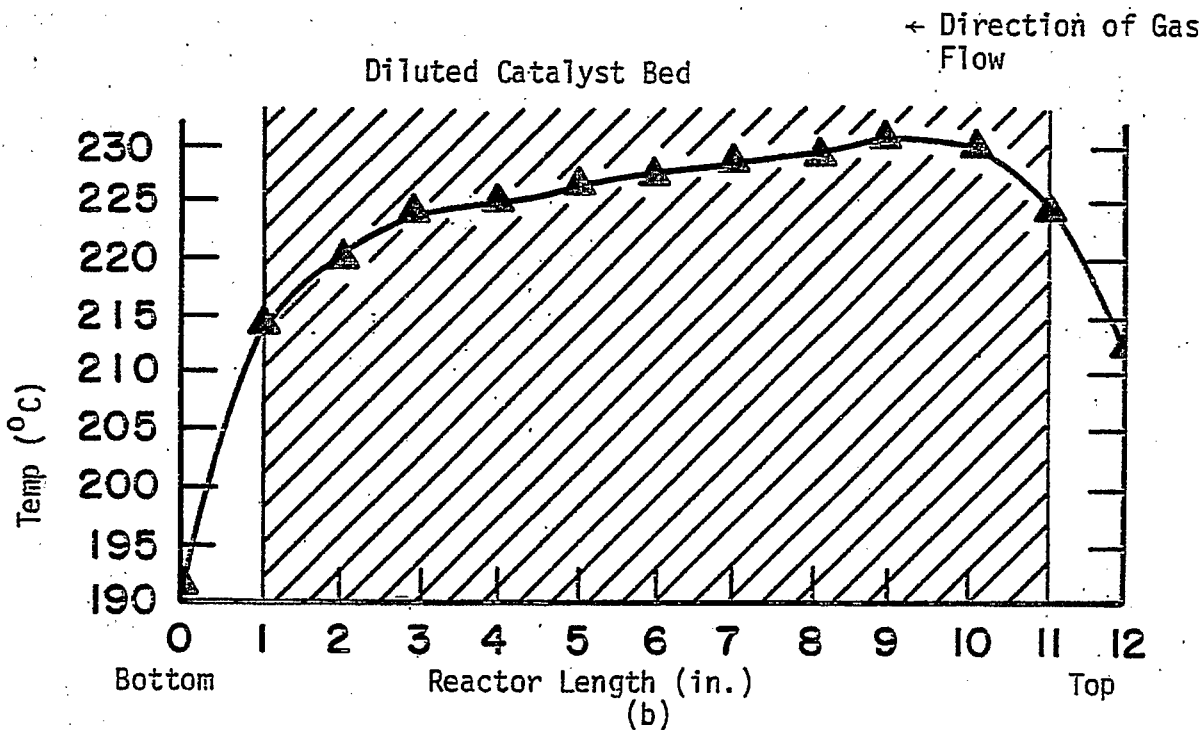
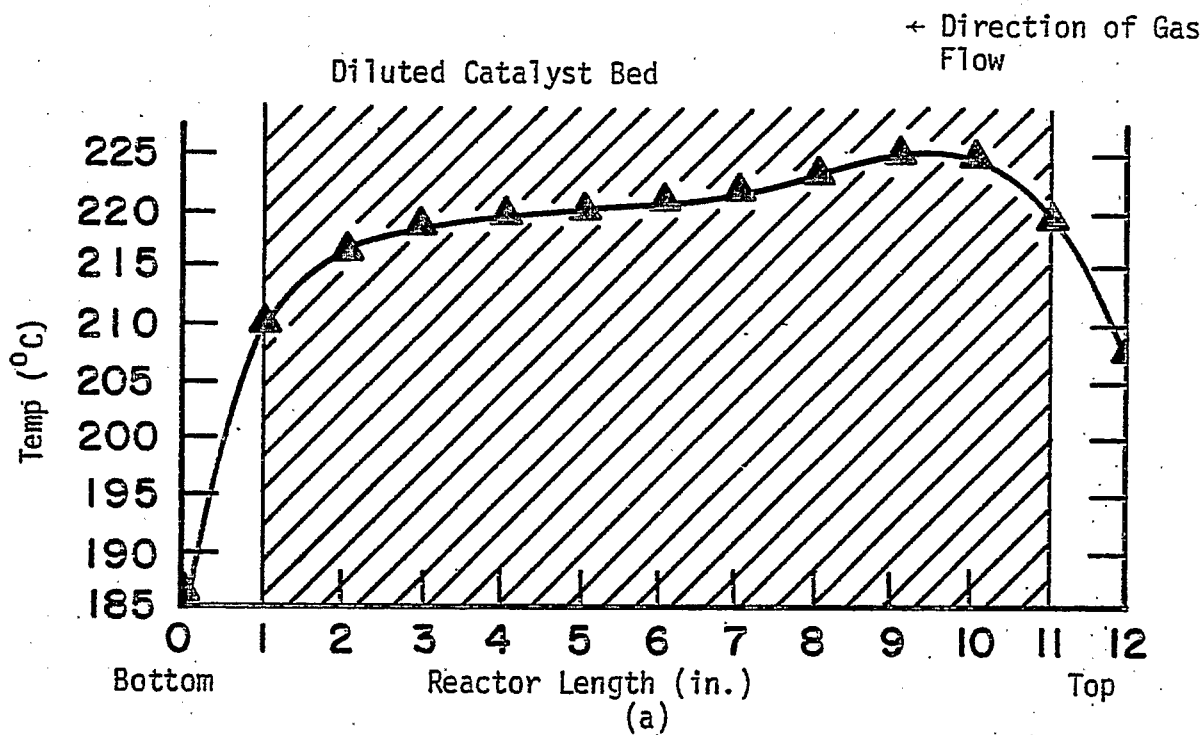


Figure 5. Temperature profiles in the diluted fixed-bed reactor: (a) 5.8% CO conversion; (b) 7.2% CO conversion (YST-4 catalyst, 8.0 g used, volumetric dilution ratio: Denstone 57/catalyst = 4/1).

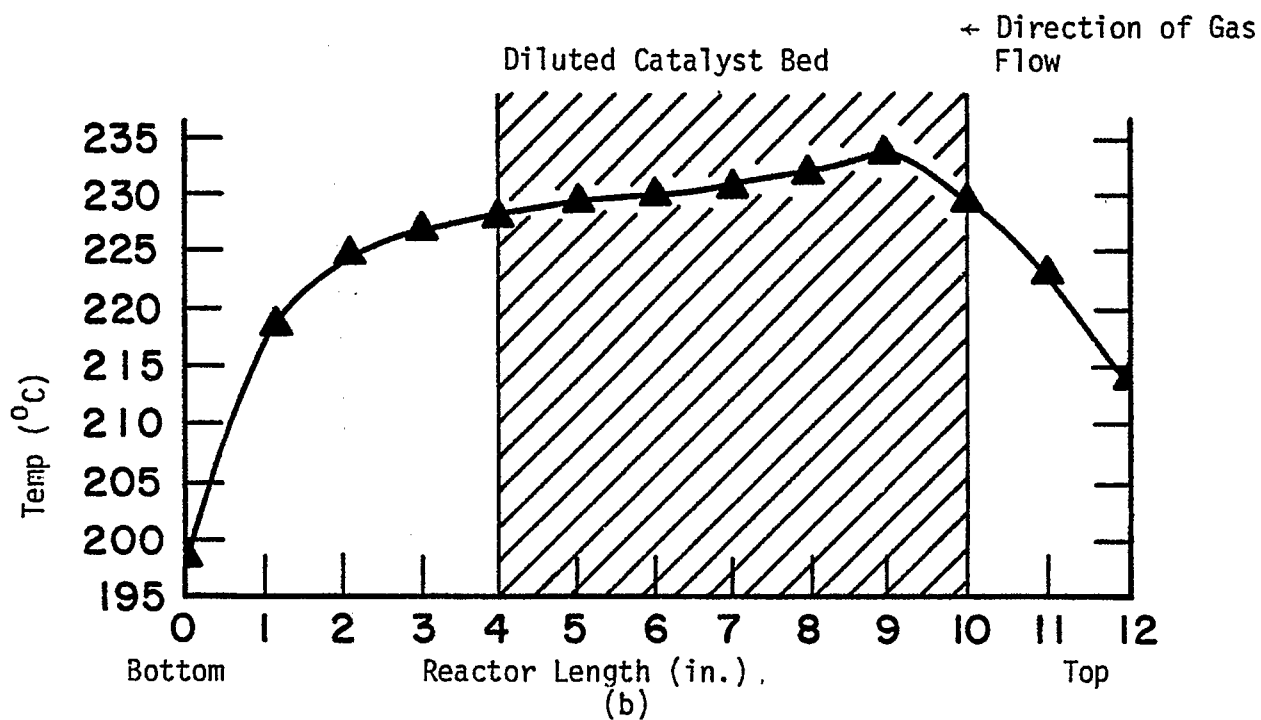
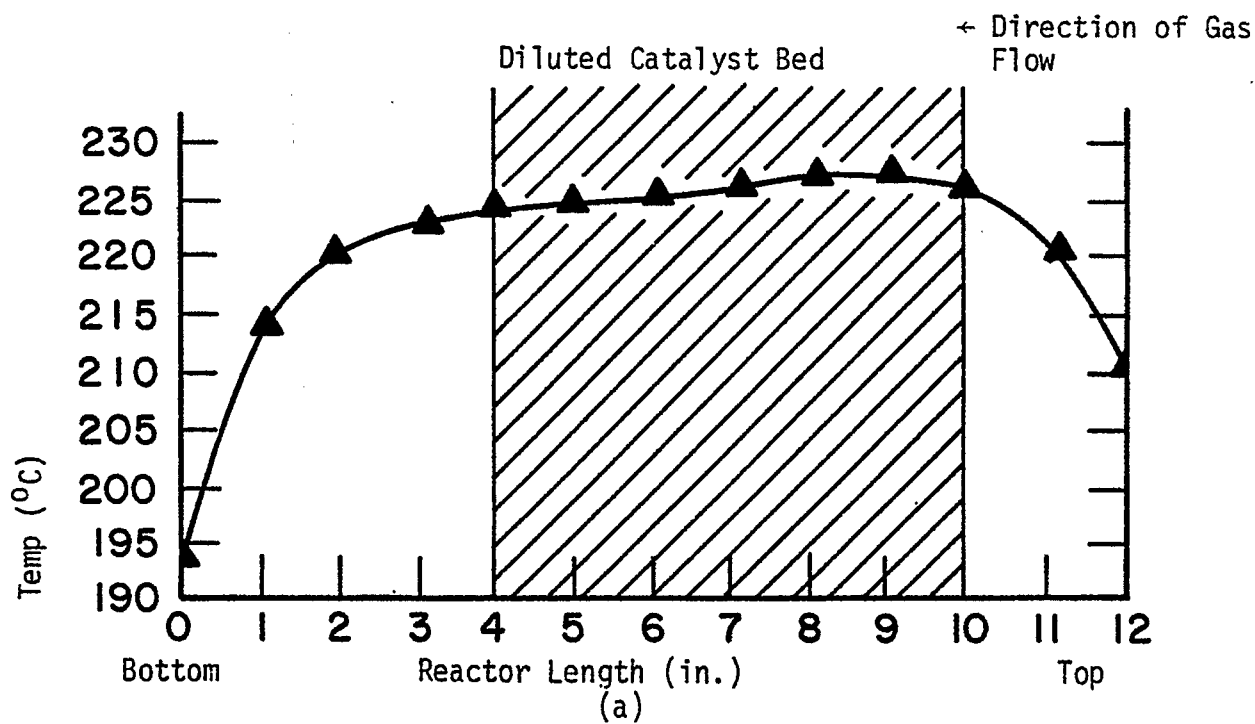


Figure 6. Temperature profiles in the diluted fixed-bed reactor:  
 (a) 7.3% CO conversion; (b) 8.9% CO conversion (YST-4 catalyst,  
 4.8 g used, volumetric dilution ratio: Denstone 57/catalyst = 4/1).

## V. Conclusions

Detailed conclusions are included in the reports for each task. Task 4 is no longer funded and has been discontinued. Tasks 14 are inactive. No work was done under Task 15.